JANUARY2019 Ph.D. in Electrical and Electronics Engineering HAMED ATYIA SOODI

UNIVERSITY OF GAZİANTEP
GRADUATE SCHOOL OF
NATURAL & APPLIED SCIENCES

DESIGN AND IMPLEMENTATION OF A SINGLE-PHASE CASCADED H-BRIDGE MULTI-LEVEL CONVERTER BASED STATCOM

Ph.D. THESIS
IN
ELECTRICAL AND ELECTRONICS ENGINEERING

BY
HAMED ATYIA SOODI
JANUARY 2019

Design and Implementation of a Single-Phase Cascaded H-Bridge Multi-Level Converter Based STATCOM

Ph.D. Thesis

in

Electrical and Electronics Engineering

University of Gaziantep

Supervisor

Assoc. Prof. Dr. Ahmet Mete VURAL

by

Hamed Atyia SOODI

JANUARY 2019

REPUBLIC OF TURKEY

UNIVERSITY OF GAZIANTEP

GRADUATE SCHOOL OF NATURAL & APPLIED SCIENCES

ELECTRICAL AND ELECTRONICS ENGINEERING

Name of thesis: Design and Implementation of a Single-Phase Cascaded H-Bridge Multi-Level Converter Based STATCOM

Name of the student: Hamed Atyia SOODI

Exam Date: January 28, 2019

Approval of the Graduate School of Natural and Applied Sciences.

Prof. Dr. A. Necmeddin YAZICI

Director

I certify that this thesis satisfies all the requirements as a thesis for the degree of Philosophy of Doctorate.

Prof. Dr. Ergun ERÇELEBİ

Head of Department

This is to certify that we have read this thesis and that in our consensus/majority opinion it is fully adequate, in scope and quality, as a thesis for the degree of Doctor of Philosophy.

Assoc. Prof. Dr. Ahmet Mete VURAL

Supervisor

Examining Committee Members:	Signature
Prof. Dr. Ergun ERÇELEBİ	…….
Assoc. Prof. Dr. Mehmet Uğraş CUMA	.....……
Assoc. Prof. Dr. Ahmet Mete VURAL	……..
Assist. Prof. Dr. Serkan ÖZBAY	……..
Assist. Prof. Dr. Tahsin KÖROĞLU	……

I hereby declare that all information in this document has been obtained and presented in accordance with academic rules and ethical conduct. I also declare that, as required by these rules and conduct, I have fully cited and referenced all material and results that are not original to this work.

Hamed Atyia SOODI

ABSTRACT

DESIGN AND IMPLEMENTATION OF A SINGLE-PHASE CASCADED H-BRIDGE MULTI-LEVEL CONVERTER BASED STATCOM

SOODI, Hamed Atyia

Ph.D. in Electrical and Electronics Engineering

Supervisor: Assoc. Prof. Dr. Ahmet Mete VURAL

January 2019

161 pages

Reactive power control is very crucial in terms of voltage stability and power quality of electrical power systems. In steady-state, during heavy loading conditions, the system voltage may be lower than its reference value, or it might be observed an increase in system voltage during light loading conditions. In either of these cases, especially shunt reactive power support is necessary to restore the system. STATCOM is one of the most versatile member of FACTS devices that is used for VAR compensation and voltage control. When compared to old compensation technologies such as fixed capacitor or SVC, STATCOM has many advantages such as faster response and small size. In this thesis, a low-power single-phase STATCOM prototype has been modelled, designed and practically implemented. The proposed STATCOM comprises of a multilevel converter having three cascaded full H-bridges. It is aimed that the proposed STATCOM can operate both in capacitive and inductive modes. It is shown by both simulations and experiments that the STATCOM injects and absorbs reactive power into/from single-phase 220V grid. A closed loop control scheme has been implemented so that the STATCOM can generate the desired amount of capacitive/inductive reactive power. Some optimization methods have been used to determine many controller parameters which provide good dynamic performance to STATCOM.

Key Words: Reactive power control, FACTS devices, Single-phase STATCOM, Closed-loop control, Controller optimization.

ÖZET

TEK-FAZ KASKAT H-KÖPRÜ ÇOK SEVİYELİ ÇEVİRGEÇ TABANLI STATCOM TASARIMI VE GERÇEKLEŞTİRİLMESİ

SOODI, Hamed Atyia

Doktora Tezi, Elektrik-Elektronik Mühendisliği Bölümü

Tez Yöneticisi: Doç. Dr. Ahmet Mete VURAL

2019

161 sayfa

Reaktif güç denetimi elektrik güç sistemlerinin gerilim kararlılığı ve güç kalitesi bakımından çok önemlidir. Durgun-halde, ağır yüklenme koşullarında sistem gerilimi referans değerinden daha düşük olabilir, veya hafif yüklenme koşullarında sistem geriliminde bir yükselme görülebilir. Bu durumların herhangi birisinde özellikle şönt reaktif güç desteği sistemin eski haline gelmesi için gereklidir. STATCOM, VAR kompanzasyonu ve gerilim denetimi için kullanılan FACTS cihazlarının en çok yönlü üyelerinden biridir. Sabit kondansatör veya SVC gibi eski kompanzasyon teknolojileriyle karşılaştırıldığında STATCOM'un daha hızlı tepki ve küçük boyut gibi avantajları vardır. Bu tezde, düşük güçlü tek-fazlı bir STATCOM prototipi modellenmiş, tasarlanmış ve pratik olarak gerçeklenmiştir. Önerilen STATCOM, üç adet kaskat tam H-köprüye sahip çok seviyeli bir çeviriciden oluşmaktadır. Önerilen STATCOM'un hem kapasitif hem de endüktif modlarda çalışabilmesi amaçlanmıştır. STATCOM'un tek-faz 220V şebekeye reaktif güç enjekte ettiği ve tek-faz 220V şebekeden reaktif güç tükettiği hem benzetimlerle hem de deneylerle gösterilmiştir. STATCOM'un istenilen büyüklükteki kapasitif/endüktif reaktif gücü üretebilmesi için bir kapalı döngü denetim şeması gerçeklenmiştir. STATCOM'a iyi dinamik performans sağlaması amacıyla birçok denetleyici parametresinin belirlenmesi için bazı optimizasyon yöntemleri kullanılmıştır.

Anahtar Kelimeler: Reaktif güç denetimi, FACTS cihazları, Tek-faz STATCOM, Kapalı-döngü denetimi, Denetleyici optimizasyonu.

To my mother, brother, wife, children and friends I dedicate this humble work

ACKNOWLEDGEMENT

In the name of Allah, the Most Gracious, the most Merciful.

First of all, I would like to express my full gratitude and appreciation for the great effort exerted by the supervisor Dr. Ahmet Mete VURAL. All thanks to him for choosing the topic and for the support and scientific guidance in my research that would otherwise not have been completed.

I would like to express my gratitude to the staff individuals from the Electrical and Electronics Department of Engineering at the University of Gaziantep and my gratitude to every single other companion for their helping me in setting up this exploration.

At last but not least, I would like to express my deepest gratitude and thanks to my family and friends especially my mother & my wife for their patience and continued support and their advice to me at all stages of my studies and life.

TABLE OF CONTENTS

LIST OF TABLES

Page

LIST OF FIGURES

Page

LIST OF SYMBOLS

AC	Alternative Current
ADC	Analog Digital Converter
ANPC	Active Neutral Point Clamped
ANN	Artificial Neural Network
APF	Active Power Filter
APOD-PWM	Alternate Phase Opposition Disposition PWM
CCC	Capacitor Clamp Converter
CHB	Cascaded H-bridge
CSC	Current Source Converter
CSAPF	Cascaded Shunt Active Power Filter
DC	Direct Current
DAC	Digital Analog Converter
DVR	Dynamic Voltage Regulator
dq	Direct-Quadrature Axis
EMI	Electro Magnetic Interference
F	Frequency
FACTS	Flexible Alternating Current Transmission Systems
FLC	Fuzzy Logic Control
GA	Genetic Algorithm
GTO	Gate Turn-Off Thyristor
H-PWM	Hybrid PWM
I	Current
IPFC	Interline Power Flow Controller
IGBT	Insulated Gate Bipolar Transistor
LS-PWM	Level Shifted PWM
LCD	Liquid Crystal Display
MLC	Multilevel Converter

MPC	Model Predictive Control
MSE	Mean Squared Errors
NPC	Neutral Point Clamped
NVC	Nearest Vector Control
NLC	Nearest Level Control
P	Active Power
PCC	Point of Common Coupling
PF	Power Factor
PI	Proportional Integral Controller
PLL	Phase Locked Loop
PWM	Pulse Width Modulation
PSO	Particle Swarm Optimization
PS-PWM	Phase Shifted PWM
PD-PWM	Phase Disposition PWM
POD-PWM	Phase Opposition Disposition PWM
PSS	Power System Stabilizer
Q	Reactive Power
ref	Parameter Reference
SAPF	Shunt Active Power Filter
SHE	Selective Harmonic Elimination
SHM	Selective Harmonic Mitigation
SFLA	Shuffled Frog Leap Algorithm
SVC	Static Var Compensation
SVM	Space Vector Modulation
SPWM	Sinusoidal Pulse Width Modulation
SSSC	Static Synchronous Series Compensator
STATCOM	Static Synchronous Compensator
T	Time
TCC	Transistor-Clamped Converter
TCSC	Thyristor Controlled Series Compensation
THD	Total Harmonic Distortion
UPQC	Unified Power Quality Conditioner
UPFC	Unified Power Flow Controller

V	Voltage
V_{BUS}	Voltage of Bus
V_{dc}	DC Link Voltage
VSC	Voltage Source Converter
ω	Rotor Speed Generator
X_L	Inductive Reactance of the Coupling Transformer
ZCD	Zero Cross Detector

CHAPTER 1

INTRODUCTION

1.1 General Overview

Steady-state and dynamic reactive power control are very critical when it comes to voltage regulation and quality of power in electrical systems [1]. Shunt compensation is frequently applied at the critical buses where the voltage magnitude is very sensitive to load changes. During heavy loading, system voltage can undershoot the reference value. Or dynamically, voltage sag can be detected following a fault in the utility system. So, system voltage should be within its permissible limits in terms of voltage stability and to provide high quality of electrical energy to consumers. Efficient voltage control becomes especially important with the insertion of specific loads, such as arc furnaces, which have high impact on voltage [1]. In many years, conventionally, shunt connected fixed capacitors had been used to generate VAR power to boost system voltage. Although this solution is very easy to apply and cheap, reactive power management is not flexible and sufficient for fast dynamic voltage control. Moreover, fixed capacitors cannot consume reactive power in cases where lowering system voltage is needed, such as in light loading conditions [2]. Later, Static VAR Compensators (SVC) have been suggested for better reactive power control. Because SVC includes both switched capacitors and reactors, reactive power can be generated or absorbed efficiently [3, 4]. Although SVC can provide better dynamic performance than fixed capacitors, SVC and fixed capacitors suffer from the fact that capacitors can generate reactive power under the given voltage. In another word, the amount of VAR power that a capacitor produces depends upon capacitor voltage. So, at the instant where the system voltage critically decreases, the capacitors cannot produce sufficient VAR power to compensate system voltage back to near its nominal value. Unfortunately, the performances of these two compensation schemes are highly dependent on distorted system conditions. This is the major drawback of capacitor utilization as reactive power source.

On the other hand, Flexible Alternating Current Transmission Systems (FACTS) has emerged as an alternative option for better operation and control of power transmission systems. FACTS was first hypothesized by Dr. Narain G. Hingorani in late 1980s and is defined as "Alternating current transmission systems incorporating power electronic-based and other static controllers to enhance controllability and increase power transfer capability". The recent stellar developments in semiconductor technology have supported broad usage of FACTS devices, especially in the last two decades. STATic synchronous COMpensator (STATCOM) is the most versatile member of FACTS device that is used for efficient VAR control and voltage compensation [5]. STATCOM is a shunt connected power electronics device with a coupling transformer [6]. When compared to older compensation technologies mentioned above, it includes a relatively smaller capacitor, providing smaller footprint for substation and more reliability. STATCOM is composed of a three-phase four-quadrant converter that has fully controllable (forced commutated) power electronic switches, such as voltage source converter (VSC), gate turn-off (GTO) thyristors or insulated gate bipolar transistor (IGBT). The function of this converter is to generate controllable three-phase AC voltage waveform with minimum harmonic content [7,8]. Earlier, multi-pulse converter topologies had been chosen for the STATCOM technology. Later, multi-level converters have been utilized since they provide more flexible and reliable design. There are two major advantages of multi-level converters. The first one is that they require smaller filter for harmonic elimination at the output. The second one is that they need no large magnetic interfaces as in case of multi-pulse converters, which greatly reduces system size and cost. Cascade H-bridge (CHB) topology is one of the multilevel converter (MLC) topologies and based on the series connection of H-bridges with separate DC capacitors [9,10,11]. This topology is recognized as the most attractive and preferred one for its modularity, redundancy, and simple layout, etc. DC capacitors should be isolated from each other since the output of each H-bridge is connected in series. Controlling the output voltage of VSC, synchronized to system voltage and exchanging the reactive power. The dynamic performance of STATCOM relies on designing proper STATCOM parameters and its controller. There are many STATCOM applications in the world. For example, ±640 MVAR STATCOM application to China Southern grid, known to be the largest application in the world, has been under service since 2011 [10]. In Canada in 2012 on two 10 kW PV-solar systems, the authors have developed "PV-STATCOM" system

was to improve voltage and power factor correction on transmission systems [12]. Another example is from our country, TUBİTAK power electronics research group designed a ±50 MVAR STATCOM for Sincan 154 kV substation and it has been active since 2009 [12,13]. When reviewed in literature, our country needs further development of STATCOM applications. With this respect, this thesis aims to design a low-power prototype single-phase STATCOM, comprised of CHB multilevel converter for dynamic VAR control.

1.2 Aim of the Thesis

In this PhD thesis, a low-power prototype single-phase STATCOM will be designed and implemented. STATCOM will be comprised of multilevel converter having two cascaded full H-bridges. STATCOM should be able to inject or absorb some VAR reactive power to/from single-phase 220V power socket. It is expected to provide some VAR reactive power at full capacitive mode and absorb some VAR reactive power at full inductive mode. A single-phase coupling transformer will be used to isolate and couple the AC side of STATCOM with the grid. The DC voltage controller of the STATCOM will be synchronized with the grid by single-phase phase locked loop (PLL). Optimization of the STATCOM control will be also studied.

1.3 Outline of the Thesis

This thesis is divided into eight chapters:

Chapter 1: In this chapter fully, an overview of thesis objectives will be outlined.

Chapter 2: This chapter examines major previous works related to this work and explains the overall STATCOM.

Chapter 3: This chapter gives a detail of the main multilevel converter topologies and their modulation techniques used for them.

Chapter 4: This chapter gives an overview of STATCOM and its applications as well function in detail.

Chapter 5: This chapter provides the basic control structure for single-phase CHB-STATCOM configurations and explains the proposed controller scheme.

Chapter 6: Simulation results of the proposed CHB based STATCOM is explained in this chapter.

Chapter 7: Experimental results of our proposed CHB based STATCOM is explained in this chapter.

Chapter 8: Summary of the results achieved and plans for future works that could be based on this work are explained in this chapter.

CHAPTER 2

LITERATURE REVIEW

2.1 Introduction

Electrical power systems are backbone of any country's economic and social progress, without which a country cannot excel in the industrial and social development. Electrical power systems' history starts from the day when first electrical system was installed to transmit the energy. Ever since that day power quality and its long-range effective transmission is under research. Operations and control of electrical power became significant as the demand for electricity increases. Many scientists and engineers around the world are working in this field to improve and provide good quality power to the consumer.

2.2 Related Works

FACTS appliances are segregated into two discrete configurations: series connected configuration or shunt connected configuration. When connected in series, FACTS devices perturb the system by introducing reactive characteristics to the system [14].

Earlier VSC provided dynamic and steady-state AC voltage and reactive power flow control. Moreover, VSC injects low harmonic current as compared to the SVC. Also by using VSC we will get higher operational agility and better dynamic response. In practice, current source converter (CSC) topology is not used for STATCOM. The reason for this is related to the higher losses on the DC reactor of CSC compared to the DC capacitor of VSC [15].

Due to the advancement of technology, STATCOM is better than the SVC now. STATCOM have faster response, better characteristics and constant current characteristics when the voltage is lower under the limited value, while the SVC have slower response than STATCOM and the current drops linearly when the voltage

lower under the limited value. Its practical advantage coupled with more research allows STATCOM to replace old SVC based technology. STATCOM is thoroughly applied to power transmission grids, in distribution systems, mainly to enhance the power quality [16]. The article "The future of high power electronics in transmission and distribution power systems" written in 2009 by Davidson and Preville the authors state briefly about the application of ideal implementation that VSC is essential for an effective implementation of STATCOM [17]. Due to limitation of earlier power electronics devices, practical implementation of VSC was infeasible as blocking voltage of older semi-conductor devices was much lower than the blocking voltage required for implementing VSC. Due to this fact, series-connection of static switches was needed which was infeasible [17].

The work in [18], presented a new technique about CHB converter. Although it is a feasible solution for the FACTS devices, the proposed technique has still limitations for its control and design. A lot of research are still being carried on CHB control and modulation. Phase-Shifted Pulse Width Modulation (PS-PWM) shows great application for CHB modulation [19,20,21].

STATCOM control is challenging and thus there are different control methods, such as PI controllers [22, 23], linear quadratic regulator [24], clustered balancing control [25], model predictive controller [26] and nonlinear passivity-based control (PBC) [27].

Benachaiba and Abdelkhlek, acknowledged to the fast development in the power semi-conductor device technology which prepared high-speed as well as electronics devices such as, MCTs, MOSFETs, IGCTS and IGBTs, utilized in active power filters which is abbreviated as (SAPF) [28].

Zhang and Suganthan, studied three separate artificial neural network (ANN) which take the complex power of the STATCOM and predict different outputs. First ANN was used to estimate voltage, and the second one was used to estimate phase angle, while the third one was to estimate the reactive power (VAR) of STATCOM. To generate a data of complex powers of the STATCOM bus, complex powers of all the load buses in the system were perturbed by gradually increasing their values and the corresponding voltages, angles, and reactive powers at the output were recorded [30]. Many research studies have been dedicated to the development of modified models for

the STATCOM such as in [31]. In [8], hardware implementation of CHB converter is described. The authors have used individual voltage balancing strategy to implement the switching circuit. Digital Signal Processor (DSP) is applied as the fundamental controller of STATCOM for generating PWM [9].

2.3 Impact of Task Done

The task of this thesis is to model, experiment, and simulate single-phase CHB-STATCOM for reactive power compensation. The modulation scheme to be used is PS-PWM. The idea of the process is to control the parameters for the good grade output which is done by STATCOM which is able to operate in capacitive and inductive mode. This work is verified thoroughly by extensive simulations and experiments.

CHAPTER 3

MULTILEVEL CONVERTER & MODULATION TECHNIQUES

3.1 Brief Overview

In 1975, the first idea related to MLC was introduced [32]. The MLC consists of power semiconductors and different sources of DC voltage. They are used for the applications which require high power conversion. The main concept of MLC is to produce high voltages for output from multiple low DC voltages. Power rating of each semiconductor device remains near to a shade of output voltage. Different DC voltages give different levels used in generation of output voltage waveform of MLC. Multiple topologies for multilevel converters are present in literature [34, 35]. Based on the topology we selected, the levels of which the converter consists of can be found. Basically, the constant values of voltage generated between the output port and a reference point in a converter will be considered as number of levels in a converter. Voltage steps are equidistant from each other. To consider in a family of MLC, the converter should have three levels (+V, -V, 0V) in each of its phase. The pros and cons of MLC is summarized below;

- MLC generates a voltage having low total harmonic distortion (THD) as well as low rate of change in $\frac{dv}{dt}$.
- Wide range of frequency spectrum for semiconductor devices. This leads to higher efficiency by lower switching losses.
- Voltage stress across power semiconductor devices is minimum as blocking voltage is much lower.
- Grid installation is easy as it guarantees transformer-less installation.

On the other hand, some of the disadvantages of MLC are:

- A lot of semiconductor devices must be used.
- Limit on the achievable levels due to hardware implementation.

Researchers have researched on MLC and its modulation techniques [35, 36]. MLC has caught the attention of many researchers due to its high controllability and higher efficiency. These converters can switch between many levels so that more details can be seen in [37,38].

3.2 Common MLC Topologies

3.2.1 Neutral Point Clamped (NPC) Converter

The Neutral Point Clamped (NPC) converter was first detailed in [39]. The main task of this converter is to provide many levels of voltage using diodes in series to capacitor banks through multiple phases. In the regular NPC topology, switching devices are cooled by using a separate heat sink. The voltage that will be generated at the output side will be half of the voltage given at input side. This is a disadvantage of NPC converter. This problem can be solved by increasing the number of switching devices and DC link capacitors.

A 3-phase and 2-Level of NPC converter is given in Figure 3.1. A 3-phase and 3-Level NPC converter is demonstrated in Figure3.2. Basically, some modification is done to 2-Level converter to make it 3-Level converter, so we can also say that a 3-Level converter is a modified version of 2-Level converter. Two extra power semiconductors are added to each phase of 2-Level converter to make it a 3-Level converter. According to the modified configuration, every switch evaluated at one half the voltage compared to 2-Level converters which have the same DC voltage. Basically, by using semiconductor of the same rating as that of 2-Level converter, the value of voltage can be increased to double of its original value in NPC converter. Also, zero voltage level is generated by NPC converter by acquiring a total of 3-Levels of voltage at the output.

It is practically infeasible to increase the levels of NPC converter beyond 5-Levels [40]. So, for this reason researchers introduce Active Neutral Point Clamped (ANPC) converter as shown in Figure3.3. This configuration is far better than NPC converter in control [41].

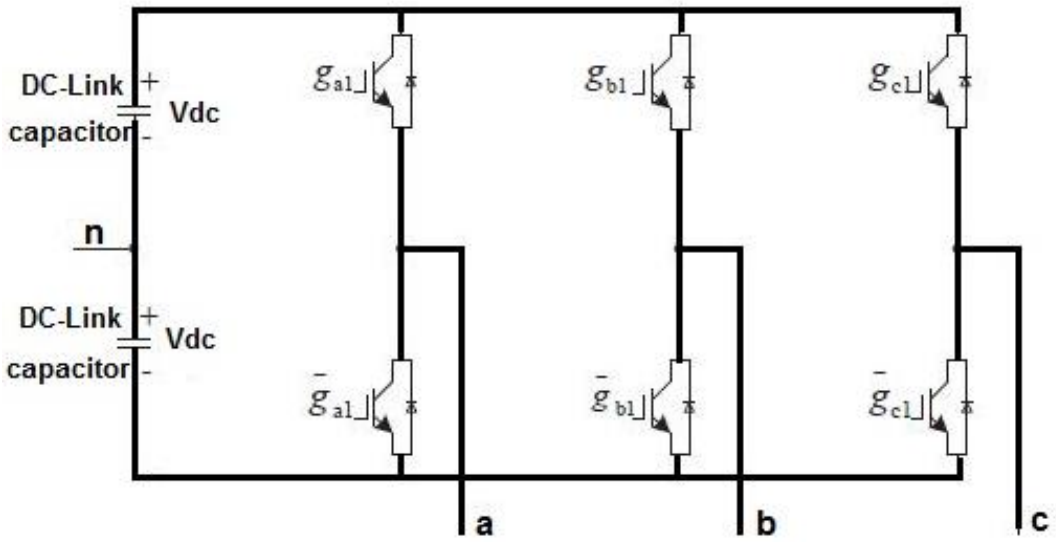

Figure 3.1 Circuit diagram of classic 2-Level converter [22]

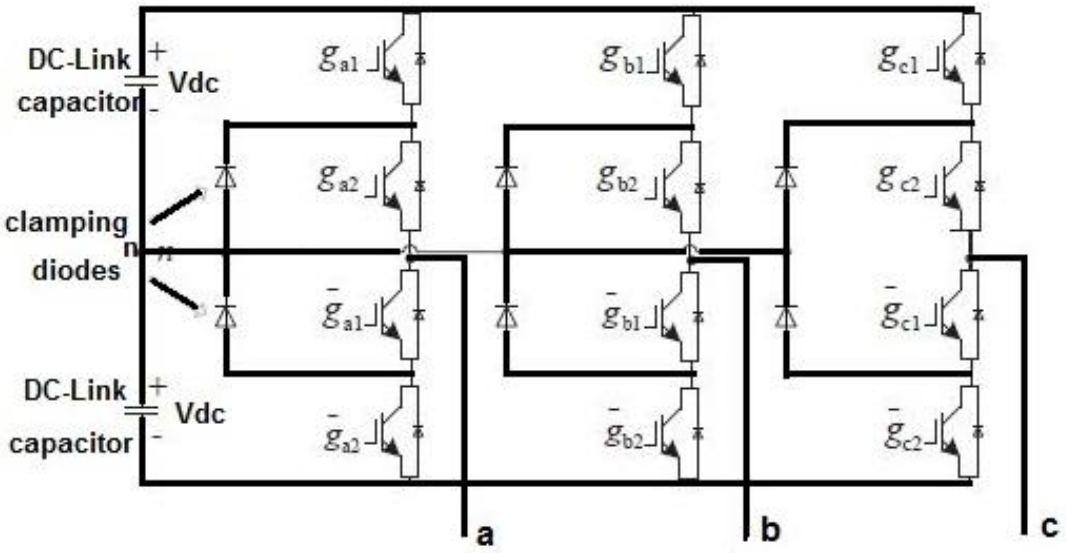

Figure 3.2 Circuit diagram of 3-Level, 3-Phase NPC converter [22]

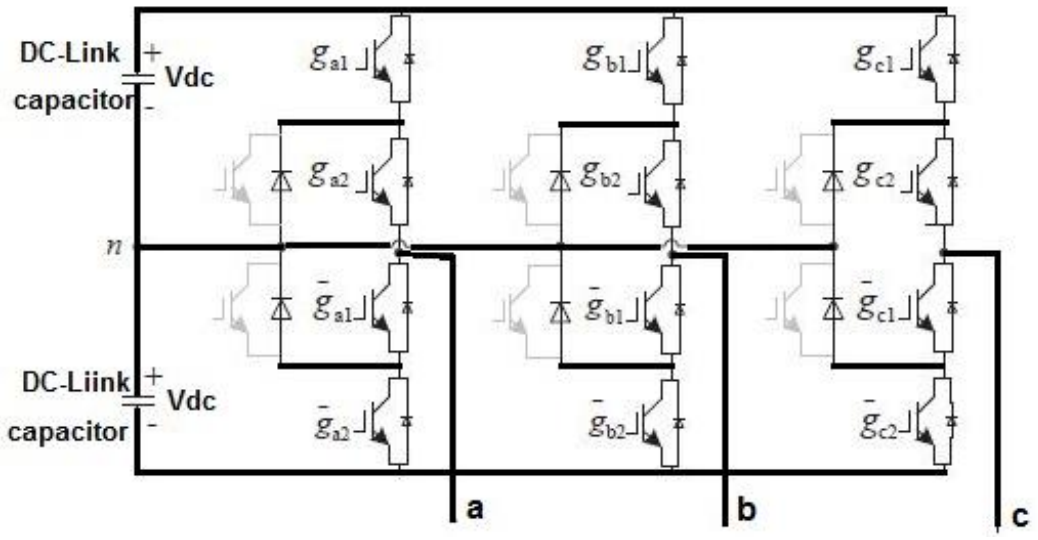

Figure 3.3 Circuit diagram of ANPC converter [22]

3.2.2 Capacitor Clamped Converter

The Capacitor Clamped Converter (CCC) is also called "Flying Capacitors Multilevel Inverter". The idea was initially incepted by Maynard et al., in the year 1992 [43]. The main idea given in this type of converter is the usage of capacitors. It consists of Capacitor Clamped switching cells (pair of power semiconductor devices together with one capacitor) which are connected in series. It is the ability of capacitors to transfer small quantity of voltage to the electrical devices. The switching states in CCC are like those present in NPC converter. Instead of clamping diodes which are used in NPC, clamping capacitors are used in this kind of MLC. Output of this MLC will be one half of the DC voltage given as input which is a disadvantage of the CCC. The CCC has the ability of switching redundancy in phase for the balancing of the capacitors. Both active as well as reactive flow of power can be controlled by CCC. One side effect can also occur and that is the switching losses and it can occur because of high frequency switching.

A 3-Level 3-Phase CCC is demonstrated in Figure 3.4, working as an alternator which provides a way to mitigate the drawbacks of NPC converter. The main difference between them is the method of clamping. The output voltage levels of the CCC are generated by adding or subtracting the clamping capacitor voltage with the DC bus voltage.

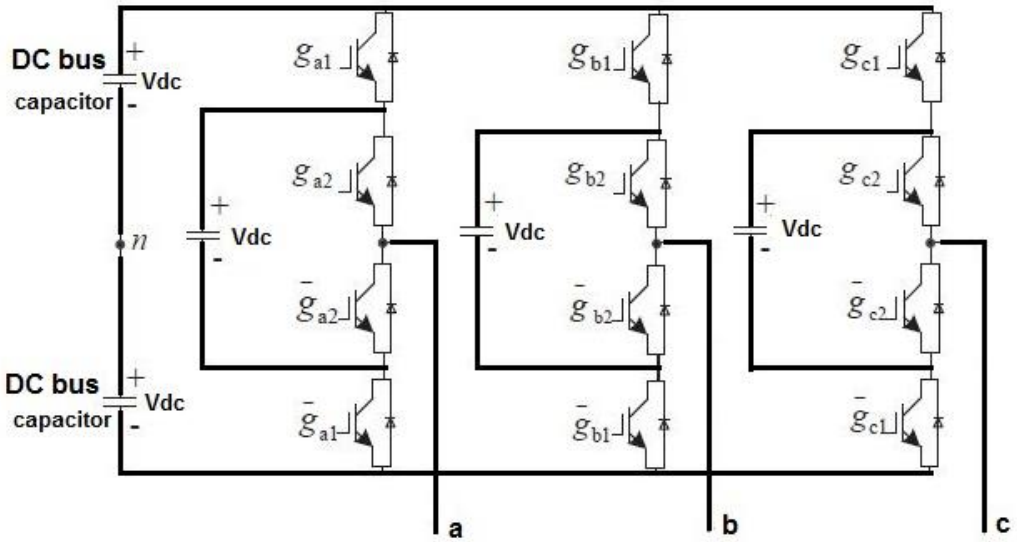

Figure 3.4 Three phase 3-Level CCC [22]

With the addition or subtraction of voltage of clamping capacitor and DC bus voltage, the voltage levels of output of CCC are generated. CCC can produce identical voltage levels for various switching states. This phenomenon can be referred as voltage redundancy. Redundancy is crucial for capacitor charge balance in CCC [33,44].

In this topology, number of capacitors depends upon number of voltage levels. This can be identified by redrawing the CCC as in Figure 3.5.

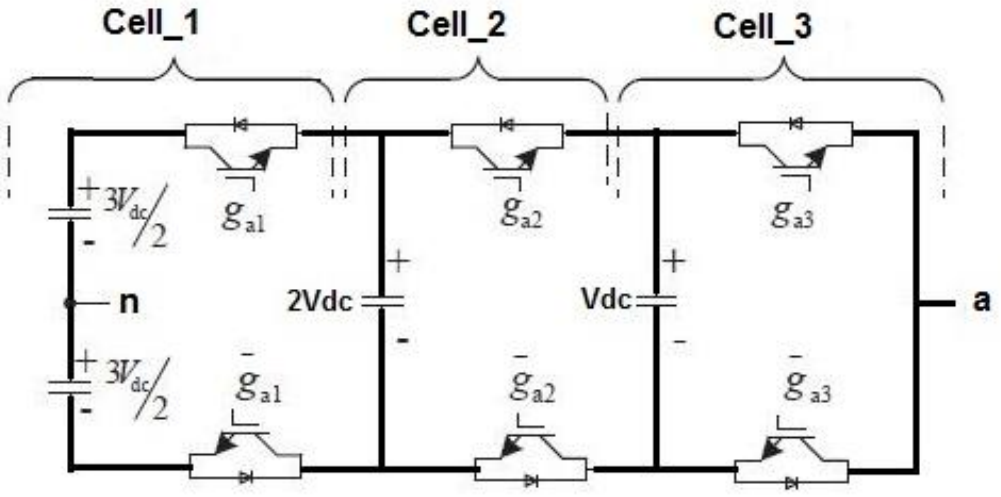

Figure 3.5 Single-phase 4-Level CCC [22]

3.2.3 Cascaded H-bridge (CHB) Converter

The concept of Cascaded H-Bridge (CHB) is one of fundamental multi-level topology. Also, in every level, small numbers of capacitors and switches are required. In this type of topology, with connected this cell in cascaded form, the first cell generates three levels as each other cell adds two more levels. The cell is referred to as H-bridge. The term "H-Bridge" is defined as the combination of capacitors and power semiconductor which generate a full-bridge. The CHB converter consists of a number of H-bridge cells and each cell has the ability to provide three different voltage levels like zero, positive DC and negative DC voltages [45].

It has multiple advantages and one of them is that it requires less number of components than NPC converter and CC converter. One more good thing about it is that its price and weight are less than NPC and CC converters. Soft-switching can also be possible by using some of recent switching methods [45].

Due to increase in demand of medium to high VSCs, the CHB converters gained a lot of attention. It consists of multiple units of single-phase H-bridge power cells, which are connected in cascade on the AC side for achieving the operation of medium voltage and generates less harmonic distortion. Isolated DC supplies are required for CHB converter operation. The constructs of CHB is limited only an odd number of levels. The use of identical power cells provides generation of multiple levels of voltage which will further cause in reduction of number of components which are used for topology.

Figure 3.6 shows the circuit diagram of single-phase 7-Level CHB converter, which consists of three identical H-bridges. The first H-bridge cell generates three levels as each other cell adds four more levels. Generally, CHB is very modular and thus easily scalable to higher levels. Each cell has low cost, desirable reliability and a highly reasonably, which affects the quality of the whole product [46].

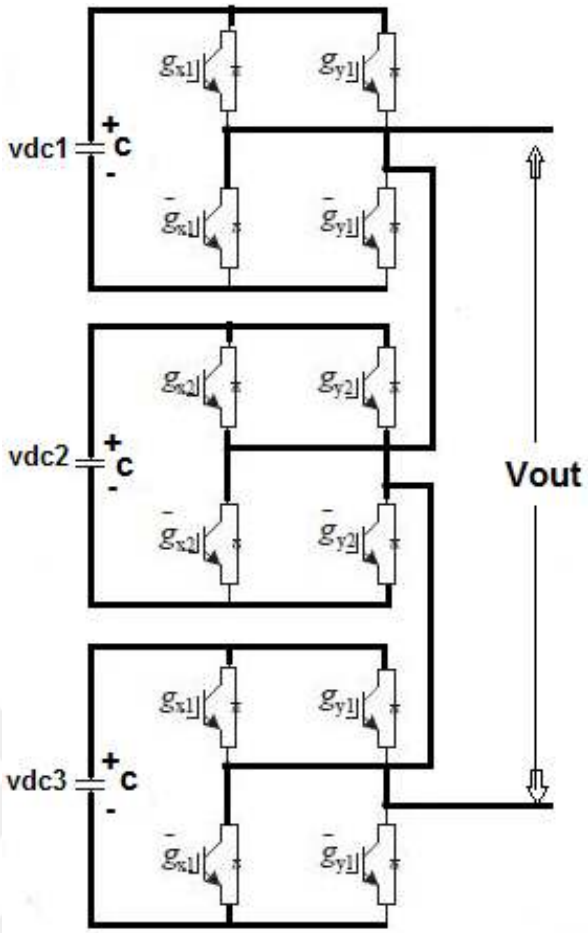

Figure 3.6 Circuit diagram of single-phase 7-Level CHB converter [45]

3.2.3.1 Asymmetric CHB Topology

This type of topology is almost like CHB topology, which is introduced in [47]. The difference is that this topology uses different values of isolated DC sources. The asymmetry generates different levels of voltage. With the use of different DC voltage values, multiple useless states are avoided occurring in conventional CHB converter topology.

This topology has a major drawback and that is related to the design of each power cell. Also it has cost effective due to cells having different ratings of power.

The harmonic cancelation of input current is difficult to achieve in this type of topology as we did in case of CHB converter topology [47]. Another drawback of this type of topology is unequal power losses and heat distribution between different power rated cells [48]. Figure 3.7 shows the circuit diagram of a single-phase CHB converter with asymmetrical (unequal) DC sources.

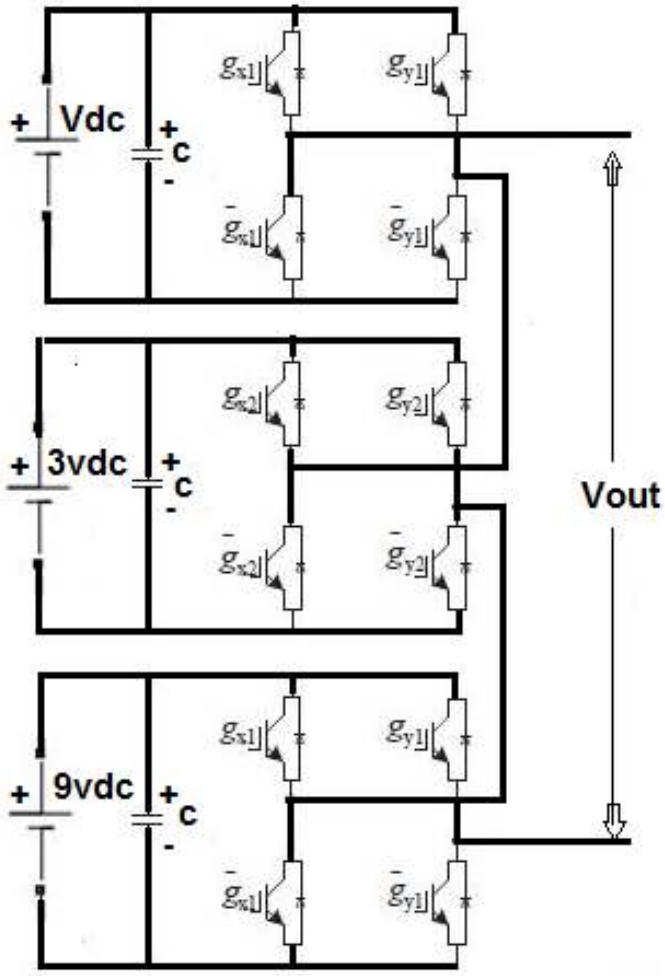

Figure 3.7 Circuit diagram of single-phase asymmetrical CHB converter [34]

3.2.3.2 CHB Converter Topology with Single DC Source

Conventional CHB converter topology uses multiple DC sources. But in case of this topology, only one DC source is utilized. The main concept here is to interface only one DC source in which the capacitors act as other DC sources. In other words, this type of converter exchanges all but the DC sources with capacitors which requires a complex control technique to keep the DC voltage levels intact [49,50]. The circuit diagram of a 7-Level CHB converter topology with a single DC source is demonstrated in Figure 3.8.

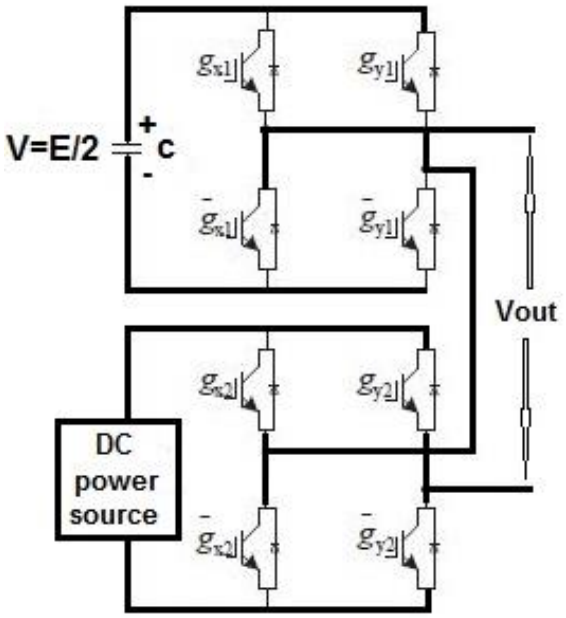

Figure 3.8 Circuit diagram of 7-Level CHB converter with one DC source [38]

3.3 Comparison of Different MLC Topologies for STATCOM Application

Common MLC topologies used in STATCOM are: CHB, CCC, and NPC converter topologies [51]. The n is referred as the number of levels. The comparison of each topology is tabulated in Table 3.1.

Main drawback in the STATCOM is that, it is connect to the grid with the help of a transformer. So now a day's research is being carried out to remove this transformer and make a STATCOM that can be applied directly to grid without using any transformer [52].

Table 3.1 Comparison of different MLC topologies for STATCOM application [22]

Structure	**NPC**	**CCC**	**CHB**
Switches per phase	$2(n-1)$	$2(n-1)$	$2(n-1)$
(Converter with n-level)			
Clamping diodes per phase	$(n-1)*(n-2)$	0	0
(Converter with n-level)			
Capacitors per phase	$(n-1)$	$\frac{(n-1)*(n-2)}{2}$ $+(n-1)$	$\frac{(n-1)}{2}$
(Converter with n-level)			
Loss distribution	Uniform with Active NPC	Uniform	Uniform
Maximum practical levels	3-5	5-7	None in theory
Availability	Low	Low	High
Modularity	No	No	Yes
Capacitor sizing	Low	High	High
Common DC source	Yes	Yes	No
Low switching	Capable	Capable with large capacitors	Capable with large capacitors

3.4 Other Multilevel Converter Topologies

MLC concept was introduced in 1970s. However, new concepts of multilevel topologies have emerged in recent years. The basic MLC topologies are already explained in section 3.3. Many other topologies are derived from these basic topologies by combining of them. Some of these derived topologies are application specific such as 5-Level HB-NPC converter, 3-Level active NPC converter, and Transistor CC (TCC) converter. The classification of major MLC topologies are presented in Figure 3.9 [53].

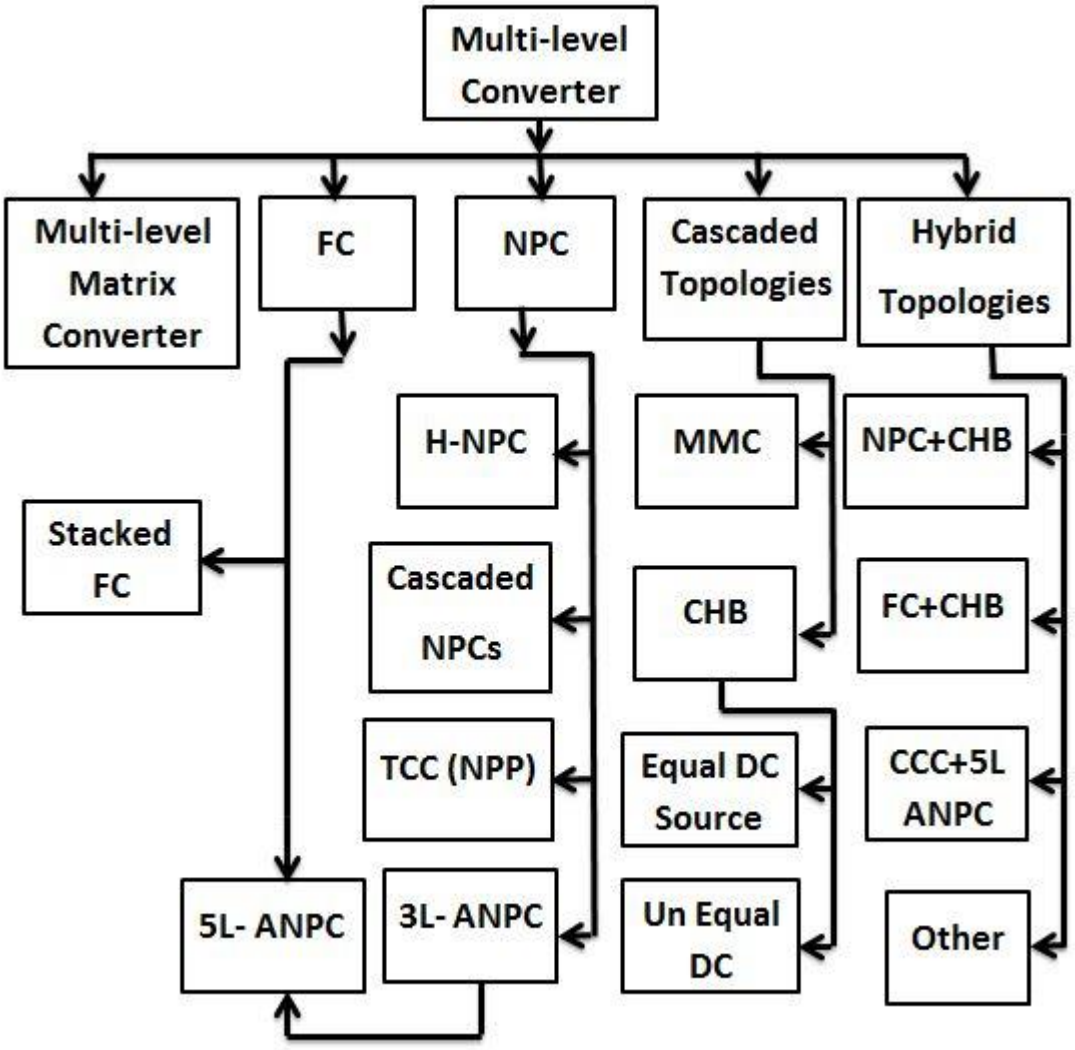

Figure 3.9 The classification of major MLC topologies [53]

3.5 Multilevel Converter Modulation Techniques

Modulation techniques are a vital part of converter control. By the use of modulation, we can control the switching instants of power semiconductor devices. Most of the modulation techniques for MLCs are summarized in Figure 3.10. Each of these modulation techniques is developed by compromising some features of converters [31,54]. These features include switching loss, distribution of switching loss, THD. These modulation techniques are explained in detail in the next subsections.

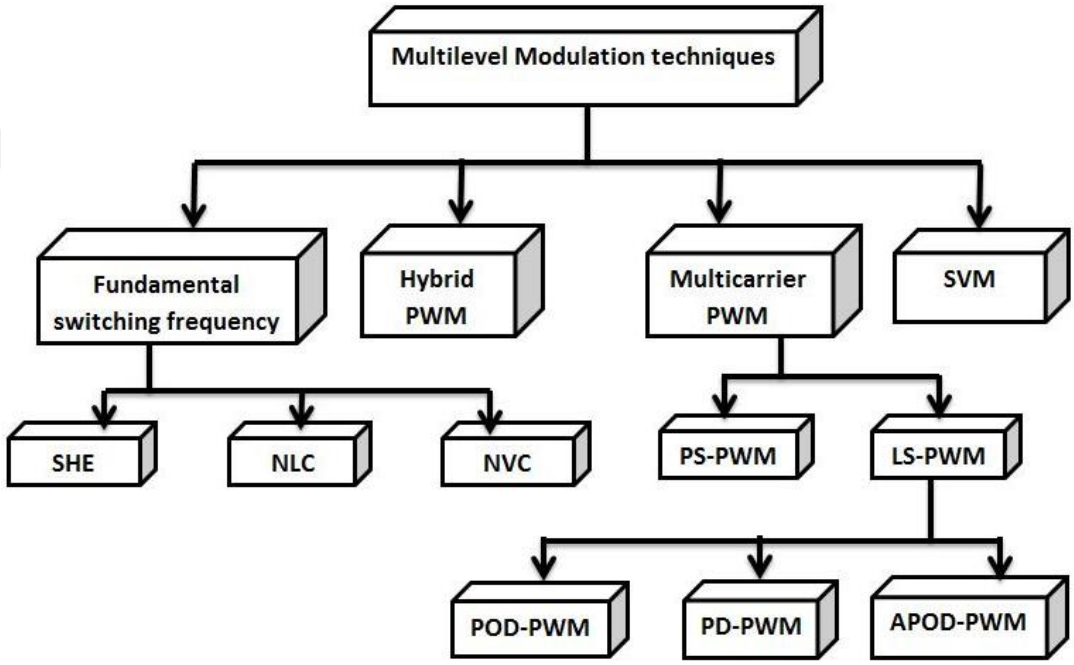

Figure 3.10 Major MLC modulation techniques [22]

3.5.1 Multicarrier PWM

There are two categories of multicarrier PWM

- Phase Shifted PWM (PS-PWM)
- Level Shifted PWM (LS-PWM)

3.5.1.1 PS-PWM

It is a commonly used technique for MLCs. Figure 3.11 demonstrates the implementation of the PS-PWM whereas Figure 3.12 demonstrates the principle of

operation of PS-PWM for single-phase 5-Level CHB configuration. By comparing reference and the carrier signal, every cell is independently modulated [54]. The reference signal is a uniform duty cycle signal while the carrier signal is a variable duty cycle signal. Reference signal is same for each cell but a shift in phase is established among the carrier signal, the phase shifts between carriers are $\frac{360^{\circ}}{n}$,where n is the number of cells [54].

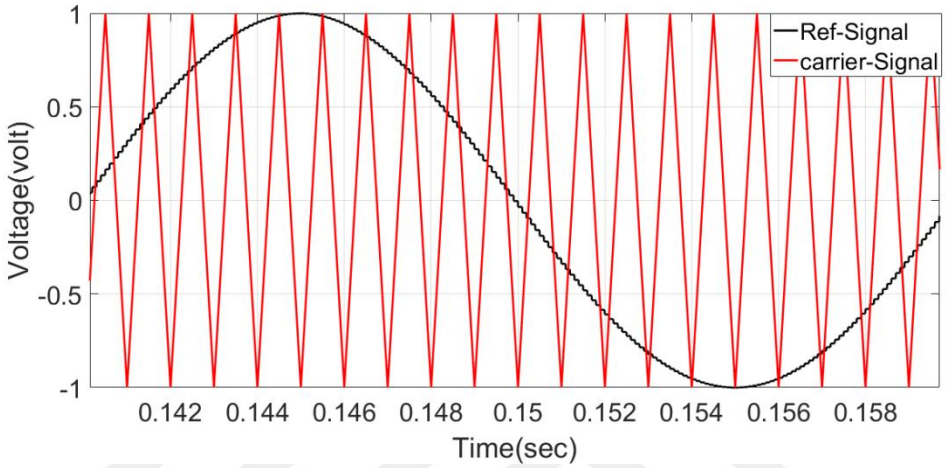

Figure 3.11 Reference single with carrier for PS-PWM

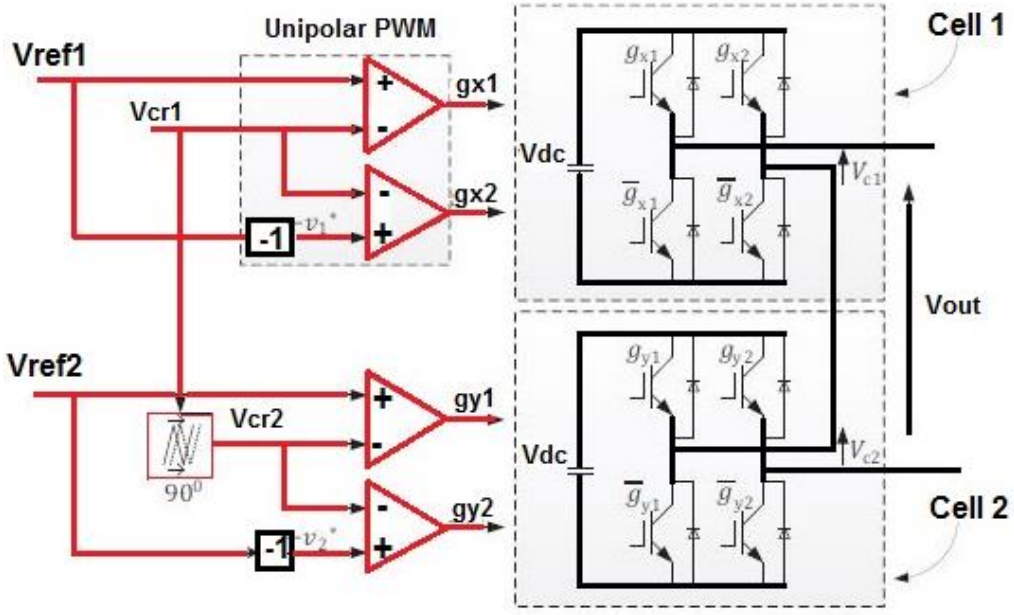

Figure 3.12 Circuit diagram of PS-PWM for single-phase 5-Level CHB configuration [22]

Active power is evenly divided between all cells because the carrier frequency and the modulation signals are same for every cell [33]. In STATCOM applications, this technique can be beneficial as once the capacitors of DC link are charged then no misbalancing will occur that reduces the THD.

3.5.1.2 LS-PWM

LS-PWM is an extension of bipolar PWM techniques. In bipolar PWM, a comparison is done between carrier signal and reference to take a decision among different levels of voltage. In this technique, the positive and negative level of switching signal comes from comparison of reference and carrier signal, if the reference voltage value at any instant is greater than carrier signal then it will give positive level and vice-versa. The operation principle and circuit diagram of LS_PWM for 1-phase are illustrated in Figure 3.13 and Figure 3.14, respectively [55,56].

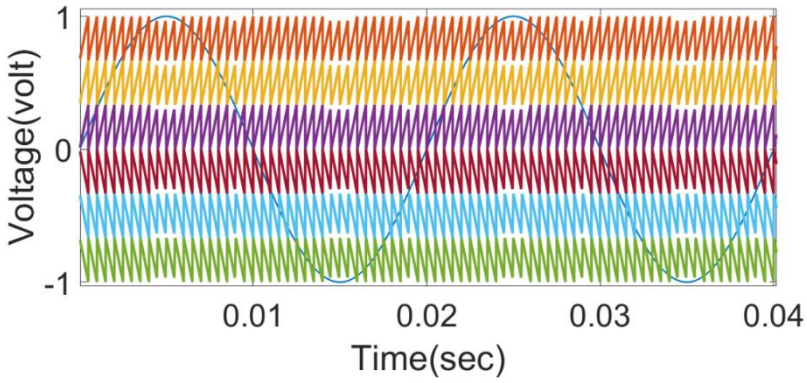

Figure 3.13 Reference single with multi-carrier for LS-PWM

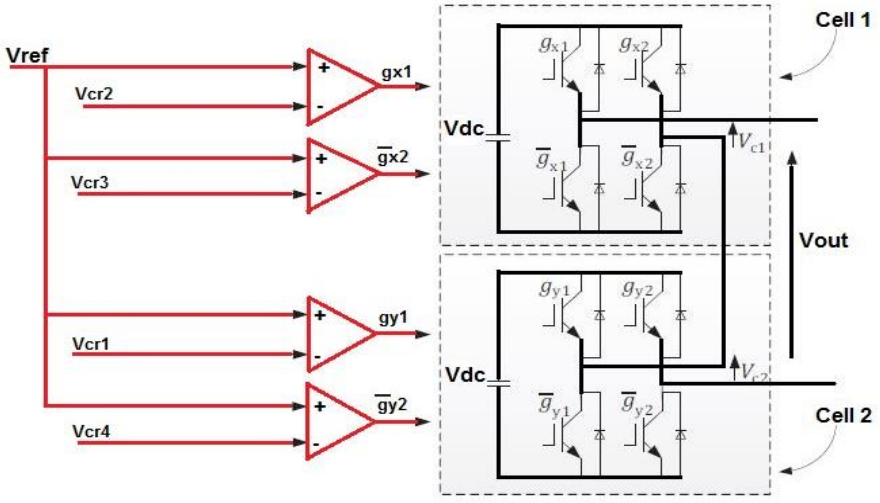

Figure 3.14 Circuit diagram of PS-PWM for single-phase 5-Level CHB configuration [22]

3.5.2 Space Vector Modulation (SVM)

In SVM, the levels of switching signal are determined using a space vector. Carrier signal follows the space vector and determines its level. First, all the switching states as well as their corresponding space vectors are converted to αβ frame. In Figure 3.15 (a), we can see the + and - signs in parentheses to show which switch in each phase is on. For example, (−, +, +) shows that in phase a lower switch and in the other two phases upper switches are on. Then the next step is to determine the reference voltage of state vector in αβ frame. After that the third step is the determination of nearest switching combination. Its operation is explained in [57,58].

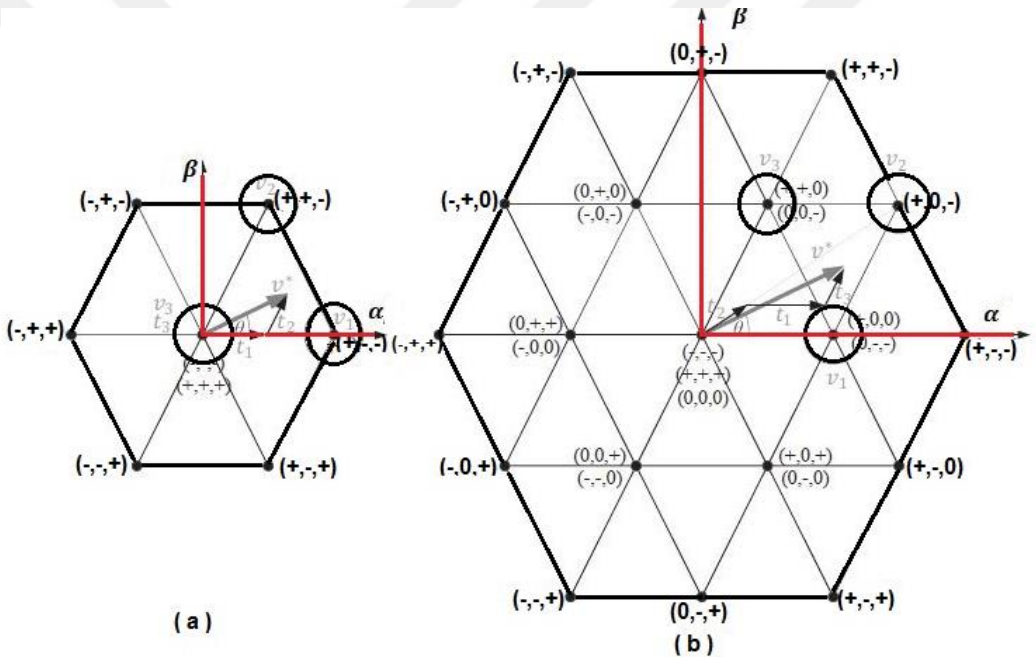

Figure 3.15 SVM principle; (a) Traditional two-level converter; (b) Three-level configuration [57]

3.5.3 Fundamental Switching Modulators

3.5.3.1 Selective Harmonic Elimination (SHE)

In SHE, we calculate the switching angle by using Fourier analysis to eliminate the low harmonics. In the first step, the Fourier series of multilevel waveform which is comprised of unknown switching angles will be determined. In the next step, the

undesired coefficient of Fourier series is set to value of zero whereas the component which is fundamental one is set to the reference value [49, 55].

3.5.3.2 Nearest Vector Control (NVC)

NVC, also called SVC (State Vector Control) is an alternative to SHE. It can generate low switching frequency. Its operation is detailed in [49,58]. The main concept is to make the reference voltage closest to the voltage vector which can be applicable to the ab frame. Voltage vectors generated by the converter are represented by dots which can be seen in the Figure 3.16, shown below. Vector is generated by the converter closest to where the reference voltage exists into the corresponding hexagon. Drawback of SVC is that it doesn't remove the low order harmonics but it can be overcome by using multilevel inverters.

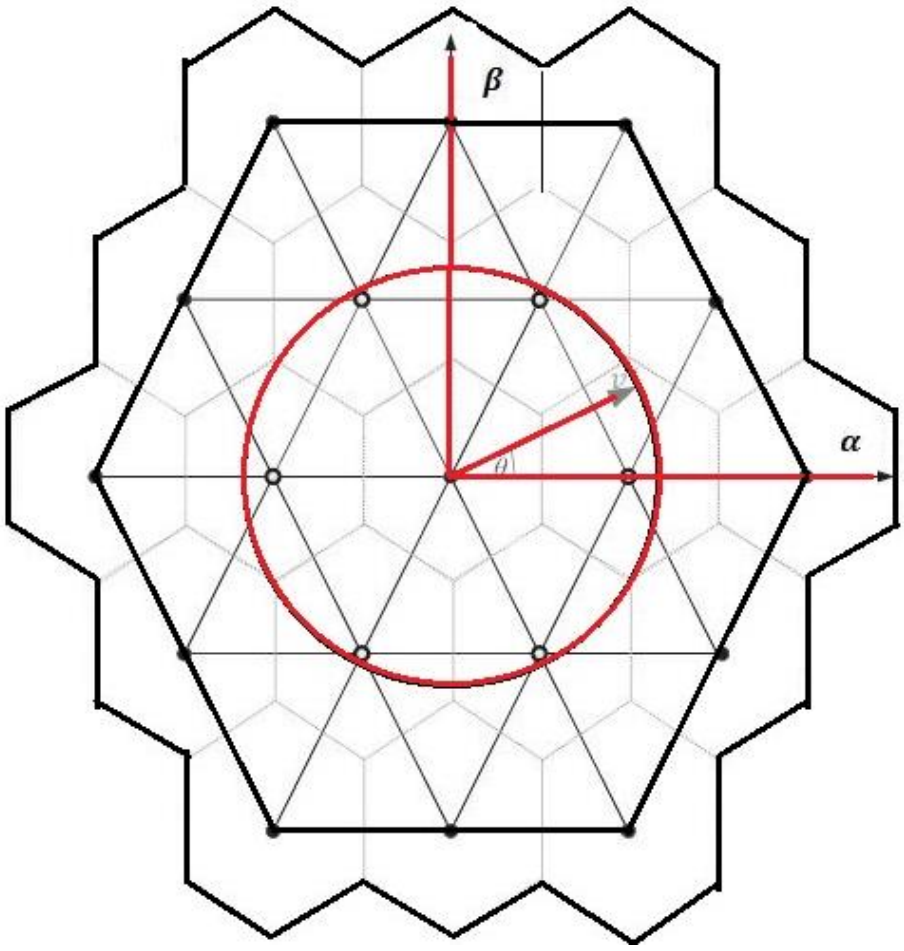

Figure 3.16 All the possible voltage vector for a three-level configuration and their corresponding hexagon [55]

3.5.3.3 Nearest Level Control (NLC)

This technique is counterpart to NVC. Main difference between each other is that NLC gives switching per phase whereas NVC cannot support this. Its operation is detailed in [58]. In NLC, the voltage level closest to the reference voltage is selected and there is also freedom to control all three phases independently. It is much simplified as compare to NVC as it is easy to find the nearest voltage level than finding nearest voltage reference. Also, NLC is recommended for high level converters. Between the three modulation techniques briefly described in the above subsection, SHE is the best as MLC operating on SHE will generate the output which will have less THD and with a high number of voltage levels [49].

3.5.4 Hybrid PWM (H-PWM)

This scheme extends PWM for hybrid/asymmetric arrangement. The basic concept of this modulation scheme is the reduction of switching losses and improvement of the efficiency of the converter by decreasing the switching frequency of high power cells. For performing this scheme, low power cells are operated by unipolar PWM and high power cells are controlled by fundamental switching frequency. The detailed description of H-PWM technique is given in [49,58].

CHAPTER 4

OVERVIEW OF STATCOM

4.1 Introduction of Power Quality

The power, in conventional terms, is defined as the flow of energy per time. The electrical energy is one of the basic requirements in almost every field of life, whether it is home or it is office. Day by day the technical advancements are making the impact on this world. Almost in every field, there is interference of automation, robots, and industries. To fulfill the input requirements for these, we need a good quality power. There are some factors which can affect the power quality of electrical power systems e.g. the variable loads, faults in lines, and etc... These situations are very critical if they last longer, even in seconds. If oscillations in the power systems are not damped effectively then the results can create an increase in the magnitude of these oscillations, which can destabilize the system and can be very harmful. Power quality defines the performance of the electric devices [58]. The electric power industry consists of the following processes: Generation of AC electrical power, transmission of generated electricity and finally the process of distributing this electricity to consumers. Stability of the electrical power systems is one of the big concerns for the operation and control of the electrical power systems. Researchers of people around the world are working in this field to improve and provide good quality power to the consumer systems [59].

4.1.1 Impact of Power Quality Problem

Poor quality of power can cause malfunction of electric devices or could completely damage them. There are many reasons in which electric power can be of poor quality. Some of the most common power quality problems and their likely effect on sensitive equipment are as follows.

4.1.1.1 Voltage Dips

Voltage sags or voltage dips are the loss in the voltage magnitude followed by a voltage recovery for a short period of time [60]. One of the major reasons behind this uncertain dip in the voltage supply to the consuming device is due to faulty and defected system [60]. Spikes in voltage magnitudes can occur when the capacitors are energized or if the inductive load is disconnected. Voltage spikes are the instantaneous rise in the voltage magnitude. A voltage surge or the voltage spike occurs when the voltage is almost 110% or more above normal level of voltage. These spikes are dangerous for electric appliances as they can severely damage them [61]. Voltage swell is defined as an increase of the voltage for few seconds at the power frequency, outside the normal tolerances, with duration of more than one cycle. Badly dimensioned power sources or badly regulated transformers can give rise to this problem. This could cause severe damage to devices and appliances [63]. This decrease in the system voltage can cause serious damages to the electric devices. Major reason of voltage sag is the system faults and also due to high demand startup currents while switching on loads. To solve these problems there are devices available in markets such as voltage regulators, uninterruptable power supplies, and power conditioners [62].

4.1.1.2 Frequency Variation

A slight variation in the frequency normally stable at 50 or 60 Hz can cause damage to electric devices. For sensitive equipment, the changes in frequency can lead to in program failure or complete shutdown of the appliance. To solve these problems there, are devices available in markets such as voltage regulators and power conditioners [63].

4.1.1.3 Harmonic Distortion

The waveforms of current and voltages are basically the sum of different sine waves with different magnitude and phase, having frequencies that are multiples of power system frequency. The deviations and distortions in the sinusoidal waveforms of the voltage and current are mostly caused by rectifiers or non-linear loads, and can lead to overload in three-phase systems, overheating of all cables and equipment, and loss of efficiency [63].

4.1.2 Power Quality Solution

Several types of power enhancement devices have been developed over the years to protect equipment from power disturbances. A simple traditional technique is to insert fixed capacitor/inductor [47,60]. For the nominal heavy load, the capacitor is inserted to inject the reactive power to improve the voltage profile at the load buses. For the light load, the inductor is used to absorb the reactive power to limit the voltage rise within the allowable regulation value. Usually, the capacitor/inductor is inserted in the system via a mechanical switch. The compensation of reactive power from the fixed compensator is varied with the square of the voltage at the point common coupling (PCC).

These simple compensations suffer from limitations, such as these techniques cannot provide the instantaneous response for load reactive power requirements, the ability of compensation is limited, and the value of fixed compensator capacitor/inductor resonates with transmission line parameters.

FACTS devices are the recent advances in power electronics, FACTS use solid-state switching devices and modern control algorithms to increase controllability and enhance power transfer capacity of existing transmission network. FACTS have gained greater interest during the last decades due to the deregulation and restructuring strategies of power systems. FACTS devices can be classified, depending on the switching properties of the power semiconductor devices and depending on the connection type to the power network, as mentioned in the next section.

FACTS gain more advantages than rotating reactive power compensators and fixed reactive elements, such as:

- High efficiency.
- Relatively fast response when compared with synchronous condenser.
- Adaptive operation. FACTS could provide continuous compensation compared with fixed reactive elements. FACTS could act as source/sink for the reactive power according to the control strategy.
- Automation. FACTS are mainly using solid-state devices so that they could be controlled by microprocessor or microcontroller.

4.2 Classification of FACTS Devices

The FACTS technology is related to the management of active power and reactive power for improvement in performance of the electrical networks. Discussion on the improvement of the quality of AC power system in previous sections leads to the point of maintaining economic and secure operation of large interconnected systems. Therefore, different types of FACTS devices can perform fast dynamic control of both real and reactive power [64].

There are two generations of FACTS devices based on the switching properties of the power semiconductor devices:

- 1^{st} generation FACTS devices with slow response times using thyristor.
- 2^{nd} generation FACTS devices with faster response times using forced-commutated power semiconductor.

The 2^{nd} generation FACTS devices have two fundamental advantages over 1^{st} generation FACTS devices:

- Use of converter instead of capacitor or reactor to generate or absorb reactive power.
- Separate and independent management of real and reactive power.

Based on the number of converters being utilized, 2^{nd} generation FACTS devices can be categorized into two main categories: single-converter FACTS devices and multi-converter FACTS devices.

Also, there are five categories of FACTS devices based on the connection type to power network:

- Shunt FACTS devices
- Series FACTS devices
- Combined Shunt-Shunt FACTS devices
- Combined Shunt-Series FACTS devices
- Combined Series-Series FACTS devices

4.2.1 Static Synchronous Compensator (STATCOM)

STATCOM is the recent replacement of SVC. It remedies the limitations of the traditional SVC. STATCOM generally utilizes high sufficient frequencies such that STATCOM produces quality output voltage and current. The main objective of the STATCOM is to supply or absorb the instantaneous reactive power to/from system at PCC. STATCOM has many advantages over SVC that STATCOM has faster response, being modular, and it can be interfaced with energy storage units, reducing system harmonics and power loss, and requires less space [67,68]. The basic STATCOM configuration is shown in Figure 4.1.

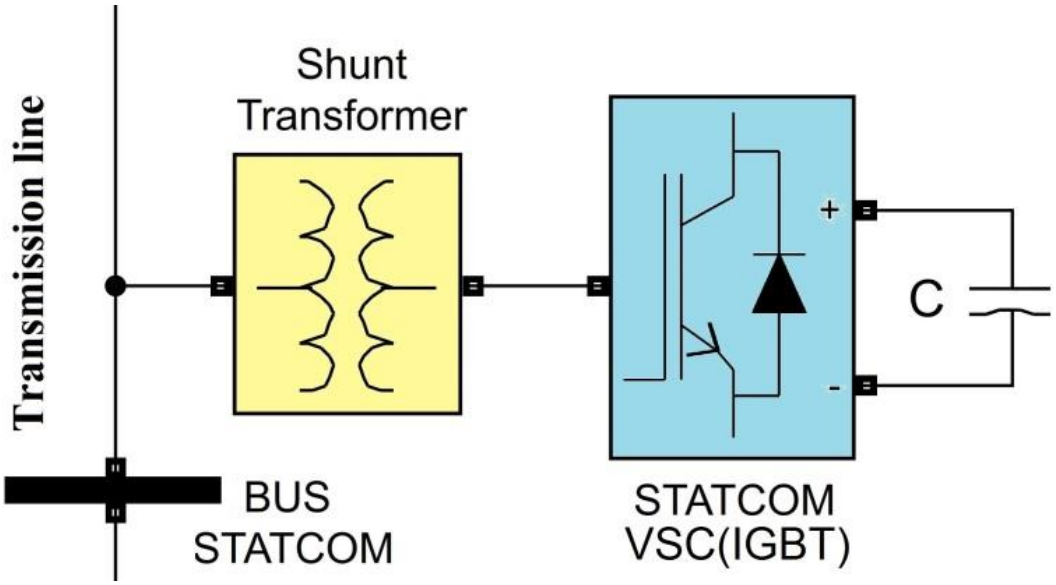

Figure 4.1 Basic STATCOM configuration [65]

4.2.2 Static Series Synchronous Compensator (SSSC)

The SSSC is connected in series to the transmission line as shown in Figure 4.2. SSSC produces a three-phase voltage whose phase angle is perpendicular to the line current that can be dynamically adjusted. With SSSC, it is possible to control active/reactive power flow on the transmission line [65].

SSSC can be regarded as a dynamic series capacitor or reactor. The magnitude and phase angle of output voltage of VSC can be controlled by changing modulation index of the VSC. in another meaning, If the VSC output voltage is 90 degrees lagging the current, SSSC provides capacitive reactive power to reduce line reactance. On the other hand, if the VSC output voltage is 90 degrees leading the current, SSSC provides

inductive reactive power to increase the line reactance. In this way, SSSC can control power flow from the transmission line to the device or vice versa [67]. SSSC is superior to other FACTS equipment and the benefits of using SSSC are [69]:

- Elimination of the bulky passive components such as reactors and capacitors.
- Technical characteristics include symmetric capability in both inductive and capacitive operation mode.

There is also a possibility of the connection of the energy source on DC side to exchange the real power with the AC network.

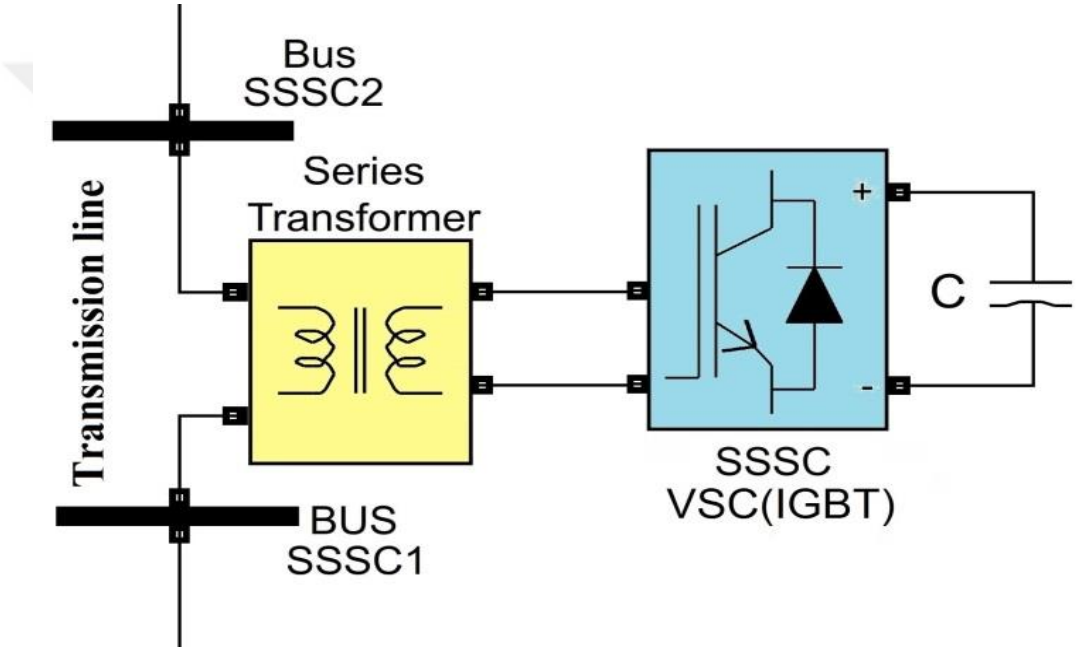

Figure 4.2 SSSC configuration [65]

4.2.3 Unified Power Flow Controller (UPFC)

A unified power flow controller (UPFC) is a FACTS device which provides series compensation, as well as independent real and reactive power flow control on the high voltage transmission system. It uses a pair of three-phase controllable VSCs, coupled through a common DC link to allow bi-directional real power flow. Main components of UPFC include two VSCs, which share a common DC capacitor and it is connected to power system through the coupling transformers. One VSC is connected in series through a series transformer and the other one is connected in shunt through shunt transformer to the transmission system. The DC terminals of both VSCs are coupled which creates a path for the active power exchange between VSCs. The active power

supplied to line by series converter can also be supplied by the shunt converter which is demonstrated in Figure 4.3 [70]. Thus, different range of the control options is also available as compared to the STATCOM or the SSSC. The capability of real power exchange enables multifunctional flexibility so that the series voltage generated by the series VSC can be injected into the transmission line with controllable magnitude and phase angle. The shunt converter is regulated in such a way to demand the DC terminal power (+ve or -ve) from line keeping the voltage across storage capacitor constant. The remaining capacity of shunt converter can also be used for the exchange of the reactive power with line to provide the voltage regulation at PCC connection. By separating the DC side, both VSCs can work in independent way. In that scenario, shunt converter is operating as STATCOM which regulates the voltage magnitude, while on the other side, the series converter is operating as a SSSC, regulating the current flow. The UPFC has multiple modes of operation: phase angle shifter emulation mode, automatic voltage control mode, line impedance emulation mode, direct voltage injection mode, and automatic power flow control mode [65].

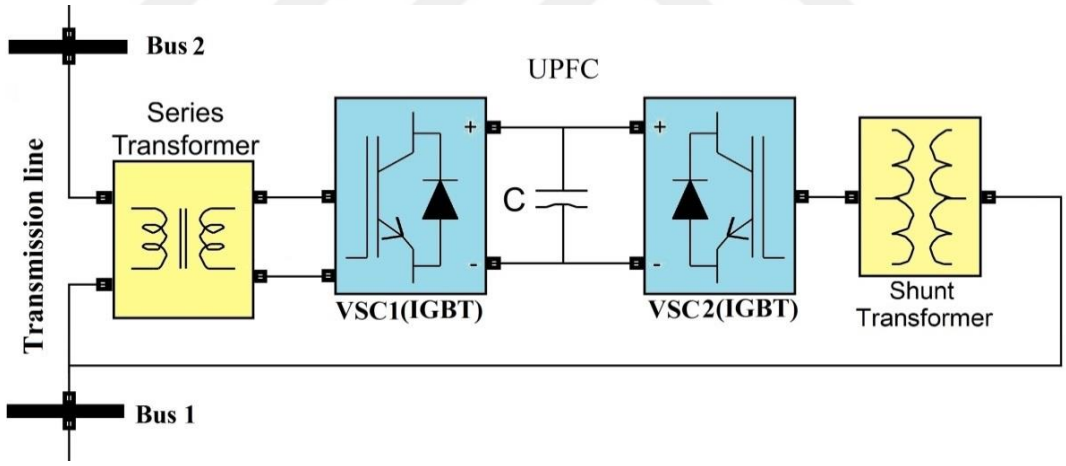

Figure 4.3 UPFC configuration [65]

4.2.4 Interline Power Flow Controller (IPFC)

IPFC is formed by the combination of a number of VSCs in series with a common DC link having series coupling transformer which is connected to the transmission line [71]. Basic configuration of IPFC consists of two VSCs. One of the VSC is used for flexible compensation for allowing independent control of active and reactive power. In addition to that, IPFC can act as a virtual transmission line so that an overloaded

line can be relieved by forwarding real power flow to the under loaded line. The simplest IPFC configuration having two VSCs is shown in Figure 4.4.

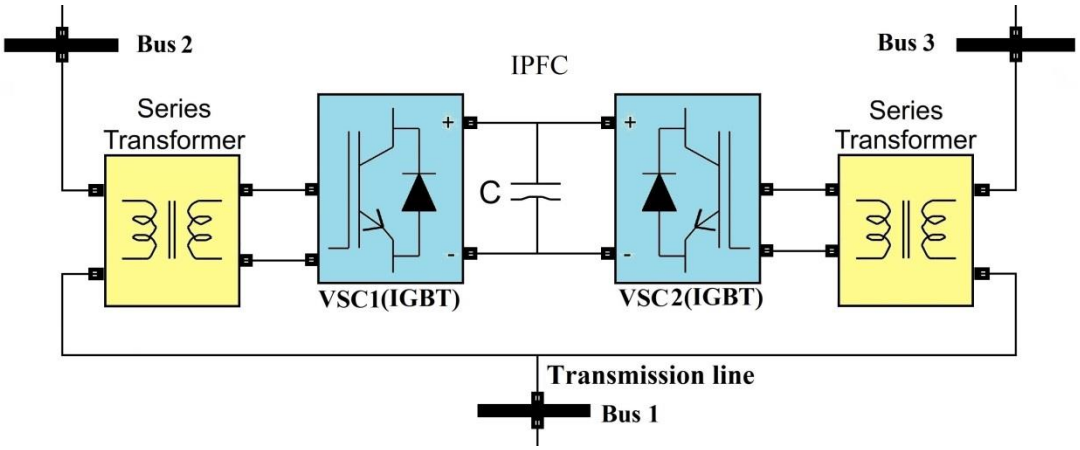

Figure 4.4 IPFC configuration [65]

4.3 STATCOM

A STATCOM is a VSC based FACTS device with the VSC behind a reactor. The VSC is created from the DC capacitor and therefore a STATCOM has a very little active power capability. This can be increased if a suitable energy storage device is connected across the DC capacitor. The reactive power of STATCOM is related with the amplitude of voltage source. For example, if the voltage at terminal of VSC is higher than AC voltage at PCC, STATCOM injects reactive power. However, when amplitude at terminal voltage of VSC source is lower than PCC, the STATCOM absorbs the reactive power from AC grid side. The response time of the STATCOM is smaller than that of a SVC, mainly due to fast switching times provided by forced commutated power semiconductors of VSC [72]. STATCOM also provides better reactive power support at the low AC voltages as compared to SVC. Since reactive power from the STATCOM decreases in a linear way with AC voltage (as current can be maintained at rated value even under AC voltage) [68].

4.3.1 History of STATCOM

It is a FACTS device of power industry which was first introduced in 1980s by Kansai Electric Power Co., Inc. (KEPCO) and Mitsubishi Motors [72]. Then in October 1986, a ±l MVAR STATCOM was put into operation. It was primitive in design that so much research was required. In 1997, Siemens installed an 8 MVA STATCOM which was

complex than STATCOMS introduced earlier. In 2001, a 175 MVAR STATCOM was developed by ALSTOM, the first cascade multilevel-inverter-based STATCOM in the world, entered commercial service at NGC (National Grid Company) East Claydon, England [72]. In the end of December 2003, two halves of STATCOM, each rated ±75 MVAR, was under development by Alstom for Northeast Utilities' Glenbrook substation. ABB has installed six STATCOM (also named SVC Light) since 1997, ABB has won a US$ 14 million order from Austin Energy, Austin, Texas, to design, manufacture and install another STATCOM based on SVC Light technologies at Pedemales Substation by October 2004. However, more research was required in the control and modulation of STATCOM [72].

4.3.2 Operating Principles of a VSC-based STATCOM

STATCOM is a shunt connected reactive power compensator. The STATCOM function is to regulate the AC voltage at the PCC to improve the voltage profile of the power system. Moreover, it can be used to enhance power system oscillation stability [73]. The STATCOM output can be regulated in such a way to regulate the AC voltage at PCC to improve the voltage profile of the power system. STATCOM can also be used to add the transient stability margin by introducing damping during power system transients. STATCOM can be based on either VSC or CSC. Both configurations utilize fast switching semiconductor components such as IGBT or IGCT, providing four-quadrant converter operation to easily change the direction of real and reactive power flows among STATCOM and the power system. A STATCOM typically consists of a step-down transformer, a GTO or IGBT or IGCT and one or more DC link capacitors. The VSC is the building block of STATCOM and of many other FACTS devices. The primary goal of a VSC is to generate an AC voltage from a DC voltage, so that it is often referred to as "DC-AC converter" or "inverter". The VSC must generate a symmetric AC voltage with controllable voltage and phase angle. The voltage difference across the transformer leakage reactance in addition to power line reactance (known as coupling reactance) produces reactive power transfer between the STATCOM and the power system. Figure 4.5 demonstrates a schematic of a one-line diagram of a STATCOM system. The VSC generates a controllable AC voltage before reactance (transformer's leakage reactance added to the line reactance). In terms of active power exchange, if the STATCOM has batteries, on its DC side, it also can inject active power into the grid. The active power transfer can be controlled using the

phase angle difference between the STATCOM terminals and PCC. When the phase angle of the power grid lags the phase angle of the VSC, the STATCOM injects active power to charge the capacitor. Unlikely, if the phase angle of the power system leads the phase angle of the VSC, the STATCOM absorbs active power from the power grid [73,74].

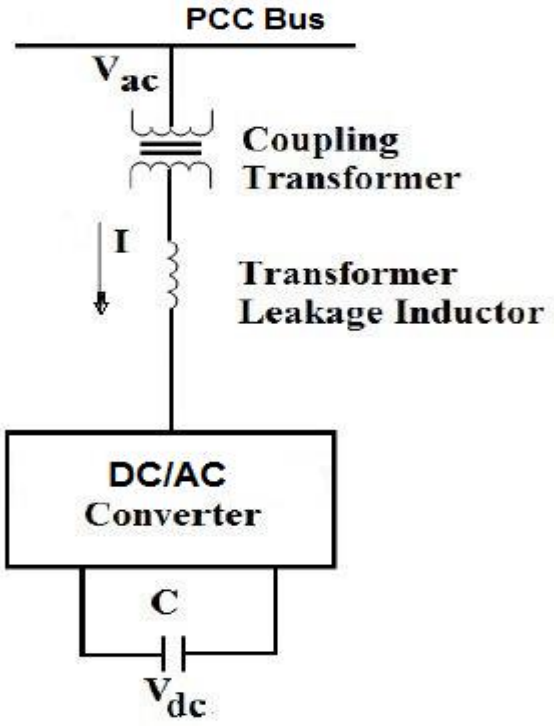

Figure 4.5 One-line diagram of a STATCOM system [74]

The STATCOM can operate in two modes.

- **Voltage Regulation Mode**

STATCOM can provide voltage support to PCC during dynamic disturbances. When operated in this mode STATCOM;

1) Absorbs VAR power from system, when system voltage is high.

2) Injects VAR power to system, when system voltage is low.

- **VAR Mode**

This mode allows the STATCOM to keep VAR power of system constant by controlling STATCOM parameters.

4.3.3 Main Components of a VSC-based STATCOM

Figure 4.6 shows a simplified single-line schematic of a VSC-based STATCOM. STATCOM usually includes a transformer, VSC, coupling reactor, and DC capacitor. Typically, the VSC is connected to the power system via a coupling transformer. Since STATCOM is usually connected to high or medium voltage power systems, the primary function of the coupling transformer is to couple the AC output of VSC with the PCC. However, the coupling transformer increases reactive current on the STATCOM side, which increases power losses associated with the leakage reactance of the coupling transformer. The VSC is the most important block of the STATCOM system. This VSC can utilize a simple two-level conventional topology or a multi-level topology. The objective of the VSC is to generate a sinusoidal AC voltage with controllable magnitude and controllable phase angle at the fundamental frequency of either 50 Hz or 60 Hz. Reactance is a key component in STATCOM operation, which allows continuous control of active and reactive power. The main functionality of this coupling reactance is, 1) to provide low-pass filtering of the VSC output waveform in order to minimize or fully cancel out undesired harmonics generated by VSC switching, 2) to provide active and reactive power control, 3) to limit short-circuit currents. In addition to coupling reactance, an output filter is usually connected at the AC side of the VSC to minimize current harmonics of STATCOM. This filter can be a single inductor or a second-order LC filter depending on the harmonic content of the output waveform. The rating of output filters depends on performance requirements and magnitude of the harmonics. Nevertheless, a typical filter for a two-level conventional converter is approximately 10% to 30% of the rated power. This value can be lower for a multilevel VSC, since multilevel VSCs produce lower harmonic content [74]. Another significant component of STATCOM is the DC capacitor to serve as constant DC voltage for proper VSC operation. Another primary function of the DC side capacitor is to provide a low-inductance path for the turned-off current. The DC link capacitor also reduces the ripples on the DC link voltage of STATCOM.

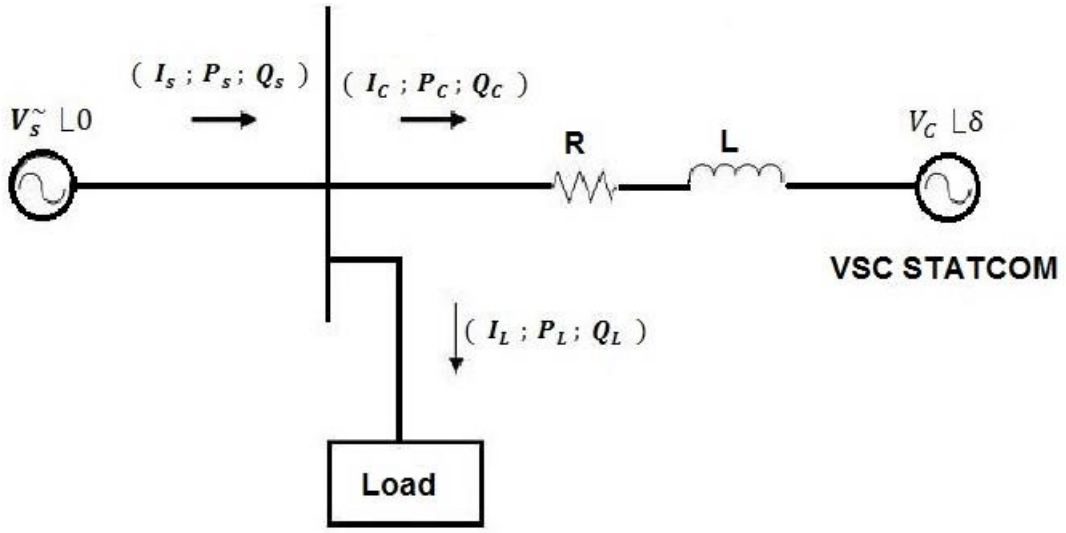

Figure 4.6 Simplified model of the STATCOM [74]

4.3.4 Power Flow in a VSC-based STATCOM System

In Figure 4.6, a schematic diagram of a STATCOM is presented, where $V_S^{\sim}$ is the rms value of the grid voltage with a zero-phase angle referred to STATCOM side, V_C is the rms value of the STATCOM fundamental voltage, Q_S , Q_C and $Q_L$are the reactive power of source, STATCOM, and load respectively. The phasor diagram of the STATCOM with equivalent total resistance and inductance between the STATCOM and the power grid is given in Figure 4.7.

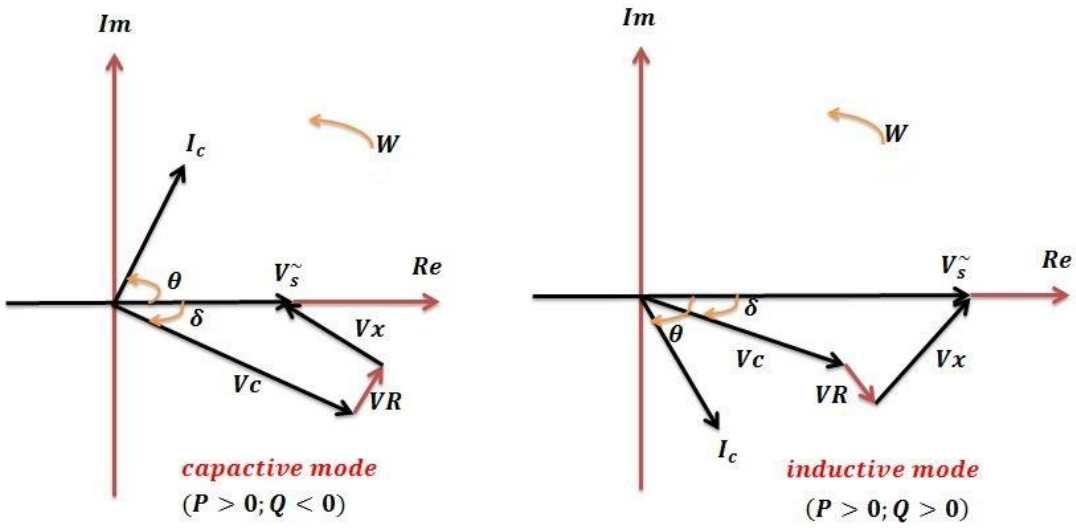

Figure 4.7 Phasor diagram of the STATCOM connected to grid [82]

As previously demonstrated in Figure 4.6, real (P_C) and reactive (Q_C) power consumed by the STATCOM from the grid can be presented by:

$$P_C = 3V_C\, I_C cos\theta \tag{4.1}$$

$$Q_C = 3V_C\, I_C sin\theta \tag{4.2}$$

Equations (4.1) and (4.2) assume that P_C flows from the grid to the STATCOM, and the STATCOM input current lags the AC supply voltage. By using Kirchhoff's voltage equations for the STATCOM shown in Figure 4.6 results in

$$V_S = V_C + V_R + V_X \tag{4.3}$$

where

$$\begin{bmatrix} V_R = I_C R \\ V_X = I_C X \\ X = 2\pi f \end{bmatrix} \tag{4.4}$$

Substituting Equation (4.4) in Equation (4.3) and using real-imaginary plane yields

$$V_S - V_C cos\delta = XI_C sin\theta + RI_C cos\theta \tag{4.5}$$

$$V_C sin\delta = XI_C cos\theta - RI_C sin\theta \tag{4.6}$$

Solving active and reactive power Equations (4.1) and (4.2) using Equations (4.5) and (4.6) results in:

$$Q_C = 3V_S\, I_C sin\theta = 3V_S \frac{V_S - V_C cos\delta}{Xsin\theta + Rcos\theta} sin\theta \tag{4.7}$$

$$P_c = 3V_S I_C cos\theta = 3V_S \frac{V_C sin\delta + RI_C sin\theta}{X} \tag{4.8}$$

Theoretically, no power loss occurs in an ideal system, resulting in no active power transfer. As a result, for an ideal STATCOM, active power should be equal to zero implying that δ is equal to zero. In this case, the AC voltage of STATCOM is in phase with the PCC voltage and the STATCOM current becomes purely reactive. Therefore, P_C and Q_C equations per-phase for a lossless STATCOM can be written as in Equations (4.7) and (4.8).

$$P_C = 0 \tag{4.7}$$

$$Q_C \cong V_S \frac{V_S - V_C}{X} \tag{4.8}$$

Figure 4.8 shows phasor diagrams of an ideal lossless STATCOM. In an ideal STATCOM, in the first condition, if V_C is lower than $V_S^{\sim}$, the STATCOM current lags, and the power grid recognizes the STATCOM as a "reactance". Now STATCOM is in inductive mode and it absorbs reactive power. In the second condition, when STATCOM is in the capacitive mode when V_c is higher than $V_S^{\sim}$, the induced current lags V_X and the power grid recognizes the STATCOM as a "capacitance". In the third condition, if V_C is equal to V_S, there is no reactive power which is injected or absorbed.

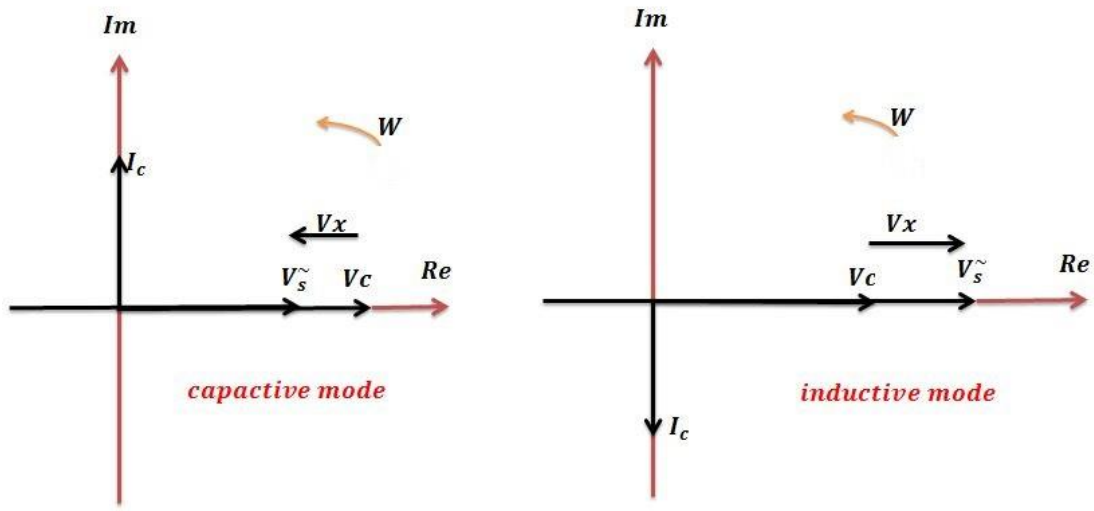

Figure 4.8 Phasor diagrams of an ideal STATCOM [74]

During transient operation of STATCOM, DC capacitor is charged and discharged periodically and active power is continuously exchanged between AC power system and STATCOM. In practice, a small amount of internal power loss is associated with the VSC and the output filter, making a small phase angle δ between the AC voltage output of the VSC and the AC voltage of power system. Figure 4.9 shows a phasor diagram of the STATCOM having loss.

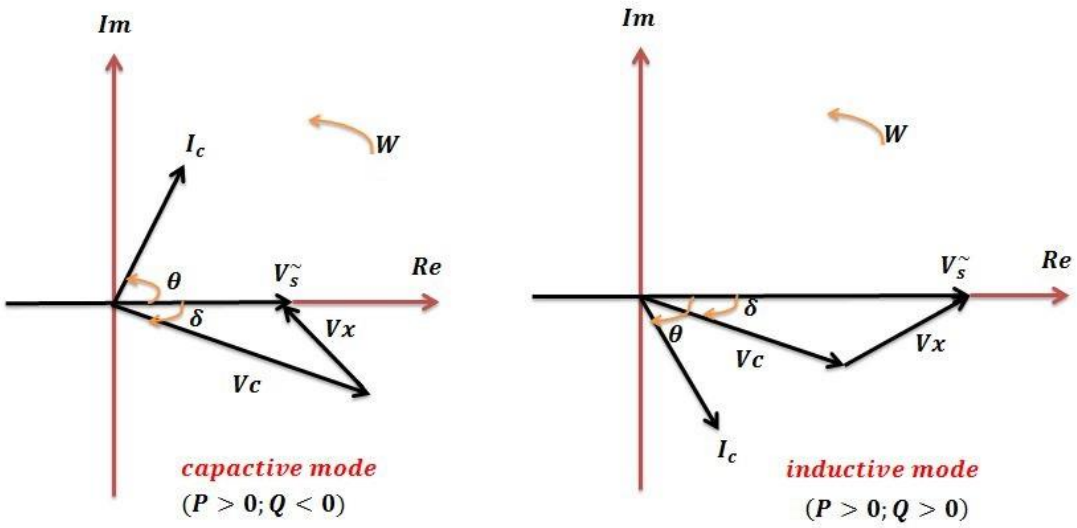

Figure 4.9 Phasor diagram of the STATCOM for R<<X [74]

4.4 Current Source Converter (CSC) Based STATCOM

A CSC based STATCOM is a shunt FACTS device. A current source is referred to as an electronic circuit that can deliver or absorb a current which is independent of the voltage across it. The DC-side energy storage element in CSC topology is an inductor. A CSC based STATCOM is illustrated in Figure 4.10. The comparison between VSC and CSC based STATCOM is summarized as follows [76]:

- As compared to VSC, CSC is more complex in terms of both power and control circuits. In CSC, filtering capacitors are used to improve the quality of AC current waveform at the output. In addition to this, these filters can also resonate with the AC side inductances.

- CSC based STATCOM doesn't have high short circuit current whereas VSC has high short circuit current. The rate of rising of fault current is limited by the reactor of CSC.

- The loss of CSC based STATCOM is higher than VSC based STATCOM. Because in former one, the inductors are present and in later one, the capacitors are present. It is known that the inductor has more power loss than capacitor.

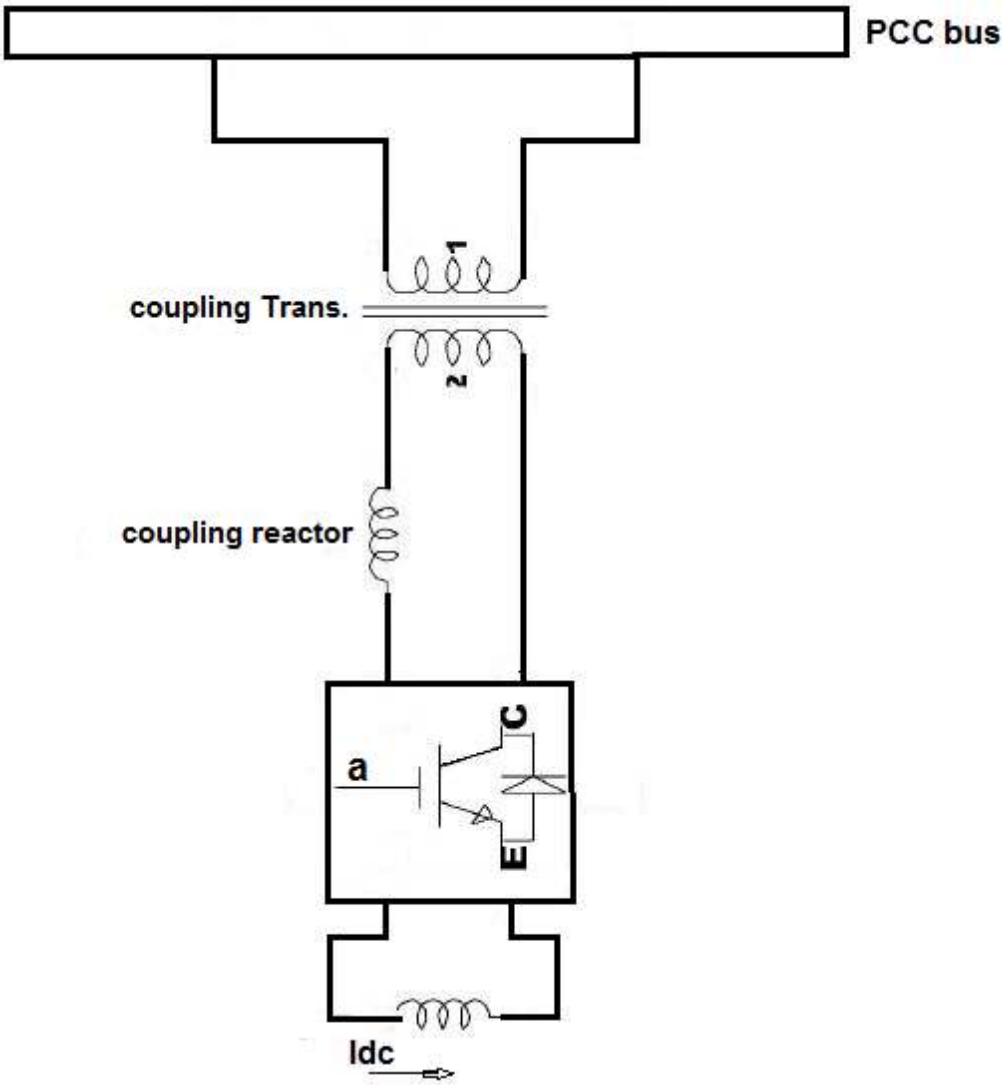

Figure 4.10 CSC based STATCOM [76]

CHAPTER 5

MODELING OF SINGLE-PHASE CASCADED H-BRIDGE STATCOM AND ITS CONTROL

5.1 Introduction

Cascaded H-Bridge (CHB) converters offer many advantages over other multilevel topologies such as high power rating by using many low-rated semiconductor devices. However, a complex control technique is required for this topology. In general, the purpose of a grid-connected VSC is to inject controlled reactive power into the grid. At the same time, the DC link voltage of the VSC must be regulated at its reference value. Both of these tasks require independent control of active and reactive power transferred between the VSC and the grid. Hence, the proposed controller for CHB STATCOM should have three major functions: The first function is to control the active power transferred between the VSC and the grid, the second function is to control the reactive power transferred between the VSC and the grid, and the third function is to keep the voltages of the CHB capacitors balanced.

In [77], a PI controller is proposed based on dq-frame. In this technique, robust synchronization of AC and DC quantities is guaranteed. As previously described, controlling power in the single-phase is much more complex than in the 3-phase systems in which the dq-transform is utilized. This chapter deals with

- How to control real/reactive power injection with CHB STATCOM in single-phase system.
- How to control real/reactive power injection with CHB STATCOM based on dq-reference frame.
- Evaluating the overall dynamic and steady-state performance of the modelled CHB STATCOM.

- Using optimization techniques to tune and enhance the closed-loop dynamic performance of the CHB STATCOM.

5.2 Power-stage Model of STATCOM with One VSC

The CHB-STATCOM connected to the grid is simulated using simulation program in order to verify the implemented control strategy. The STATCOM consists of identical full H-bridges connected in series from their AC sides. Each H-bridge has an individual DC link made by a DC capacitor. The converter output is connected to the power system via coupling reactance which is used for source connection with the system and filter out the current coupling transformer is used for adjusting voltage levels between the STATCOM converter and PCC. STATCOM enhances the power quality of system by compensating the reactive power. Figure 5.1 shows the basic structure of a STATCOM connected parallel with the main power line at the PCC**.**

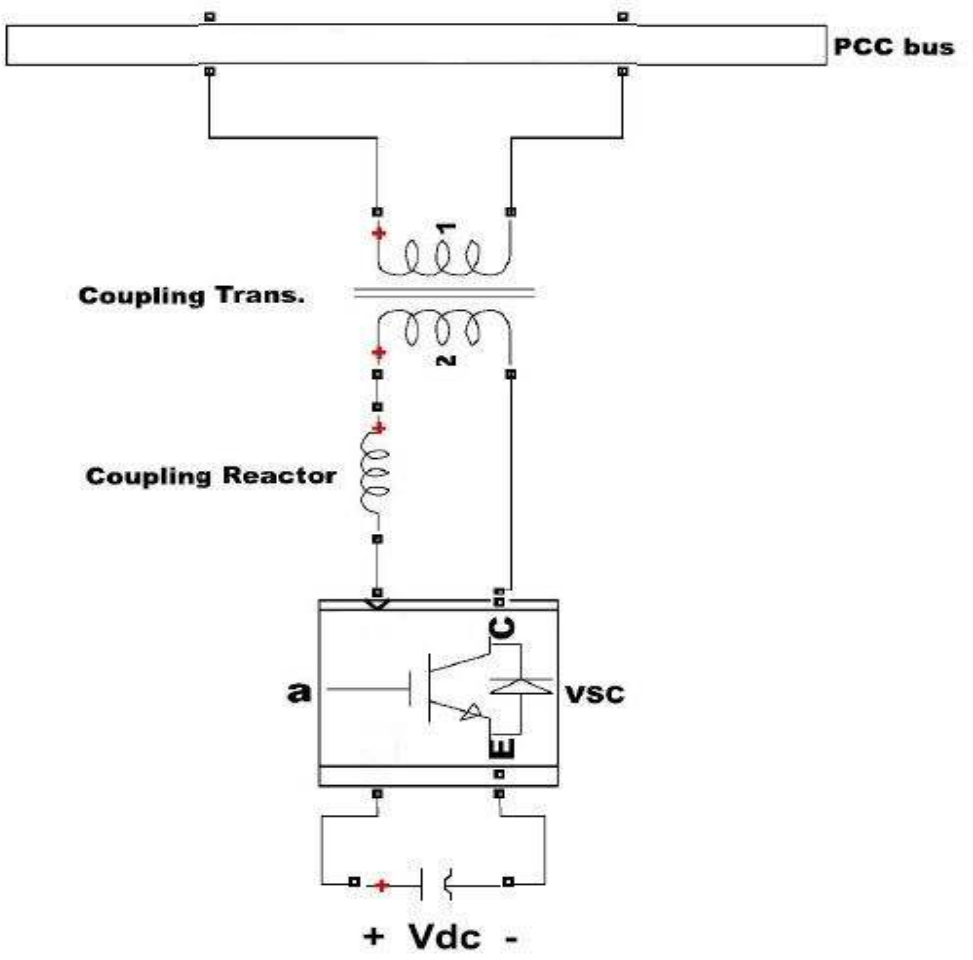

Figure 5.1 Power-stage model of STATCOM with one VSC

5.3 Power-stage Model of CHB STATCOM with More VSCs

CHB converters are constructed by cascading N number of H-Bridges at their AC sides. This CHB converter can generate $2N + 1$ levels at its output phase voltage. In case of utilizing identical DC sources for each DC side of the H-Bridge, the voltage unbalance problem in DC sides of the H-Bridges is not normally observed. However, if capacitors are used at the DC side of each H-Bridge, voltage unbalance and ripple problem can become dominant. Normally DC voltage balancing is realized by strategically controlling the active power supplied to each H-bridge [80]. Several advantages of CHB are possible. CHB topology is capable of reaching high output voltage levels. Also it has the ability to successfully balance the capacitor voltages for high number of levels. CHB cells have less price and weight. In case of faulty cell, we can replace it easily and swiftly. Each of the H-bridge produces three-level voltage outputs, i.e. positive, zero and negative. These voltages are then summed up together to form AC voltage waveform. The magnitude of phase-a AC output voltage is given as follows:

$$V_{out} = V_{c1} + V_{c2} + V_{c3} + \ldots\ldots + V_{cM} \tag{5.1}$$

where M is the number of H-Bridges per phase, V_c is the output voltage of each H-bridge. The structure of CHB converter is modular which means that we can simply make the output voltage waveform better by adding more identical H-bridges in the circuit. The DC capacitor connected to the DC side of each H-bridge acts as a temporary energy storage device. Sinusoidal pulse width modulation (SPWM) is an switching technique for controlling CHB converters. In principle, SPWM works by comparing a reference sinusoidal waveform with a triangular waveform in order to generate the firing (switching) signals for power semiconductor switches of CHB VSC. The CHB VSC has been designed and simulated using the simulation program. The 7-Level CHB is illustrated in Figure 5.2. The circuit consists of twelve power semiconductor switches in three series CHBs. IGBT has been chosen as power semiconductor switch. Both two IGBTs are connected in series in half H-bridge.

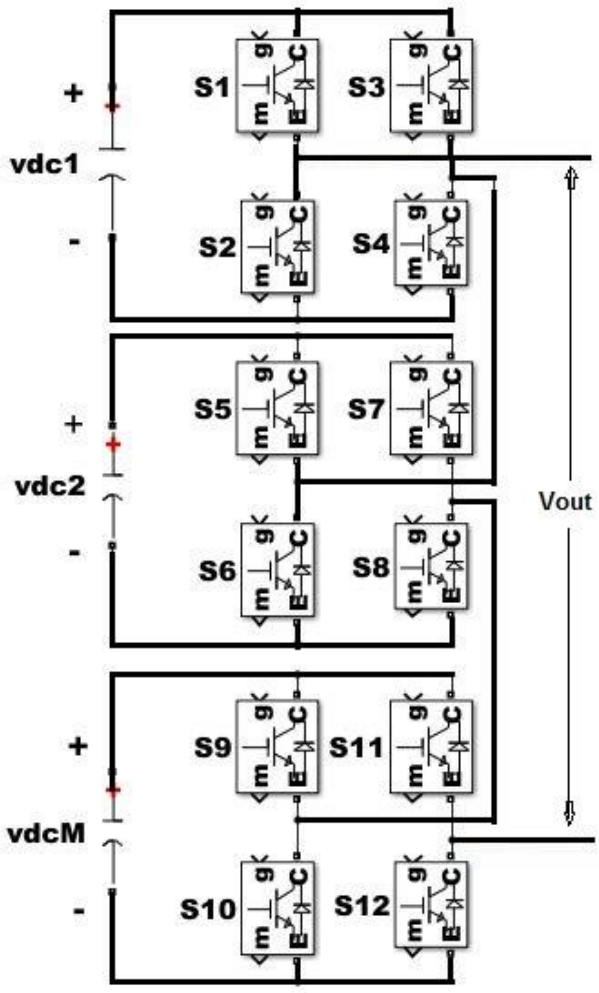

Figure 5.2 Power-stage model of CHB STATCOM with three H-bridges

5.4 Phase Locked Loop (PLL)

The main objective of phase locked loop (PLL) is to determine the phase angle of the phase-a grid voltage (θ), which is required to perform the coordinate transformation and produce the reference voltage [81]. The law governing the PLL is given by:

$$\frac{dw}{dt} = \alpha_{pll}^2 \varepsilon \tag{5.2}$$

$$\frac{d\theta}{dt} = 2\alpha_{pll}\varepsilon + w \tag{5.3}$$

where α_{pll} is the closed loop PLL bandwidth. Synchronization speed and bandwidth of PLL are inversely related. Figure 5.3 shows the basic block diagram of PLL.

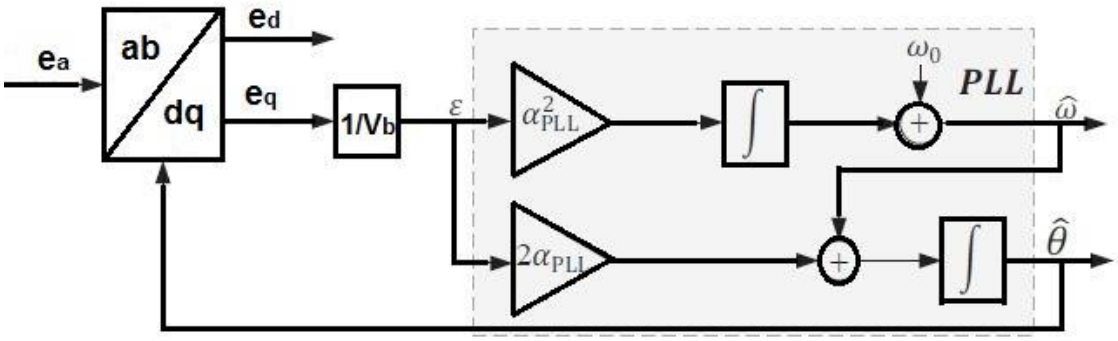

Figure 5.3 Basic block diagram of PLL [22]

Figure 5.4 depicts the simulation block diagram of PLL which has three main components: PID controller, a voltage-controlled oscillator (VCO) and filter. This block is used to track the phase of the voltage signal and it outputs the angle wt.

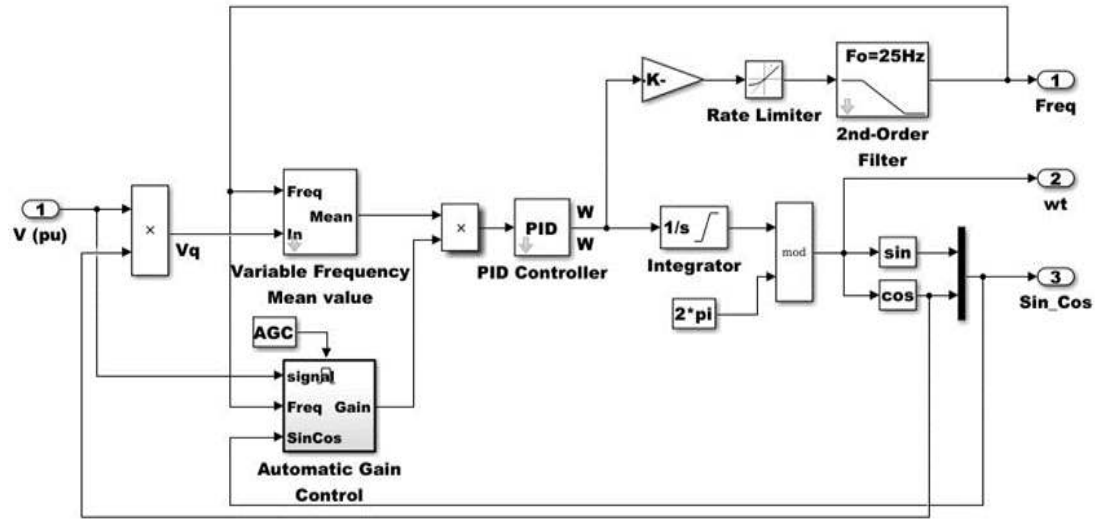

Figure 5.4 Simulation model of PLL

5.5 Modelling of Controller System For Single-phase CHB Based STATCOM

5.5.1 Active and Reactive Power Controllers

5.5.1.1 PI Control Scheme

The main goal of the designed single-phase CHB based STATCOM is to provide dynamic VAR compensation to the utility grid. Hence, active and reactive power must be efficiently controlled. In the proposed controller, the power transfer (active and reactive) between the converter and the power grid is managed by adjusting phase shift angle (between the voltage of the converter and the AC power supply) and modulation index, respectively. The modulation index of STATCOM is governed to provide reactive power control. On the other hand, to control active power transfer between STATCOM and the grid, the phase shift angle is used. The function of the phase shift angle controller is to keep the DC link voltage constant at the reference value [82]. Figure 5.5 depicts the complete PI control schematic of the proposed controller system.

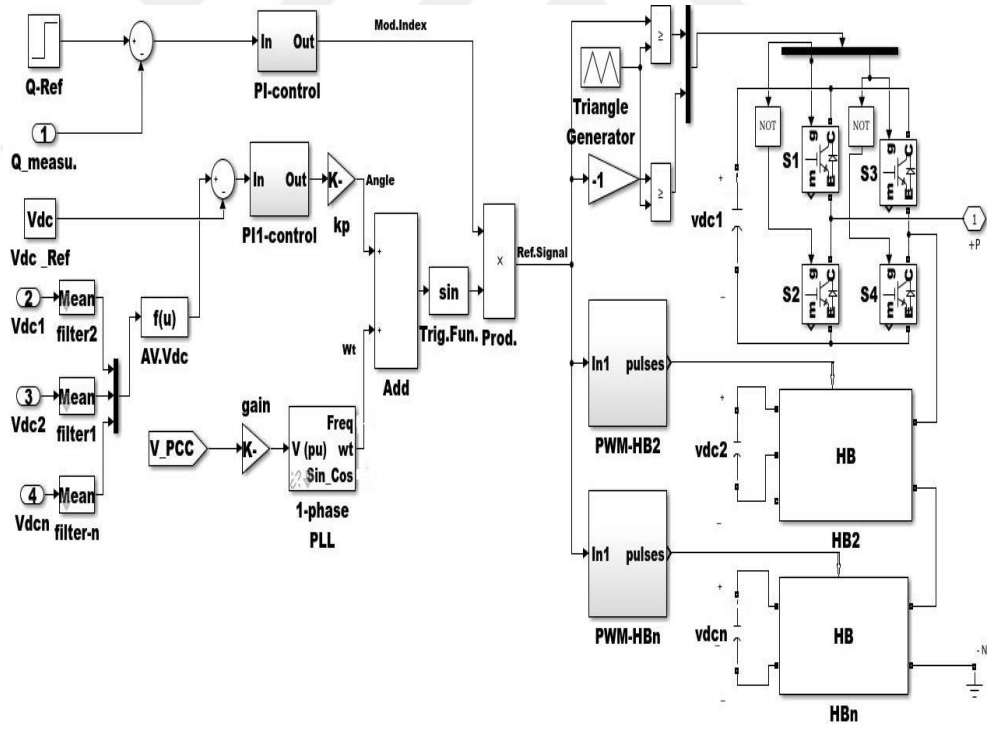

Figure 5.5 Complete schematic of the proposed PI controller system

First assumption is that, the change in modulation index mainly affects Q, whereas a change in the phase shift angle mainly affects *P*. The power flow between a STATCOM and line is regulated by the Equations (5.4) and (5.5). The inductive

reactance given in Equations (5.4) and (5.5) X is the summation of the reactance of the power line and the reactance of the transformer which couples the STATCOM to the power grid.

$$P_s = \frac{E_c E_s}{X} \, sin\delta \tag{5.4}$$

$$Q_s = \frac{E_s^2 - E_c \, E_s cos\delta}{X} \tag{5.5}$$

In Equation (5.4) and (5.5) E_C is the STATCOM fundamental voltage , E_S is the value of the grid voltage , and δ is the phase angle between the voltage of the grid and the STATCOM. By varying the magnitude of the voltage of the STATCOM, reactive power can be controlled. The general relation between the STATCOM output voltage and the DC link voltage is as follows:

$$E_C / N E_{DC} = m \tag{5.6}$$

where E_{DC} is the DC link voltage value, and m is the modulation index. Hence the equation for the active and reactive power now becomes

$$P_s = \frac{m E_{DC} E_s}{X} \tag{5.7}$$

$$Q_s = \frac{E_s^2 - m E_{DC} E_s cos\delta}{X} \tag{5.8}$$

Equation (5.7) and Equation (5.8) regulate the operation of STATCOM. Hence, the reactive power supplied or absorbed by STATCOM to or from power grid is determined indirectly by controlling reactive power. The amount of the target injected or absorbed reactive power (Q_{ref}) is then compared with the output STATCOM reactive power. The resulting error is called "Q_{error}" processed by a PI controller to determine the modulation index (m). Figure 5.6 demonstrates the schematic of the reactive power controller. On the other hand, the DC link voltage of the converter is compared with a reference value (V_{dcref}). The resulting error is sent to another PI controller. The output of this PI controller is used to determine the phase shift angle between the converter output voltage and the grid voltage. Figure 5.7 shows the schematic of the DC link voltage controller.

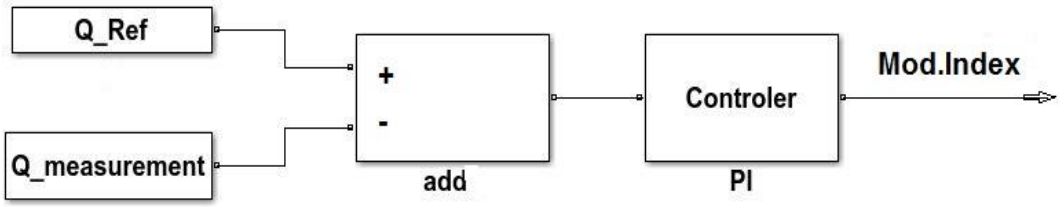

Figure 5.6 Schematic of the reactive power controller

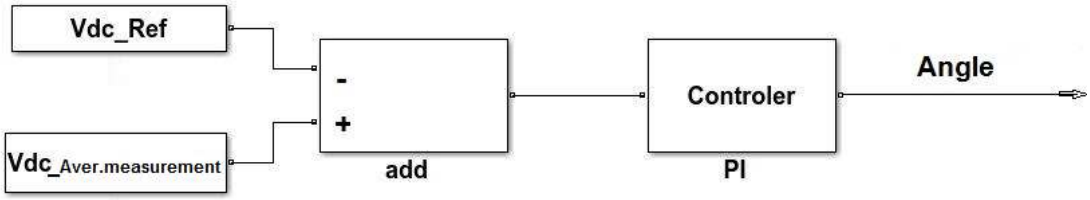

Figure 5.7 Schematic of DC link voltage controller

5.5.1.2 Fuzzy Logic Control Scheme

In this work, the main function of fuzzy logic control (FLC) is to generate two signals: modulation index by comparing the reactive power with the reference reactive power and phase shift angle by comparing the average measured DC voltage of CHB with the reference DC voltage. A fuzzy control system is the one which is based on fuzzy. It is a multi-valued logic in which there are many values for a given option, i.e, it is an approach to computing based on the degree of right and wrong rather than the absolute right and wrong unlike Boolean logic (0 means false and 1 means true). We can have a partial truth in fuzzy logic which ranges between completely true and completely false [83]. The cores of a fuzzy control system are the followings:

- Input/output is defined in the form of membership function.
- Rules are developed which is used in network adjustment.
- The network is programmed.

5.5.1.2.1 Fuzzy Systems

Fuzzy systems are pretty simple in terms of concept. They just contain three stages i.e: an input stage, a processing stage and an output stage. The input stage is used to map the non-fuzzy input values like that of sensor output, switches or thumb wheels to fuzzy inputs using the membership functions and truth values. The processing stage evaluates the input values using the developed rules and then generates the output for each of the corresponding input and then combines the result of the rules. The output stage takes the results from the processing stage which is in fuzzy input form and converts it into corresponding control output values. To build a fuzzy logic system, followings are the steps involved in build a fuzzy logic system: define the inputs and outputs of the system, develop membership functions, generate rules, and simulate the fuzzy logic system.

5.5.1.2.2 Linguistic Variables

These variables are different from the typical variables, with which we are familiar in a sense that these variables are closer to our natural language.

5.5.1.2.3 Membership Functions

These functions are used to map the mathematical inputs to fuzzy linguistic terms and vice-versa. There are many different types of membership functions such as trapezoidal, singleton, sinusoidal, triangular membership function, and etc...

The membership function used in this work was the triangular membership function. The triangular membership function is defined in Equation (5.9) by three parameters; "a" which represents lower limit, "b" which represents the upper limit "b" and "m" which represents the mean value where $a < m < b$, [84].

$$tri(x: a, b, c) = \begin{cases} 0 & x \leq a \\ \dfrac{(x-a)}{(m-a)} & a < x \leq m \\ \dfrac{b-x}{b-m} & m < x < b \\ 0 & x \geq b \end{cases} \tag{5.9}$$

The results of the inputs x and y after passing through the triangular membership function will be according to the following and if the value of x lies between $-1e^9$

and $-\frac{x_a}{2}$, then the output would be negative big (NB), if the value of x lies between $-x_a$ and 0, then the output would be negative medium (NM), if the value of x lies between $-\frac{x_a}{2}$ and $\frac{x_a}{2}$, then the output would be zero (Z), if the value of x lies between 0 and x_a, then the output would be positive medium (PM), if the value of x lies between $\frac{x_a}{2}$ and $1e^9$, then the output would be positive big (PB).

Similarly, for the second input (y), the following rules are generated, as depicted in Figure 5.8.

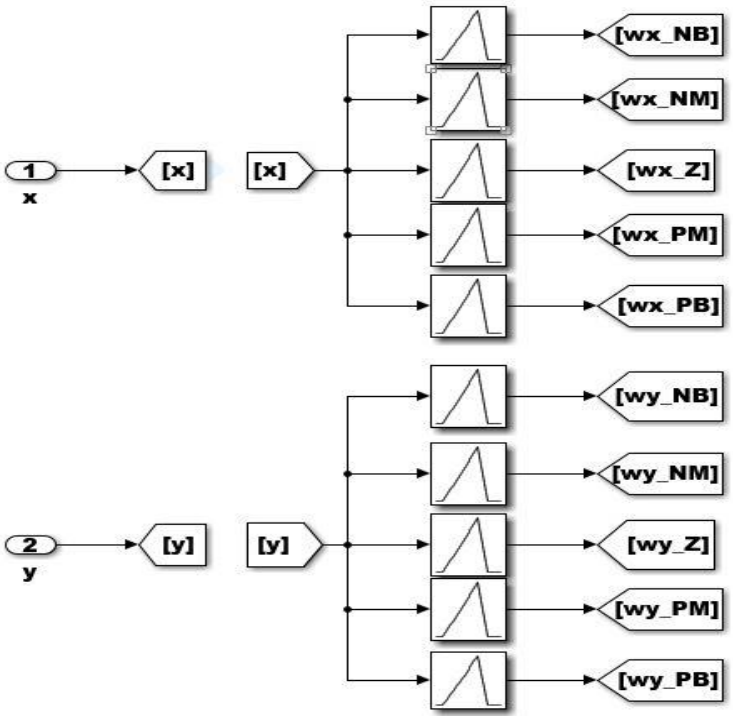

Figure 5.8 Evaluation of inputs according to membership function

5.5.1.2.4 Generated Rules

Followings are the rules developed and implemented in control system for single–phase CHB based STATCOM:

- Rule 1: If x is negative big and y is negative big then z is negative big
- Rule 2: If x is negative big and y is negative medium then z is negative big
- Rule 3: If x is negative big and y is zero then z is negative big
- Rule 4: If x is negative big and y is positive big then z is positive medium

The last step is the defuzzification step i.e. the conversion of fuzzy input to numerical values [84]. The defuzzification step is defined in Equation (5.10) by three parameters; "z" which represents defuzzified value, "W_{ij}" which represents the evaluating the inputs , and "Z_{ij}" which represents evaluating the firing strength of each rule.

$$\frac{\sum W_{ij} * \sum Z_{ij}}{\sum W_{ij}} = Z \tag{5.10}$$

5.5.1.2.5 FLC of Reactive Power and DC Link Voltage Controller

In the present work, the measured reactive power of the system was compared with the reference reactive power. The output was then passed through the error gain block and then given as input (x) to the controller. The second input to the controller block was the output of the error dot gain whose input was the difference of the measured and reactive power. Figure 5.9 shows the FLC of reactive power and DC link voltage of STATCOM.

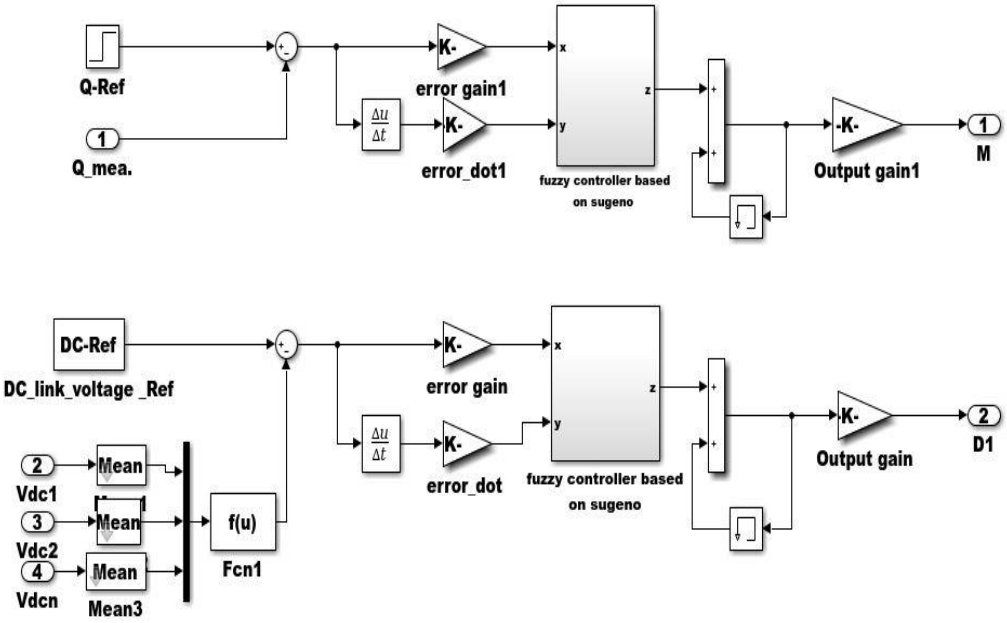

Figure 5.9 FLC of reactive power and DC link voltage of STATCOM

5.5.2 Modeling of the Single-Phase STATCOM in Rotating Reference Frame

For determining a mathematical model of any dynamical system, we need some equations that define the dynamics of that system. These equations can be derived by the help of steady-state response of system. The power circuit of single-phase CHB-STATCOM with an arbitrary number of n cells per phase is shown in Figure 5.10.

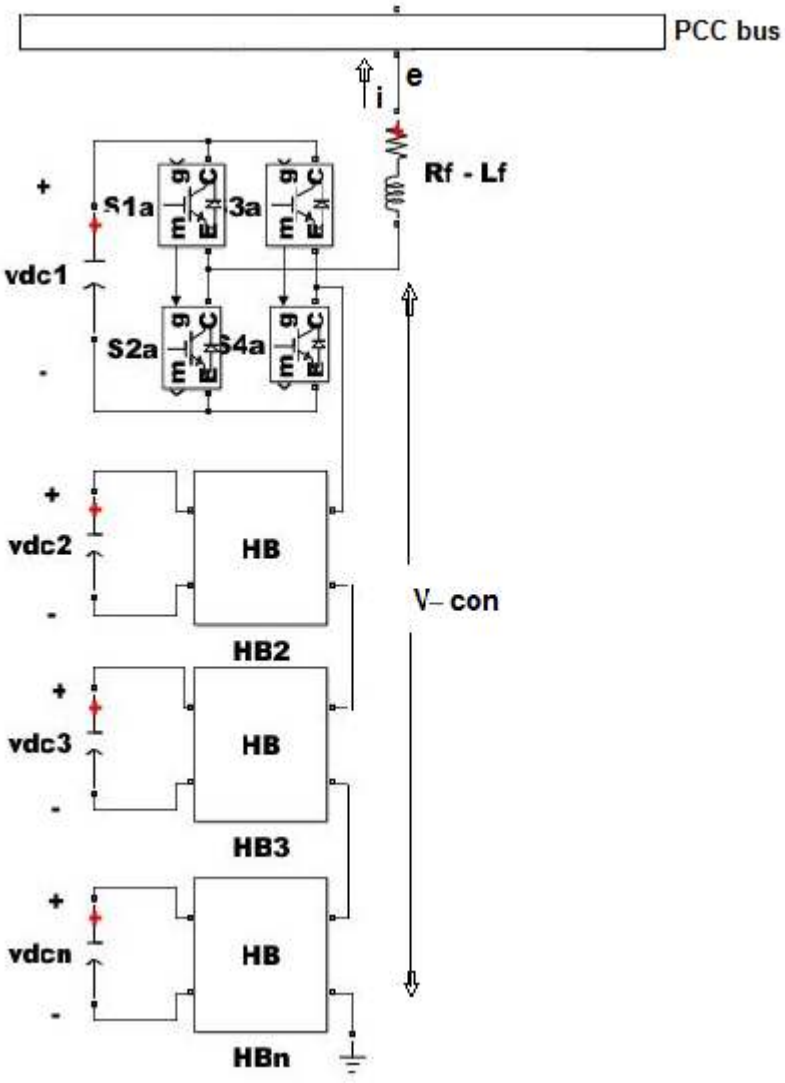

Figure 5.10 Power circuit of single-phase CHB-STATCOM

Using Kirchhoff's voltage law, we get;

$$L_f \frac{di}{dt} + R_f i + e = n s_c v_{dc} \tag{5.11}$$

where i is the phase current, e is the line-to-neutral voltage of PCC, R_f and L_f are the resistance and leakage reactance of the actual power transformers, v_{dc} is the average voltage of all the DC link voltages, n is the total number of cells/phase, and s_c is the switching function (which can be$+1, -1$ and 0).

Using the exchanged active power between the PCC and the converter, the dynamic equation of the DC side for one cell is obtained as:

$$p = \frac{dw}{dt} = \left(\frac{1}{2} C_{dc} \frac{d}{dt} v_{dc}^2\right) = \frac{p_a - \frac{R_f |i|^2}{2}}{n} - \frac{v_{dc}^2}{R_{dc}} \tag{5.12}$$

where w and p are the energy stored in the DC link capacitor and the active power flows in the cells respectively, C_{dc} is cell capacitor, R_{dc} is an additional resistor connected in parallel to the capacitor and represents the overall losses in the DC side, and p_a is the active power absorbed from the grid. In order to simplify the dynamic equations, the switching functions are replaced with the modulation index [22].

$$\mathrm{s_c} = \mathrm{m_c} \tag{5.13}$$

AC side output voltage in the single-phase CHB converter can be written as:

$$Vcon = m_c \, n \, v_{dc} \tag{5.14}$$

By replacing Equation (5.13) into Equation (5.11), a single-phase system can be directly converted into αβ frame without any matrix transformation. An imaginary variable is obtained by shifting the original signal (voltage/current) by 90 degrees, as follows:

$$\begin{bmatrix} x_\alpha \\ x_\beta \end{bmatrix} = \begin{bmatrix} xsin(wt) \\ xsin(wt - 90) \end{bmatrix} \tag{5.15}$$

The $\alpha\beta$ components of STATCOM converter voltage can be written as.

$$Vcon_{\alpha} - e_{\alpha} - R_f i_{\alpha} - L_f \frac{di_{\alpha}}{dt} = 0$$
$$Vcon_{\beta} - e_{\beta} - R_f i_{\beta} - L_f \frac{di_{\beta}}{dt} = 0 \tag{5.16}$$

The real and imaginary circuits constitute the frame of the single-phase STATCOM system, which can be transferred into the dq-frame through the following equation:

$$T_{\alpha\beta-dq} = \begin{bmatrix} sin\,\omega t & -cos\,\omega t \\ cos\,\omega t & sin\,\omega t \end{bmatrix} \tag{5.17}$$

In rotating dq-frame, Equations (5.16) and (5.17) can be expressed as;

$$\begin{bmatrix} v_d \\ v_q \end{bmatrix} + R_f \begin{bmatrix} I_d \\ I_q \end{bmatrix} + L_f \frac{d}{d} \begin{bmatrix} I_d \\ I_q \end{bmatrix} + w_s L_f \begin{bmatrix} -I_q \\ I_d \end{bmatrix} = \begin{bmatrix} vd_{con} \\ vq_{con} \end{bmatrix} \tag{5.18}$$

where, $w_s = 2\pi f$ which is the frequency of the grid voltage . In terms of space vectors, Equation (5.18) is expressed by Equation (5.19) in which v_{dq}, i_{dq} and vdq_{con} are instantaneous space vectors of the single-phase PCC voltage, grid current and converter output voltage in dq- reference frame, respectively.

$$v_{dq} + R_f\, i_{dq} + L_f\, \frac{d}{dt}\, i_{dq} + w_s L_f i_{dq} = vdq_{con} \tag{5.19}$$

In the steady-state condition, Equation (5.19) becomes Equation (5.20), where, v_{dq}, i_{dq} , and vdq_{con} stands for the steady-state space vectors of PCC voltage, grid current, and converter output voltage in dq-frame, respectively.

$$v_{dq} + R_f\, i_{dq} + w_s L_f i_{dq} = vdq_{con} \tag{5.20}$$

In terms of the steady-state conditions, the d-axis of the reference frame is aligned along the PCC voltage position. Assuming and neglecting resistor, the current flowing between the PCC and the STATCOM is given according to following equation:

$$I_{dq} = \frac{vdq_{con} - v_{dq}}{jx_f} = \frac{vd_{con}}{jx_f} + \frac{vq_{con}}{jx_f} - \frac{v_d}{jx_f} \tag{5.21}$$

where x_f is the reactance of the filter and actual power transformer. The voltage v_d is constant and v_q is zero. Thus, the instantaneous active $p(t)$ and reactive power $q(t)$ transferred from the AC system to the STATCOM system are proportional to d-axis and q-axis currents, respectively, as shown by Equations (5.22) and (5.23) [85].

$$p(t) = \frac{Vd * Id + Vq * Iq}{2} = \frac{VdId}{2} \tag{5.22}$$

$$q(t) = \frac{VqId - VdIq}{2} = -\frac{VdIq}{2} \tag{5.23}$$

5.5.2.1 Control Design and Algorithm

The control system used for CHB-STATCOM consists of an inner current control loop, which is used to control the converter output current, and an outer DC link voltage controller, which is used to control the DC capacitor voltages. Figure 5.11 shows the overall block diagram of the implemented control system. A PLL estimates the grid voltage phase angle needed for the coordinate transformations. The DC link voltage controller determines a reference value for the d-component of the current based on the selected DC link voltage reference. Reference value for the q-component of the current is determined either by the reactive power controller or voltage controller. The outputs of the controller are transferred to Cartesian coordinates using dq-ab transformation [84]. The main control blocks are described in the following section.

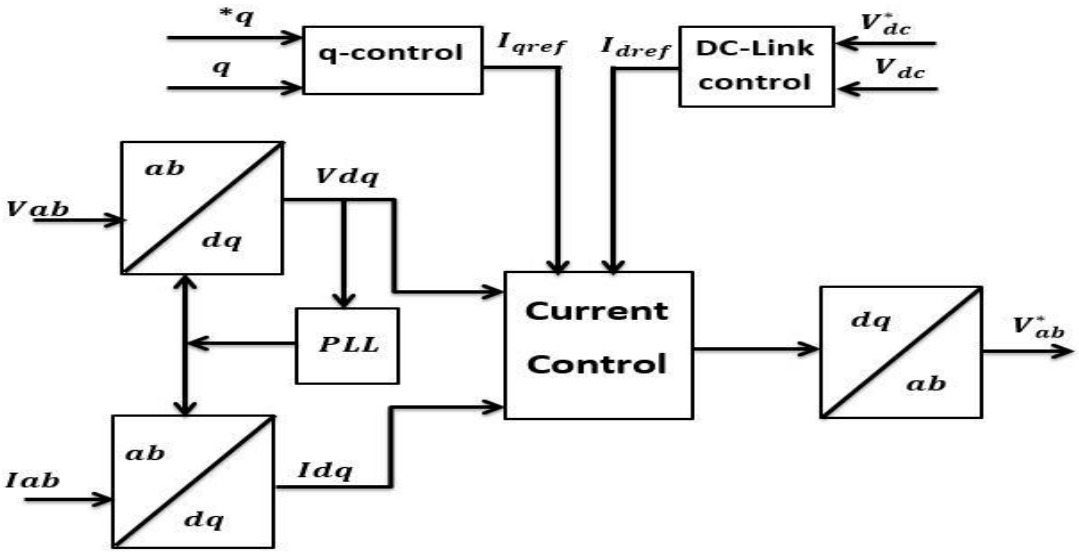

Figure 5.11 Overall control block diagram of CHB-STATCOM

5.5.2.2 Current Control Loop

To derive the control law, Equation (5.19) can be written in the Laplace domain as:

$$i_{dq}L_f s + R_f i_{dq} + e_{dq} + j\omega L_f i_{dq} = nm_{dq}v_{dc} \tag{5.24}$$

and therefore, the law governing the current control is given as below:

$$\left(k_p + \frac{k_i}{s}\right)\left(i^*_{dq} - i_{dq}\right) + e_{dq} + j\omega L_f i_{dq} = nm_{dq}v_{dc} \tag{5.25}$$

where i^*_d and i^*_q are the reference direct and quadrature currents, k_p is the proportional and k_i is the integral gain of current control. The proportional and integral gains of the implemented controller can be easily found by shaping the closed-loop transfer function to have the same response as a first-order low-pass filter of bandwidth.

$$G_i = \frac{i^*_{dq}}{i_{dq}} = \frac{sk_p + k_i}{L_f s^2 + s(R_f + k_p) + k_i} = \frac{\alpha_i}{s + \alpha_i} \tag{5.26}$$

where 'α_i' is the bandwidth of the filter [22]. The proportional and integral gains of the controller can be found as:

$$k_p = \alpha_i L_f \tag{5.27}$$

$$k_i = \alpha_i R_f \tag{5.28}$$

5.5.2.3 DC Link Voltage Control

The aim of the DC link voltage controller is to generate the required reference d-component of the current regulator control. The equivalent circuit configuration is shown in Figure 5.12. Note that all DC capacitors are assumed to be connected in series.

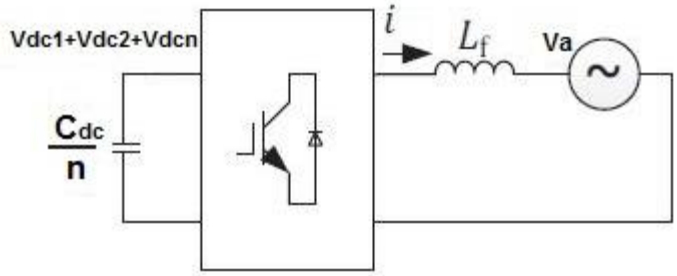

Figure 5.12 Equivalent circuit configuration of STATCOM

Assuming a lossless system, the active power on the AC side and the power on the DC side of the converter can be written as follows:

$$p_{dc} = \frac{dw}{dt} = \frac{1}{2}\frac{C_{dc}}{n}\frac{d}{dt}(v_{dc1} + v_{dc2} + \cdots .. + v_{dcn})^2$$
$$= \frac{n}{2}C_{dc}\frac{d}{dt}\left(\frac{v_{dc1} + v_{dc2} + \cdots .. + v_{dcn}}{n}\right)^2 \quad (5.29)$$

$$p_{ac} = \frac{|v_a||i|}{2} = \frac{n}{2}C_{dc}\frac{d}{dt}(v_{cl})^2 \quad (5.30)$$

Here v_{cl} is the average of all DC link voltages, and v_a is the voltage of PCC. Since both AC and DC side real powers are equal, the Equation (5.30) can be written in Laplace domain as:

$$nC_{dc}sv_{cl}^2 = |v_a||i| \quad (5.31)$$

Here i is the active current and can be calculated using reference DC link voltage. By using PI controller with proportional gain, the active current can be calculated as:

$$i_d = k_c(v_{dc}^{*2} - v_{cl}^2)cos(\theta) \quad (5.32)$$

where "θ" is grid voltage angle, $\cos(\theta)$ is used to generate AC currents that are in phase with the grid voltage, v_{dc}^* is the DC link reference voltage and v_{cl} are the average of all DC link voltages. The amplitude of the active current component from Equation (5.32) can be replaced into Equation (5.31) as follows:

$$nC_{dc}sv_{cl}^2 = |v_a||\, k_c(v_{dc}^{*2} - v_{cl}^2)cos(\theta)| \tag{5.33}$$

Simplifying the results, the transfer function of the DC link controller can be calculated as follows [86]:

$$G_{cl} = \frac{v_{cl}^2}{v_{dc}^{*2}} = \frac{k_c \frac{|v_a|}{nC_{dc}}}{s + k_c \frac{|v_a|}{nC_{dc}}} = \frac{\alpha_{cl}}{s + \alpha_{cl}} \tag{5.34}$$

where the proportional gain k_c is defined as [86]:

$$k_c = \frac{nC_{dc}\alpha_{cl}}{|v_a|} \tag{5.35}$$

5.5.2.4 Individual DC Link Voltage Controller

The concept of individual DC link voltage controller is to add an extra control loop to improve the modulation index for every cell and therefore provide required active power for the individual DC link voltage balancing. Every modulation index is distinguished by the amplitude and the phase angle of the reference signal. The method which is proposed in the work [80] enhances the amplitude and the phase angle of every modulation index to provide the active power which is required for each cell. Modification is done in the modulation index by using the voltage vector superposition method, proposed in [82]. This method is a robust method. Thus, the method which is used in [22] is used here for individual DC link voltage controller. For STATCOM applications, the reactive component of current is normally much greater than active component ($i_q \gg i_d$). With this fact and also considering a fast and precise current controller ($i_{qref} \approx i_q$), it is possible to estimate current in each of phase as follows:

$$i^{\wedge} = i_{qref} sin(\theta) \tag{5.36}$$

The upper script " ˆ " is used for the indication of the estimated quantities. The amplitude of the current is multiplied $\sin(\theta)$, because the current is leading or lagging by 90 degrees with the voltage. Figure 5.13 shows the block diagram of the individual DC link voltage controller.

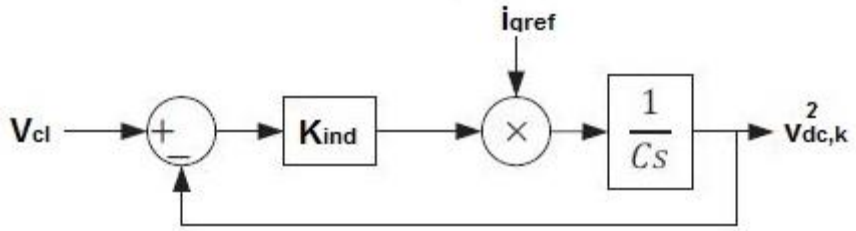

Figure 5.13 Closed loop block diagram of the individual DC link voltage controller

In each cell, the corresponding voltage components are calculated as:

$$v_i^k = k_{ind}(v_{dc,k}^2 - v_{cl}^2)sin(\theta) \tag{5.37}$$

The $v_{dc,k}$ is the DC link voltage of 'k_{th}' cell of H-bridge . The voltage components are AC in nature and constitute active power, in phase with the currents. These component voltages balance the individual DC link voltages. This controller is accountable for controlling DC link voltage in each cell. The active power for each cell can be written as:

$$\frac{1}{2}Cs(v_{dc,k}^2) = \frac{|v_i^k||i\hat{}|}{2} \tag{5.38}$$

Substituting the values from Equation (5.36) into (5.38), we can obtain the closed-loop transfer functions for individual DC link voltages to average DC link voltages as low-pass filter transfer function [90]:

$$G_{ind} = \frac{(v_{dc,k}^2)}{v_{cl}^2} = \frac{\frac{k_{ind}i_{qref}\sqrt{2}}{C\sqrt{3}}}{s + \frac{k_{ind}i_{qref}\sqrt{2}}{C\sqrt{3}}} = \frac{\alpha_{ind}}{s + \alpha_{ind}} \tag{5.39}$$

The proportional gain k_{ind} is given as:

$$k_{ind} = \frac{\sqrt{3}C\alpha_{ind}}{\sqrt{2}i_{qref}} \tag{5.40}$$

5.5.2.5 Dq-Controlling Scheme

Current decoupling method is used to control the AC current and voltage output from STATCOM. The single-phase dq-transformation is used to transfer voltage and current of STATCOM from real and imaginary circuits by substituting them into the α-β frame and transforming them into the dq-frame. A delay is applied to generate two stationary α-β frame in a single-phase system. PLL is applied to synchronize the STATCOM output voltage with grid terminal voltage, hence output of PLL will be in form of sinusoidal changing. Herein, dq-transformation is performed on the resultant signals in form of DC signal. A PI controller is used to generate and control the output voltage in the DC capacitors and for reactive power regulation. This is achieved as in Figure 5.14. Two loops are used: OUT loop and IN loop. Firstly, OUT loop is used to generate I_{dref} which underlies capacitor voltage controller. In OUT loop, a PI controller is used to generate I_{dref} to control the capacitor voltage. Similarly, I_{qref} is produced by OUT-loop to regulate the reactive power. The IN loop is implemented in the rotational reference framework which is synchronized with the PCC voltage E_d^*.This voltage is obtained by comparing I_d with the internal real current reference, while E_q^* is obtained by comparing I_q with the external reactive current reference I_{qref} and components are transformed back to $\alpha\beta$ coordinates and are normalized by capacitor voltage and the resulting values of reference voltage are used further on as modulation indices for the PWM generation.

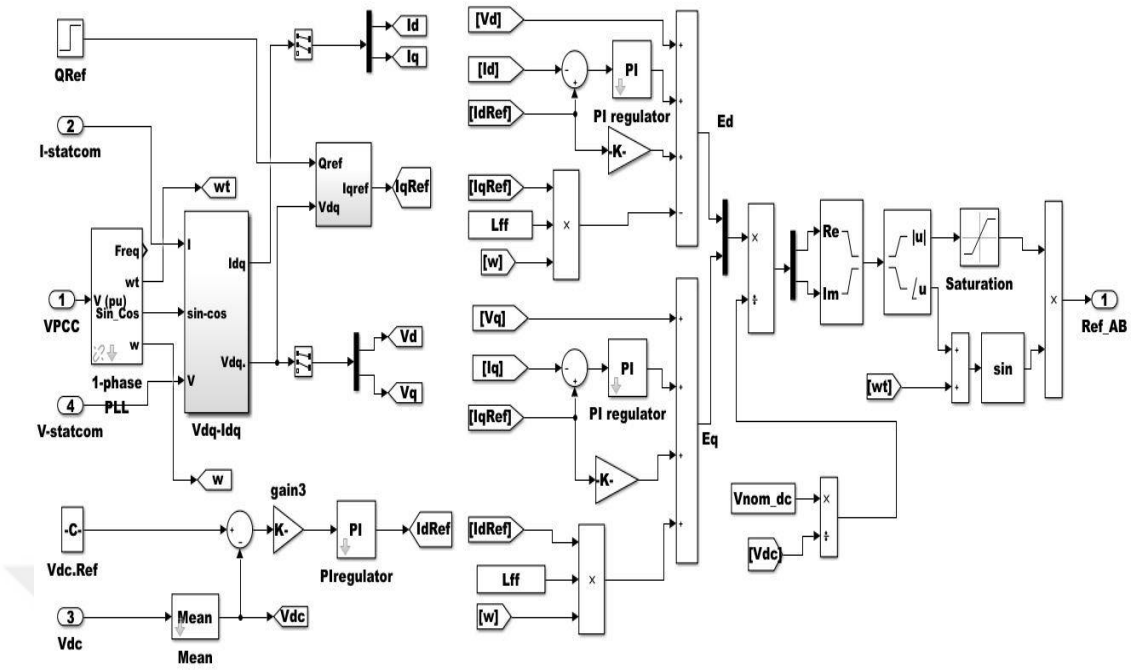

Figure 5.14 dq-Control strategy

5.5.2.6 PI Controller Design Using Optimization Algorithms

The overall STATCOM control system with optimization algorithms is shown in Figure 5.15. The external reactive current reference i_{qref} is determined by using particle swarm optimization (PSO), accelerated particle swarm optimization (APSO) and gravity search algorithm (GSA) for tuning the reactive power controller of STATCOM system and using it in the inner current controller. The inner controller regulates the STATCOM current, while the DC link voltage controller regulates the real power P flowing into the STATCOM to compensate power switch losses. Hence the charging and discharging of the capacitor voltage of the STATCOM are accomplished, DC link voltage controller is used to directly control the DC voltage magnitude and calculate the reference current I_{dref} which is used in inner current regulator. The purpose of the individual DC link voltage controller is not to allow the DC link voltage of each cell to diverge from the reference voltage, V_{dc}.

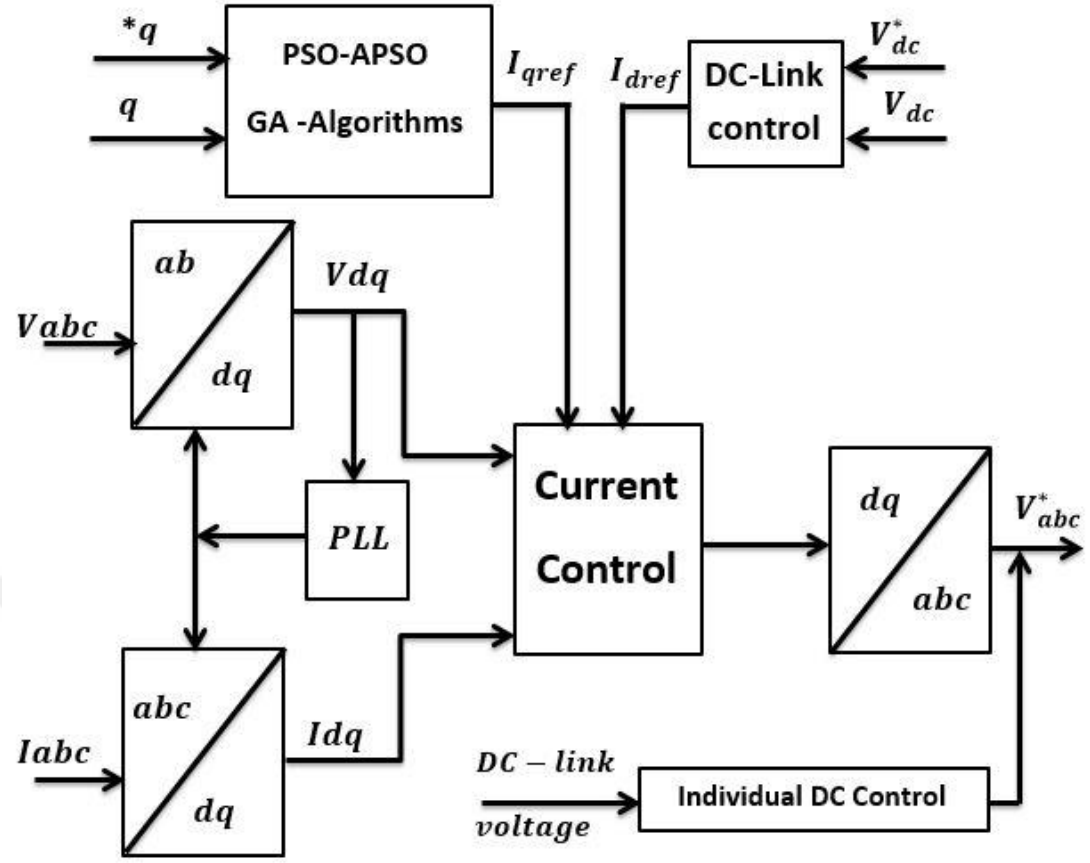

Figure 5.15 STATCOM control system using optimization algorithms

5.5.2.7 Overview of Optimization Algorithms

5.5.2.7.1 Particle Swarm Optimization (PSO)

PSO is an optimization technique which is based on swarm intelligence. PSO takes its inspiration from swarms found in nature such as fish or birds [88]. PSO converges towards the optimal solution by first creating a population of feasible solutions at random and then encouraging the rest of the solutions (known as particles) to move towards the best available solution. Thus, particles are evolved through cooperation and competition. Each particle 'i' can be treated as a point represented in D-dimensional space, being represented as $x_i = (x_{i1}, x_{i2}, \ldots, x_{iD})$ There are two types of best solutions present in the entire set: Particle's own best solution over the course of iterations is denoted by P_{best} (called cognitive learning), which is denoted as $P_{best} = (P_{i1}, P_{i2}, \ldots, P_{iD})$ while the entire swarm's best solution is denoted by G_{best} (called social learning). At each iteration 'k', each particle at position $X_{(K)}$ takes

a step towards the P_{best} and G_{best} which is known as velocity (denoted $V_{(K)}$). The velocity is calculated using particles own best experience and entire swarms best experience and can also be represented in D-dimensions $V_i = (v_{i1}, v_{i2}, \ldots, v_{iD})$. Each particle calculates velocity in next iteration as follows:

$$\mathrm{v_i(k+1)} = \mathrm{w_{i.}v_i(k)} + \mathrm{c_1.rand.}\left(\mathrm{P_{best}} - \mathrm{x_i(k)}\right)\mathrm{c_2.\ rand.}\left(\mathrm{G_{best}} - \mathrm{x_i(k)}\right) \quad (5.41)$$

where 'w' is the inertia constant, c_1 is the cognitive constant, and c_2 is the social constant. The function $rand()$ generates a random number between 0 and 1. Each of these constants have impact on the rate of convergence. Clerc has calculated the optimum values of these parameters as $c_1 = c_2 = 1.494$ and $w = 0.729$ [89]. The PSO requires a cost function, which in this case would be the system's desired behavior. In the predefined number of iterations, the PSO continues its operations to move towards the most optimum solution. The particles position in the next iteration '$k+1$' is calculated as follows:

$$X_i(k+1) = v_i(k+1) + X_i(k) \quad (5.42)$$

The initial population for PSO can be assumed based after some trial-and-error calculations. It has been proposed by the architects of PSO that an initial population of 20-100 particles usually produce similar results. However, the problem at hands also effects the optimal population [90].

5.5.2.7.2 Accelerated PSO (APSO)

Unlike the standard PSO, which uses both the global and local best positions of the particles to calculate particle's velocity in the next iteration, APSO only utilizes global best [91]. The reason for using local best in PSO is linked to increase the diversity in the search space; which is surrogated in APSO by applying randomness. With this setting, the algorithm 'accelerates' towards the optimality, unless the problem at hand in highly non-linear [92]. The updated version of Equation (5.41) will be:

$$v_i(k+1) = w_{i.}v_i(k) + c_1.rand + c_2.rand.\left(G_{best} - x_i(k)\right) \quad (5.43)$$

5.5.2.7.3 Gravity Search Algorithm (GSA)

GSA is intended to be based on the law of gravity, in which different solutions tend to attract each other in the given search space based on the relative distances between the solutions and their masses (or qualities) [93]. The solutions are simulated as set of agents behaving as point masses in *N*-dimensional space with masses m_i and position x_i. All the solutions attract each other and since the particle with best cost has the heaviest mass, the other objects are attracted towards it. Each particle has four associated features: position, inertial mass, gravitational mass, and passive gravitational mass. The position of each object is represented in *N*-dimensional space as $X_i = (x_{i1}, x_{i2}, \ldots, x_{iN})$. The masses are dependent on the cost function. The heavier the mass, the better its cost is and the slower it will move in the search space. The force between two particles 'i' and 'j' at time 't' is calculated as

$$F_{ij}(t) = G(t)\frac{M_{pi}(t)M_{aj}(t)}{R_{ij}(t)+\epsilon}(x_j(t) - x_i(t)) \tag{5.44}$$

In Equation(5.44), M_{aj} is the active gravitational mass of object 'j', M_{pi} is the passive gravitational mass of object 'i', $G(t)$ is gravitational constant at time 't', and $R_{ij}(t)$ is the Euclidian distance between two agents i and j. Here $R_{ij}(t)$ is used in place of $R_{ij}^2(t)$ because it delivers better results [93]. The movement of each agent 'i' is characterized by the acceleration, which is directly proportional to the force applied on the agent and inversely proportional to the inertial mass of the agent. This is shown below:

$$a_i = \frac{F_{ij}}{M_{ii}} \tag{5.45}$$

In the original algorithm, the forces and accelerations are calculated in each dimension separately. For dimension 'd', Equation (5.44) is modified as Equation (5.46) as follows:

$${F_{ij}}^d(t) = G(t)\frac{M_{pi}(t)M_{aj}(t)}{R_{ij}(t)+\epsilon}({x_j}^d(t) - {x_i}^d(t)) \tag{5.46}$$

The gravitational constant G, is initialized and reduced with time to control the search accuracy. Similarly, the acceleration of dimension 'd' is rewritten in Equation (5.47) as:

$$a_i{}^d = \frac{F_{ij}{}^d}{M_{ii}} \tag{5.47}$$

Most importantly, the velocity of an agent 'i' in the next time interval '$t+1$' is calculated as a fraction of its velocity in current time 't' plus its acceleration (or change in velocity). Hence, its velocity and position in the next time interval '$t+1$' for the dimension 'd' are given in Equations (5.48) and (5.49) as:

$$v_i{}^d(t+1) = rand_i . v_i{}^d(t) + a_i{}^d(t)) \tag{5.48}$$

$$x_i{}^d(t+1) = x_i{}^d(t) + v_i{}^d(t+1) \tag{5.49}$$

In Equation (5.48), $rand$ is a random number in the interval [0, 1]. The gravitational and inertial masses are calculated using the fitness function. Assuming the inertial and gravitational masses to be equal, based on the theory of general relativity, they are calculated using the following equations:

$$M_{ai} = M_{pi} = M_{ii} = M_i \qquad \textit{for } i=1,2,\ldots..,\ N \tag{5.50}$$

$$m_i(t) = \frac{fit_i(t) - worst(t)}{best(t) - worst(t)} \tag{5.51}$$

$$M_i(t) = \frac{m_i(t)}{\sum_{j=1}^{N} m_j(t)} \tag{5.52}$$

In Equation (5.51), the $fit_i(t)$ represents the fitness value of the agent 'i', while $best(t)$ and $worst(t)$ are the best and worst values of the entire population set at time 't', respectively.

5.5.3 Modeling STATCOM Control Based Active Power Filtering

5.5.3.1 Cascaded Shunt Active Power Filter (CSAPF)

The cascaded shunt active power filter (CSAPF) has topologies which are almost like that of STATCOM. The CSAPF is used for the elimination of harmonics. The CSAPF makes up the harmonics of the load current by putting the equal but opposite harmonic compensating current. In this case, it can be said that the CSAPF filter works properly as a current source, eliminating the harmonic components which are produced by load. But the phase of current is shifted by 180º. Figure 5.16 illustrates single-phase CSAPF topology [94]. A VSC is used as SAPF in [95]. It is dominated so as to to draw the compensating current to or from the utility as it calls off harmonics on AC side, namely, this APF gives the opposite of the non-linearity towards the nonlinearities of the load. In addition of load current, the compensating current injected by SAPF also have harmonics, together they make source current purely sinusoidal. The necessary item of the CSAPF is achieved by compensating the reactive power and eliminating the harmonics of the load current [94].

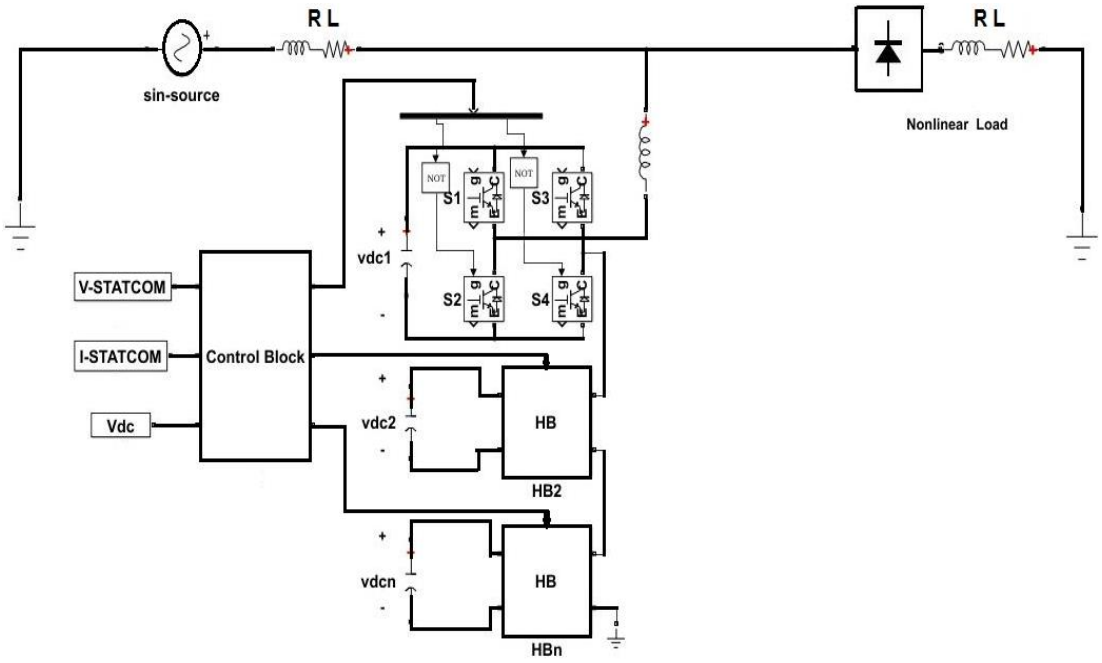

Figure 5.16 Single-phase CSAPF topology

5.5.3.2 Power Flow for Ideal Compensation

The power flow for the ideal compensation of SAPF is demonstrated in Figure 5.17. The total instantaneous power which is drawn by the nonlinear load can be given as:

$$P_{L(t)} = P_{f(t)} + P_{r(t)} + P_{h(t)} \tag{5.53}$$

where, $P_{f(t)}$ is the instantaneous fundamental real power absorbed by the load. $P_{r(t)}$ is the instantaneous reactive power drawn by the load and $P_{h(t)}$ is the instantaneous harmonic power drawn by the load.

With the achievement of the unity power operation and drawing the sinusoidal currents from the of utility, the APF is required to supply all the reactive and harmonics power demand of the load. At the same time the CSAPF will draw real component of power active filter that will form a right component of the power " P_{loss}" of utility to provide the switching losses and to maintain the steady DC link voltage. Thus, for the ideal compensation the following conditions should be fulfilled [96].

$$P_s = P_f + P_{loss} \tag{5.54}$$

where, P_s is the total real power supply by the source, P_{loss} is the fundamental real power loss component of the CSAPF, P_f is the fundamental real power absorbed by the load. For ideal compensation, the reactive power supplied by the source becomes $Q_s = 0$. The total real power drawn by the load is given as:

$$P_L = P_f + P_h \tag{5.55}$$

where, P_L is the total fundamental real power absorbed by the load. P_h is the fundamental harmonic power drawn by the load. The total reactive power drawn by the load given as:

$$Q_L = Q_f + Q_h \tag{5.56}$$

where, $Q_L$is the total fundamental reactive power drawn by the load. Q_f is the fundamental reactive power absorbed by the load. Q_h is the fundamental harmonic power drawn by the load. The total real power supplied by the SAPF is given as:

$$P_c = P_h - P_{loss} \tag{5.57}$$

where, P_c is the total fundamental real power supplied by the SAPF. The total fundamental reactive power (Q_c) supplied by SAPF is given as:

$$Q_c = Q_f + Q_h \tag{5.58}$$

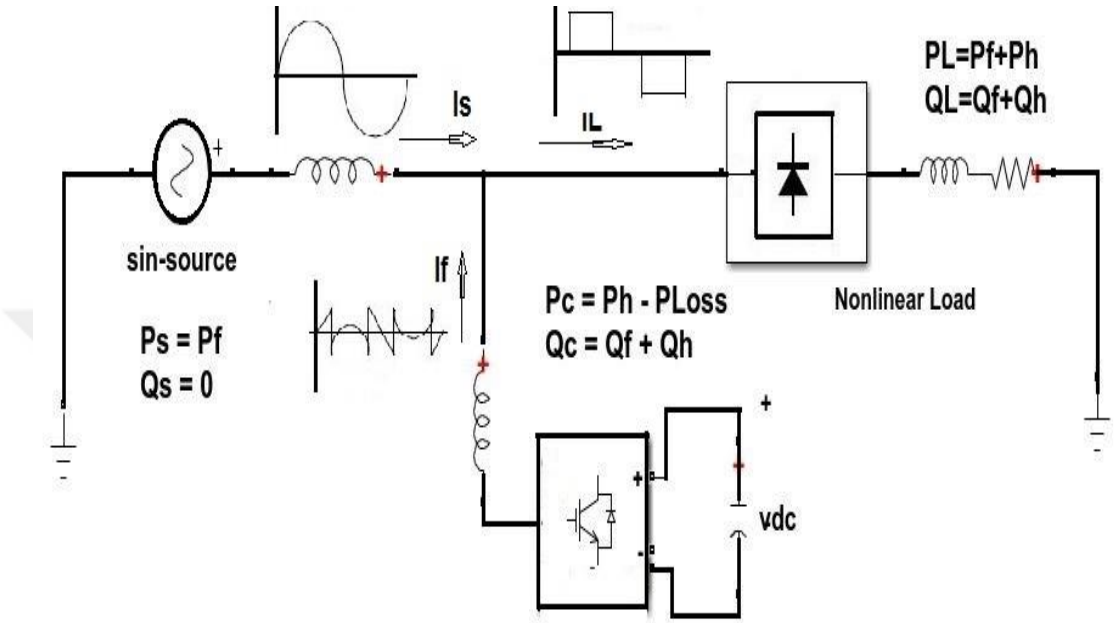

Figure 5.17 Shunt active filter power flow for ideal compensation

5.5.3.3 Control Strategy of CSAPF

To gather the reference compensation currents, it is needed to inject reactive and harmonic power into network at PCC of the nonlinear load and it is due to the instantaneous active and reactive power method. The curious method of a SAPF can be made without the active energy source units [97]. Figure 5.18 demonstrates the average power supplied by the source for instantaneous active and reactive power.

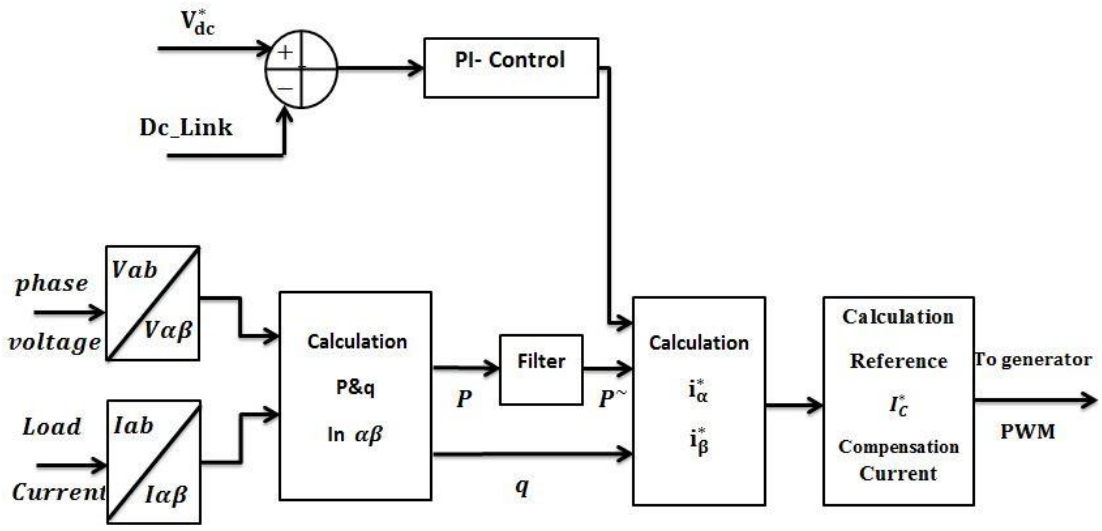

Figure 5.18 Block diagram of the proposed control system

The p-q theory is based on the Clarke transform of voltage and current [98]. The instantaneous values of the single-phase voltages and the currents in α-β coordinates are taken from following equations:

$$\begin{bmatrix} v_\alpha \\ v_\beta \end{bmatrix} = \begin{bmatrix} v(wt+\theta) \\ v(wt+\theta-90) \end{bmatrix} \tag{5.59}$$

$$\begin{bmatrix} I_\alpha \\ I_\beta \end{bmatrix} = \begin{bmatrix} I(wt+\emptyset) \\ I(wt+\emptyset-90) \end{bmatrix} \tag{5.60}$$

The instantaneous active and reactive powers in $\alpha\beta$ coordinates are calculated with the following expressions:

$$P(t) = V_{\propto}(t)I_{\propto}(t) + V_{\beta}(t)I_{\beta}(t) \tag{5.61}$$

$$q(t) = V_{\propto}(t)I_{\beta}(t) - V_{\beta}(t)I_{\alpha}(t) \tag{5.62}$$

The values of P and q can be expressed from Equation (5.61) and Equation (5.62) respectively in terms of DC components along with the AC components, i.e;

$$P = P^{-} + P^{\sim} \tag{5.63}$$

$$q = q^{-} + q^{\sim} \tag{5.64}$$

where, P is the instantaneous power, P^{-} is the dc component of the instantaneous power, $P^{\sim}$ is the ac component of the instantaneous power, which does not have

average value, and it is related to the harmonic currents caused by the AC component of the instantaneous real power. q is imaginary instantaneous power, q^{-} is stands for the DC element of the imaginary instantaneous power, and it has a relation to the reactive power made by the basic components of currents in addition to voltages , $q^{\sim}$ is stands for AC component of the instantaneous imaginary power and has a relation to the harmonic currents which is caused by AC component of immediate reactive power. To make up the current harmonics and the reactive power which are generated by the nonlinear loads, it is confirmed that the reference signal of SAPF has to be included in the values of $P^{\sim}$and $q^{\sim}$. The reference currents, in this case, obtained by the SAPF which are gathered with the explanation below:

$$\begin{bmatrix} I_{c\alpha}^{*} \\ I_{c\beta}^{*} \end{bmatrix} = \frac{1}{V_{\alpha}^{2} + V_{\beta}^{2}} \begin{bmatrix} V_{\alpha} & V_{\beta} \\ V_{\beta} & -V_{\alpha} \end{bmatrix} \begin{bmatrix} P_{L}^{\sim} \\ q_{L}^{\sim} \end{bmatrix} \tag{5.65}$$

The control strategy of SAPF includes both controllers. The first one is used to compensate the reactive power or production of the currents to leave out undesired harmonics. In steady state the real power supplied by the source should be equal to the real power demand of the load plus some small power to compensate the losses in the active filter. Thus the DC link voltage can be maintained at a reference value [95,96]. The value of average voltage across the terminals of the capacitors should be kept constant. By providing or absorbing the active power on electrical network, the regulation of the DC capacitor voltage is achieved. The compensation of reactive power brought storage capacity (C) which absorbs fluctuations of the power when the harmonics occur, in addition to the active power control and by losses of converter. It should be made by keeping the value of the average voltage constant across the terminals of the capacitor. Here we are using the DC component for the generation of reference current hence it is called "indirect method". The load requires only fundamental active part of the source current.

5.5.4 STATCOM Control Based on Artificial Neural Networks

5.5.4.1 Introduction

Recently, the increase of non-linear loads has badly affected the power quality due to the inherent voltage fluctuations in these types of loads and has also raised question on the long-term stability of the power systems and their associated instruments.

Hence, more research studies have been dedicated to improve the power quality and efficiency through variety of different techniques. The planning, implementation, control and maintenance of power systems initiate with the power flow calculations, which constitute the crux of any power system. Over the past few decades, many different solutions have been proposed for the load flow problems. The most important of these techniques have been reviewed in [99]. At any instant, the power systems experience varying operating conditions and the power flow calculations ensure that the operation of the system is within the bounds of the stability criterion. The power flow equations are complex non-linear algebraic equations which are usually written in computer programs, and run over the course of the operation for dynamic analysis. Usually, these equations are solved in multiple iterations and hence require substantial processing and memory requirements [100,101]. One of the primary methods used for the solutions of non-linear equations is Newton-Raphson method [100]. In this section, the proposed an alternative approach to this method, which is based on machine learning algorithms. More specifically, propose the use of Artificial Neural Network (ANN) for estimating the STATCOM parameters such as voltages, phase angles and reactive powers. ANN is a very powerful tool which can be used for the data fitting operations as well as classification problems [103].

5.5.4.2 Overview of ANN

Artificial neural network (ANN) is an excellent machine learning algorithm for the regression and classification problems, which can estimate the data by emulating the functionality of human brain. It works in different layers each with certain number of neurons and weights. The ANN can be used to estimate non-linear systems even when the input data is sophisticated and contains redundant and corrupt information. Due to the non-algorithmic nature, ANN doesn't try to approximate the solution like the conventional techniques which are used for solving the load flow equations.

A neural network is composed of nodes called neurons, at each of which the inputs from previous layers are accumulated after being multiplied with some weights. The neurons are the fundamental processing units which are interconnected with each other in a certain pattern. The human brain comprises of trillions of interconnections between the neurons. It is estimated that there are 10 billion neurons present which are interconnected through 10^{14} links [105]. An isolated worthless neuron becomes

powerful when interconnected with other neurons in the network. In a similar fashion, ANNs are comprised of inter-linked neurons, whose arrangement depends on the type of application. Each neural network has the following basic layers:

Input layer: This layer just comprises of passive nodes whose sole job is to transmit the input to the next layer and therefore the number of nodes in this layer is equal to the number of inputs to the network.

Hidden layer: This is the most important layer of the network which consists of arbitrary number of sub-layers, each containing different number of neuron. This layer processes the data from the input layer by multiplying it with the weight factors.

Output layer: This layer interfaces the internal layers with the outputs and therefore the number of nodes in this layer are equal to the number of outputs. Nodes in this layer are active since they process the data received from the internal layers before transmitting it to the output. A schematic of the connections in ANN is shown in Figure 5.19.

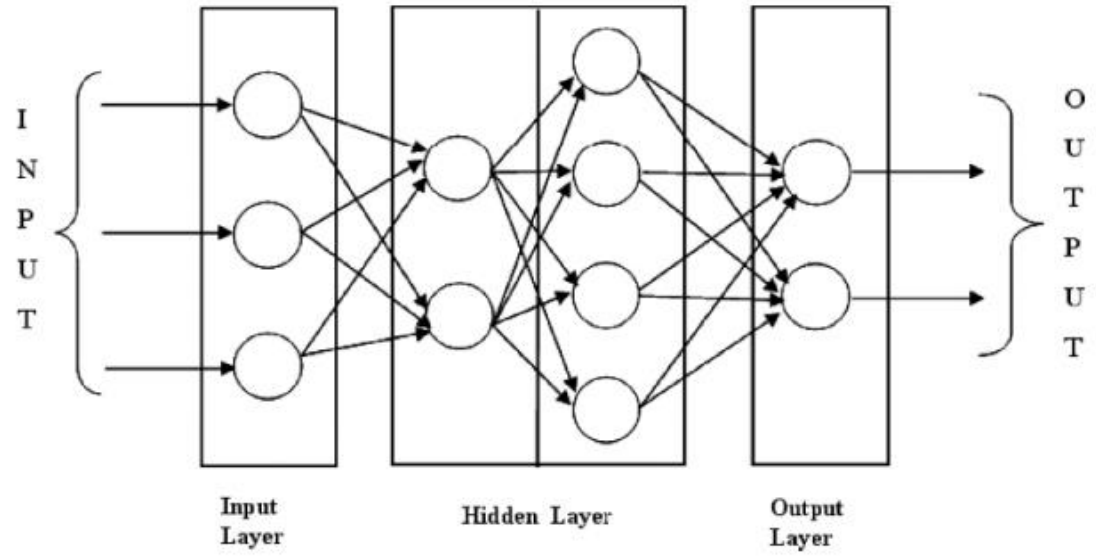

Figure 5.19 The layers of ANN

This interconnection improves the performance of the system over the traditional numerical analysis schemes. Structure of the artificial neuron is shown in Figure 5.20. As obvious, the inputs are received in the hidden layer after being multiplied with weights. These weighted inputs are summed and passed through the transfer function to produce the output. A transfer function's job is to restrict the widely ranging inputs

and map them to a finite output and that's why it is also called 'squash'. At each node 'j', the weighted-input sum is represented by the equation:

$$S_j = \sum_{i=1}^{n} X_i W_i \tag{5.66}$$

The output of the neuron 'j' is written as 'Q_j':

$$O_j = T_j(S_j) \tag{5.67}$$

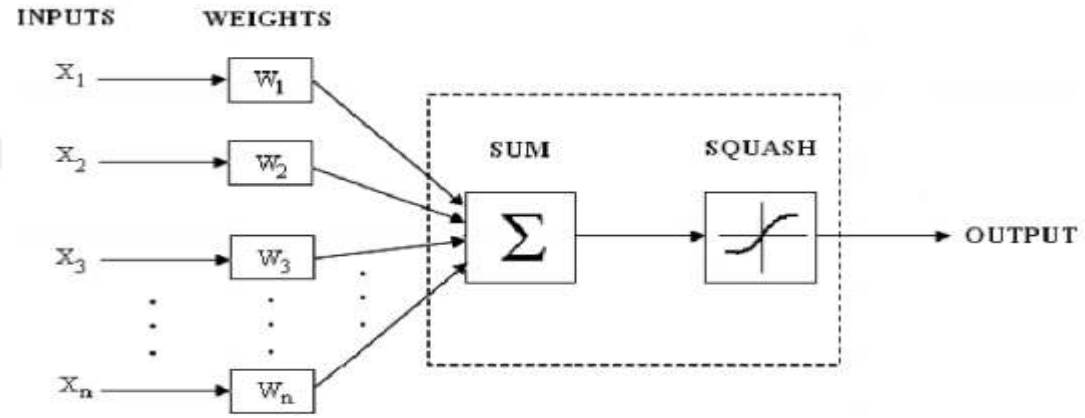

Figure 5.20 The structure of ANN [106]

ANN must be trained for the specific dataset before starting to make its own decisions. Therefore, ANN works in two parts: i) training ii) testing. In training phase, part of the dataset is fed to the ANN along with the determined output. The output obtained from the neural network is compared with the original output (also called target) and the error is fed back to the network to adjust the weights accordingly. When the weights produce optimum result, with minimum error, the ANN is ready to be tested.

The ANNs are usually trained using back-propagation method which is a variant of the Least Mean Squares Method due to its activation function which is analytic continuous function. The back-propagation method is based on steepest-descent algorithm, which seeks to find the minimum error by adjusting weights in the direction of lowest error. The error is taken and back-calculated to converge to the optimum solution. Thus, in essence, the error propagates in the backward direction and that is why it is called back-propagation method. The error at the neuron 'j' is calculated as:

$$E_j = \frac{1}{2}\left(R_j - O_j\right)^2 \tag{5.68}$$

The total error 'E' in all neurons becomes:

$$E = \sum_j E_j = \frac{1}{2}\sum_j \left(R_j - O_j\right)^2 \tag{5.69}$$

To minimize the total error, the weights are adjusted by adding a weight change (ΔW) to the original weights after each iteration. In this respect, a parameter 'α', which is the learning rate is used along with the gradient descent algorithm to define the weight changes as:

$$\Delta W_{kj} = -\alpha \frac{\partial E}{\partial W_{kj}} \tag{5.70}$$

where $0 < \alpha \leq 1$, this means that if the gradient is positive, the weight change is negative and vice versa, to ensure that the solution converges towards the least error. The solution in the next iteration becomes:

$$W_{kj}' = \Delta W_{kj} + W_{kj} \tag{5.71}$$

However, back-propagation sometimes stuck in the local minimum. One solution is to use this technique with other methods such as the one proposed in [106]. Another solution is to use meta-heuristic methods to fine-tune the neural networks.

5.5.4.2.1 PSO Based ANN

PSO is an excelled optimization technique which can be used to tune the weights of the ANN. The overview of PSO was already explained in the previous section.

5.5.4.2.2 Shuffled Frog Leap Algorithm (SFLA) Based ANN

SFLA is another population based meta-heuristic which works in a way which closely resembles the PSO [107]. This method converges to the optimal solution by evolution of memes which are carried by the particles (called frogs in this regime), which exchange information with each other. Each frog has an associated cost and during each iteration, the frogs try to improve their cost. The frogs are the carrier of memes which consist of memo types. This algorithm combines both deterministic and random approaches. In deterministic part, the algorithm uses response surface information to

search for the optimal solution. On the other hand, the random part allows the algorithm to instill robustness and flexibility. Initially, the algorithm generates random solutions (frogs) just like PSO. The cost of all the frogs are calculated and frogs are ranked according to ascending order of their cost. Then, starting from the top position, the frogs are partitioned into communities called memeplexes. Within each of these memeplexes, the frogs share their memes or ideas with other frogs and therefore each memeplex evolves on its own in terms of the cost. In each memeplex, the frogs with the best and worst costs (P_B and P_W) are noted. The next step is to improve the position of the worst frog (P_W). The new position of the worst frog is updated as:

$$U = P_W + S \tag{5.72}$$

where 'S' defines the step size (similar to the velocity in PSO) and it is calculated as:

$$S = min(rand * (P_B - P_W), S_{max}) \tag{5.73}$$

for positive step

$$S = max(rand * (P_B - P_W), -S_{max}) \tag{5.74}$$

for negative step

where S_{max} is the maximum step size allowed and rand generates a random number between 0 and 1. At each iteration, the worst frog is moved closed to the best frog and the cost of the new position U is calculated. If the cost is better than the previous cost, the new position is assigned to the worst frog, else another step size is calculated as:

For positive step

$$S = min(rand * (P_X - P_W), S_{max}) \tag{5.75}$$

For negative step

$$S = max(rand * (P_X - P_W), -S_{max}) \tag{5.76}$$

Here P_X is the position of the global best frog in all memeplexes. Once again, the new position's cost is compared with the worst frog's cost. If it is better, the new position replaces the old worst frog, else this frog is terminated, and another random frog is generated. After predefined number of iterations, the frogs in the memeplexes are

reshuffled. In this way, memeplexes become richer with new ideas and quality of the meme gets improved.

The important parameters in SLFA are the total number of memeplexes and number of frogs in each memeplex. As the size of each memeplex increases, the probability of converging to the global optima also increases, however, this also increases the computational demand. As proposed in [108], the number of memeplexes can be set in the range of 10-100, while the number of frogs in each memeplex can vary from 5 to 300. However, this is imperative that optimum values for these parameters can be obtained through testing the algorithm with different combinations.

5.5.4.2.3 Genetic Algorithm (GA) Based ANN

GA proposed by Dr. David Goldberg [109] is another optimization algorithm. This algorithm is based on the natural selection and genetics which are derived from the Darwanian concept of survival. The solutions consist of binary strings with exchange information with each other through different operations. Usually, the solutions are represented in terms of binary strings. The initial solutions are randomly generated and their cost is calculated. The genetic algorithm performs three basic operations on these solutions.

Reproduction is the process of copying the strings according to their fitness, which implies that higher fitness incurs more chances of survival.

Crossover is the process of probabilistically choosing two parents of a new solution (called child) based on their fitness value. Furthermore, the crossover site is also chosen at which the two parents are split.

Mutation randomly changes the bit values of the newly born child, because there are chances that a bit might remain unchanged by previous operations. This function can also be used to modify the newly born children which are not feasible.

Genetic algorithm can be used to optimize the weights of the ANN. The steps for this optimization are as under:

1. In the first step, the weights of the neural network are initialized as real number.

2. The neural network is run with the combination of weights in step 1 and the output of the network is compared with the original network. In this way, each solution's fitness value is recorded.

3. The solutions are chosen probabilistically among the set of all solutions based on their fitness values with a probability.

4. A crossover is applied between the two selected parents in each iteration to create a child solution. This involves selection of parents as well as the selection of split (crossover) site.

5. Mutation operation takes the child and randomly changes random number of entries. This child is now placed in the population set. In the next iteration, this child would be candidate for the parent.

5.5.4.3 Modeling of Power Systems

Each power system is composed of multiple buses, which are interconnected with each other via transmission lines. The buses can be of two types either they can be generator buses or the load bus. The admittance matrix (Y_{BUS}) or the admittance matrix is used to represent the interconnection of different buses. Since the entries of the matrix are mostly zeros so the Y_{BUS} can represent the transmission lines in a better way as compare to the bus impedance matrix (Z_{BUS}). But, the Y_{BUS} does not include the admittances which are linked with load connected to buses and the STATCOM controller. This representation is demonstrated in Figure 5.21. The steady-state model of system is illustrated by the equations of the static load flow for real and reactive powers of buses along with equality constraints of transmission network. The equation of the static load flow for a specific bus is written in terms of the voltage magnitudes and the phase angles of all buses which are connected to that bus [104]. The equation of the load flow for the real "P_i" and the reactive power "Q_i" of bus 'i' are given as:

$$P_i = \sum_{j=1}^{N} |V_i||V_j||Y_{ij}| \cos(\delta_i - \delta_j - \theta_{ij}) \tag{5.77}$$

$$Q_i = \sum_{j=1}^{N} |V_i||V_j||Y_{ij}| \sin(\delta_i - \delta_j - \theta_{ij}) \tag{5.78}$$

In Equations (5.77) and (5.78), "$|V_i|$" is magnitude of the voltage at the bus 'i', whereas "$|V_j|$" is voltage magnitude of the 'jth' bus connected to bus 'i'. 'δ' represents the corresponding phase angle of voltage and "N" is the total number of the buses in the system. "$|Y_{ij}|$" and "θ_{ij}" are the magnitude and the phase angle of the admittance respectively between the buses 'i' and 'j', "Y_{ij}" can be obtained from the admittance matrix "Y_{Bus}" of bus system, which is represented as:

$$Y_{Bus} = \begin{bmatrix} Y11 & Y12 & Y13 & \cdots & Y1N \\ Y21 & Y22 & Y23 & \cdots & Y2N \\ Y31 & Y32 & Y33 & \cdots & Y3N \\ \vdots & \vdots & \vdots & \ddots & \vdots \\ YN1 & YN2 & YN3 & \cdots & YNN \end{bmatrix} \tag{5.79}$$

Here $Y_{XY} = -y_{XY}$ is the negative of line admittance from bus "x" to bus "y", containing the real and the imaginary part. "y_{xy}" is calculated as:

$$y_{XY} = \frac{1}{R} + j\frac{1}{X} = G + jB \tag{5.80}$$

where 'G' is the conductance of line and 'B' is the susceptance (R and X being the resistance and reactance). The self-admittance terms Y_{XX} can be calculated as:

$$Y_{XX} = y_{X0} + y_{X1} + y_{X2} \ldots + y_{XX-1} + y_{XX+1} \ldots + y_{XN} \tag{5.81}$$

For each of the load bus, there are two equations for the corresponding real and the reactive powers, while there are four unknown variables of the voltages and the phase angles. Therefore, these equations are needed to be solved using the non-linear iterative methods. The most common method is the Newton-Raphson method, which requires the Jacobian of the equations. The Jacobian of the above equations can be given as:

$$\begin{bmatrix} J^1 & J^2 \\ J^3 & J^4 \end{bmatrix} \begin{bmatrix} \Delta\delta \\ \Delta|V| \end{bmatrix} = \begin{bmatrix} \Delta P \\ \Delta Q \end{bmatrix} \tag{5.82}$$

In Equation (5.82), sub-Jacobian entries are defined as $J^1 = \partial P/\partial\delta$, $J^2 = \partial P/\partial|V|$, $J^3 = \partial Q/\partial\delta$, and $J^4 = \partial Q/\partial|V|$. With addition of the STATCOM, the equations of bus connected to STATCOM are slightly enhanced.

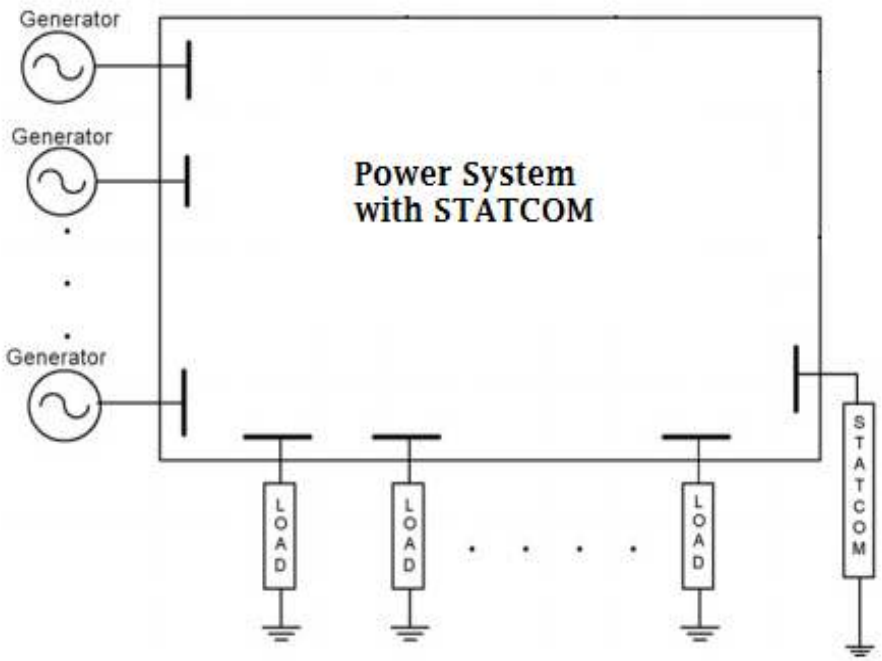

Figure 5.21 Power system representation with STATCOM [104]

5.5.4.4 Power System with STATCOM

The main purpose of STATCOM is to regulate voltage and the reactive power of power systems. Figure 5.22 demonstrates the equivalent circuit diagram of the STATCOM, which is connected to bus 'k'.

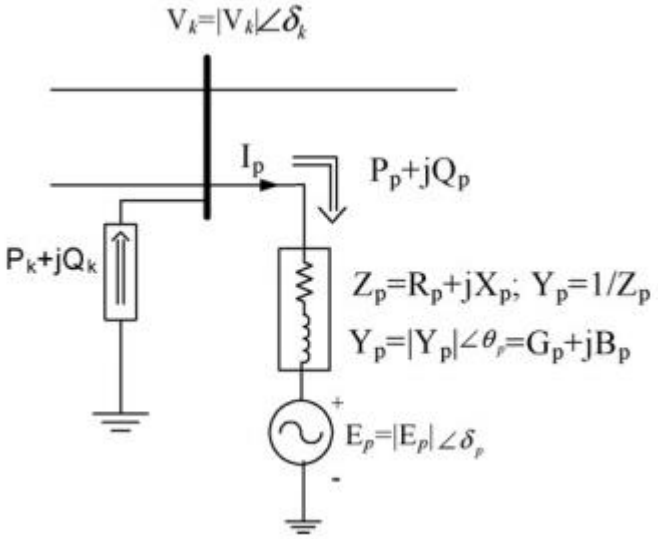

Figure 5.22 The equivalent circuit of STATCOM [104]

In Figure 5.22, STATCOM is represented by controllable voltage source with the voltage E_P and the phase angle δ_P which is connected in series with the impedance Z_P. Y_P is the admittance of link. Since admittance is complex, so the real part of impedance represents the real power losses P_P of the devices which are installed on system e.g. converters etc. The leakage inductances of coupling transformer represent the imaginary part of reactance power loss Q_P. This model of the STATCOM is connected in parallel to bus k, whose net reactive and real powers are represented as P_k and Q_k, respectively. STATCOM will inject or absorb the reactive power to keep the voltage magnitude of the bus k $|V_k|$ constant (normally at 1.0 pu) if it is being operated in the Voltage Control Mode. With the introduction of the STATCOM, the equations for the power flow are changed only for bus k, to which the STATCOM is connected. These equations are given as:

$$P_k = P_p + \sum_{j=1}^{N} |V_k||V_j||Y_{kj}| \, cos(\delta_k - \delta_i - \theta_{kj}) \tag{5.83}$$

$$Q_k = Q_p + \sum_{j=1}^{N} |V_k||V_j||Y_{kj}| \, sin(\delta_k - \delta_i - \theta_{kj}) \tag{5.84}$$

Therefore, for bus k, original equation is modified by addition of real and the reactive powers (P_P and Q_P) of STATCOM device. These powers can be further written as:

$$P_p = G_p|V_k|^2 - |V_k||E_p||Y_p| \, cos(\delta_k - \delta_p - \theta_p) \tag{5.85}$$

$$Q_p = -B_p|V_k|^2 - |V_k||E_p||Y_p| \, sin(\delta_k - \delta_p - \theta_p) \tag{5.86}$$

It is evident from Equations (5.85) and (5.86) that the STATCOM at the bus k has introduced two new variables which are voltage E_P and the phase angle δ_P. But now, $|V_k|$ is a known variable which have a predefined value. Therefore, the solution to solve the problem using Newton-Raphson method requires one more equation. By principle, in the steady-state operation, the real power which is consumed by STATCOM should be zero. Since the equation for the voltage source power should be equal to zero, the following equation is written as:

$$P_{Ep} = Real[E_p I_p{}^*] \tag{5.87}$$

$$P_{Ep} = -G_p|E_p|^2 - |V_k||E_p||Y_p|\,cos(\delta_p - \delta_k - \theta_p) \tag{5.88}$$

With this modification in Equation (5.88) of Bus k, the Jacobian matrix for the updated system is represented as:

$$\begin{bmatrix} J^1 & J^2 & J^3 \\ J^4 & J^5 & J^6 \\ J^7 & J^8 & J^9 \end{bmatrix} \begin{bmatrix} \Delta\delta \\ \Delta|V| \\ \Delta\delta_p \end{bmatrix} = \begin{bmatrix} \Delta P \\ \Delta Q \\ \Delta P_p \end{bmatrix} \tag{5.89}$$

5.5.4.5 Methodology

In this study, we have estimated the output voltages, phase angles and reactive power of the STATCOM bus using ANN with different algorithms for the training. The datasets were taken from the standard IEEE bus systems. The first step is to solve Equations (5.77) to (5.89) using any standard numerical analysis technique such as Newton-Raphson. The Newton-Raphson is an iterative method that solves the equations iteratively using assumptions in the start. The STATCOM is connected to an appropriate load bus k and the voltage magnitude $|V_k|$, phase angle δ_k and reactive power Q_k of the modified bus are also calculated using the above-mentioned equations. In order to generate large data for the STATCOM bus, the real and reactive powers of all the load buses were perturbed by increasing their values in proportions of their original values. The voltages, phase angles and reactive powers of all the buses are calculated after each perturbation. In this way, a large dataset is obtained in which the inputs are the real and reactive powers of the buses after each perturbation and the outputs are corresponding values of STATCOM bus voltage magnitude $|V_k|$, phase angle δ_k and reactive power Q_k. The whole dataset is randomly divided into two parts such that 70% of the data is used for the training of the ANN and the remaining 30% is used for testing. Three separate ANN were used: the first one is used to estimate the voltage magnitude, the second one to estimate the phase angle of the STATCOM bus, while the second one is used to estimate the reactive power. In the standard operation, the ANN has been trained using the back-propagation method which is explained in the previous section. Furthermore, the ANN is also trained using PSO, SFLA and GA.

5.6 Summary

In this chapter, four efficient techniques have been presented for the compensation of reactive power using single-phase CHB converter based STATCOM. The STATCOM provides reactive power to the system at PCC, when the STATCOM is in capacitive mode and absorbs the reactive power from the system when the STATCOM is in inductive mode. At first, we simulated the system using PI controllers and then a FLC is used. These two controllers are used in each of the control schemes: DC voltage regulation and reactive power regulation.

The designed PI controller for the STATCOM regulates reactive power at the PCC. The controller is based on individual balance control loop which helps in avoiding capacitor voltage drifting and increases the stability of the system. The system has been derived to control the model based on mathematical equations. The PI controller contains adaptive gains for the VAR regulator, which are optimized using three optimization techniques including PSO, APSO, and GSA.

Different optimization techniques such as Back-Propagation, PSO, SFLA and GA are used for the training and fine-tuning of feed forward neural networks, for the estimation of STATCOM voltages and reactive power. Finally, to enhance the performance of power system, CSAPF was used to reduce harmonics. In addition, CSAPF was also realized for reactive power compensation in power systems.

CHAPTER 6

SIMULATION RESULTS

6.1 Introduction

In this chapter, the four proposed controllers and modulation and simulation of the single-phase cascaded H-bridge multi-level converter based STATCOM have been implemented using a computer software. Modeling and control are discussed in detail, and results are tabulated. The performance of the PI controller is compared with FLC in Section 6.2. Modeling and control simulation results of single-phase CHB-STATCOMs circuits by using dq-control based on the synchronous rotating reference frame have been discussed in Section 6.3. The results of optimization techniques used for estimating the gain of PI controller are discussed and the role of STATCOM in power buses for the voltage regulation of the buses have been discussed in Section 6.4. Finally, in Section 6.5, modeling and result analysis of single-phase CHB-STATCOM based on the SAPF are discussed.

6.2 Simulation Model of Active and Reactive Power Scheme

The whole system is modeled in simulation program. A single-phase voltage source has been connected to the nonlinear (inductive and capacitive) load and four series CHBs circuit. IGBT has been chosen as the power semiconductor device. A transformer connects power system to STATCOM. Complete model of the system is shown in Figure 6.1. Simulation without STATCOM is carried out with inductive load power (450W and 450 VAR), for the time from zero to 7 seconds and with capacitive load power (450 W and 450 VAR) for the time from 7 to 14 seconds with power factor 0.7 for each load as shown in Figure 6.2. Table 6.1 is summarizing the model parameters.

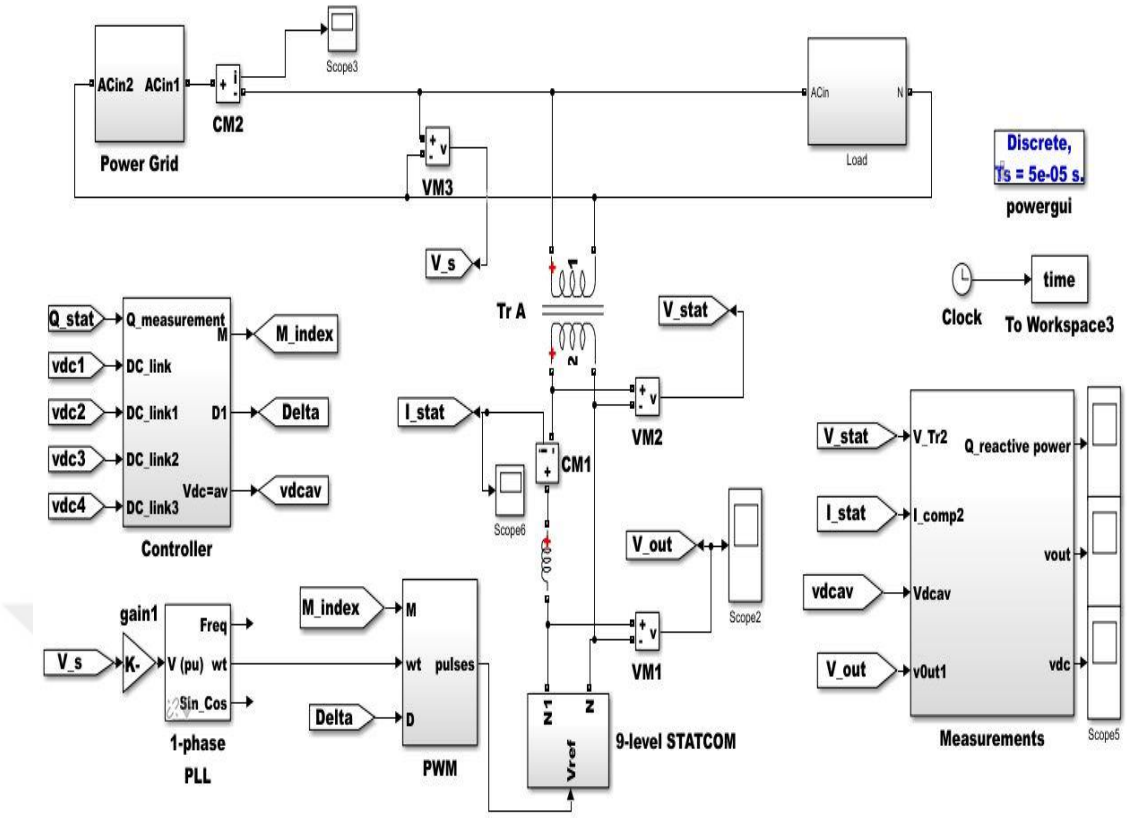

Figure 6.1 Block diagram of the complete system

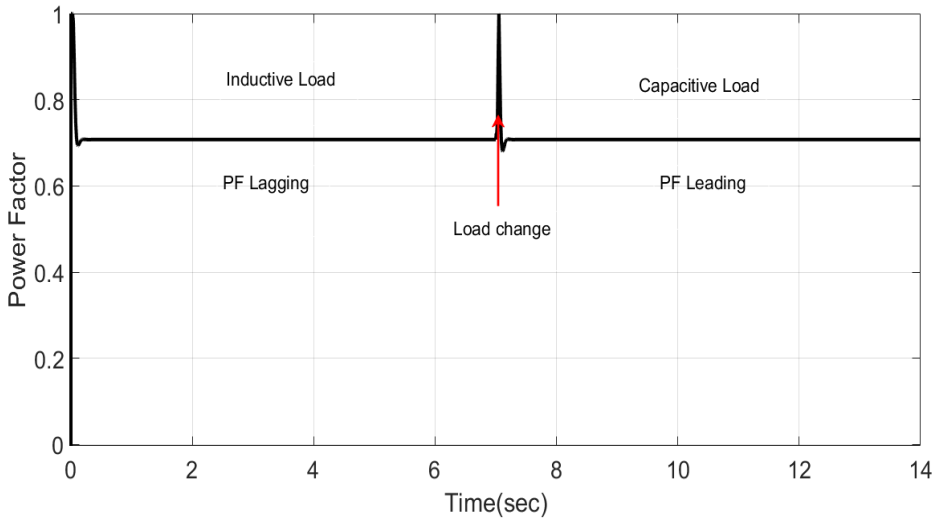

Figure 6.2 Power factor of the PCC without STATCOM

Table 6.1 The model parameters

Type	Parameter	Value
Source	Peak Amplitude	311.12 V
	Frequency	50 Hz
Load	Nominal Voltage	220Vrms
	Active Power	450 W
	Inductive Reactive Power	450 VAR
	Capacitive Reactive Power	450 VAR
DC Link	Reference DC Link Voltage	40 V
PLL	Regulator Gain (k_P)	180
	Regulator Gain (k_I)	32000
	Regulator Gain (k_D)	1
Coupling Transformer	Nominal Power	5000 VA
Winding-1 Parameters	Voltage	220 V
	Resistance	0.0005 pu
	Inductance	0.0005 pu
Winding-2 Parameters	Voltage	110 V
	Resistance	0.0005 pu
	Inductance	0.0005 pu

6.2.1 Simulation Result of Active and Reactive Power Scheme with PI Control

For testing, reactive power reference signal for STATCOM is generated as shown in Figure 6. 3. Figure 6.4 depicts nine level output voltage waveform of STATCOM with lagging power factor. The STATCOM voltage and current are shown in Figure 6.5. The average DC link capacitor voltage is shown in Figure 6.6.

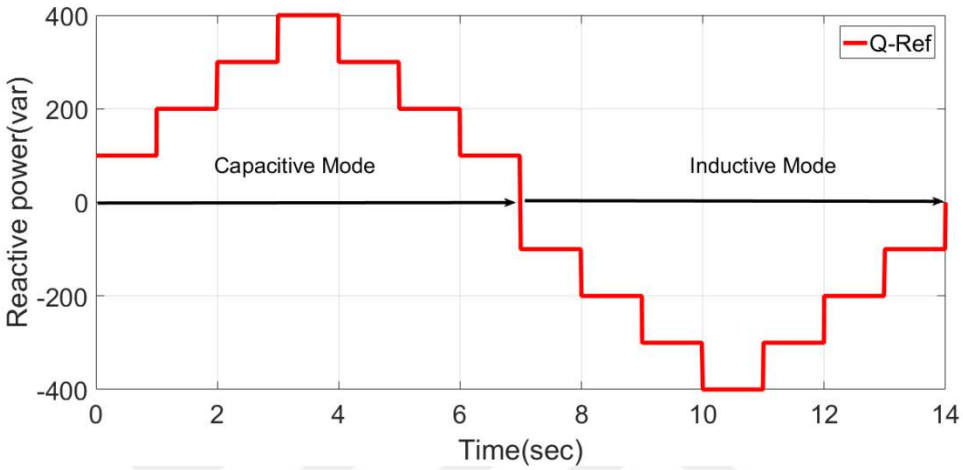

Figure 6.3 Reactive power reference signal for STATCOM

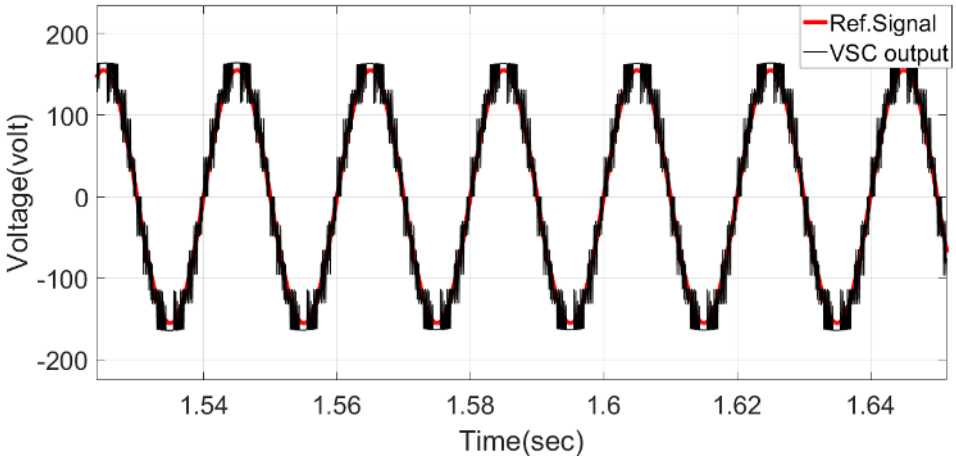

Figure 6.4 Nine-level STATCOM output voltage waveform and reference signal under PI control

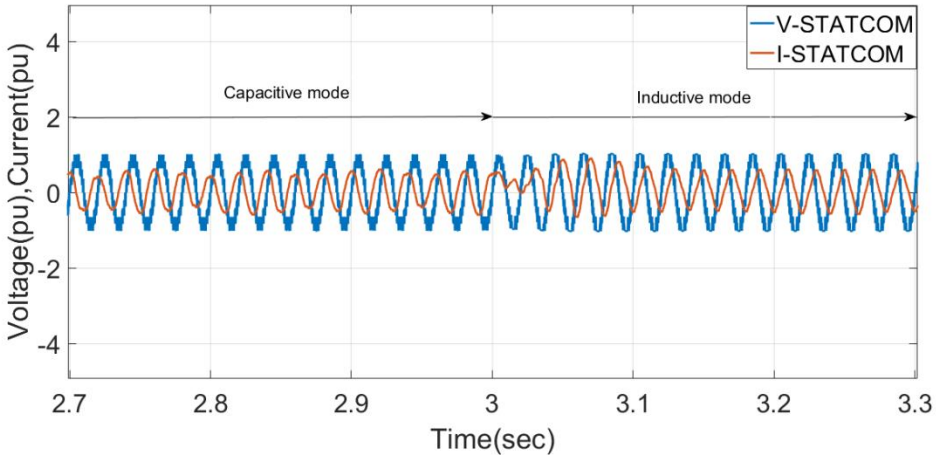

Figure 6.5 Nine-level STATCOM voltage and current in inductive and capacitive modes

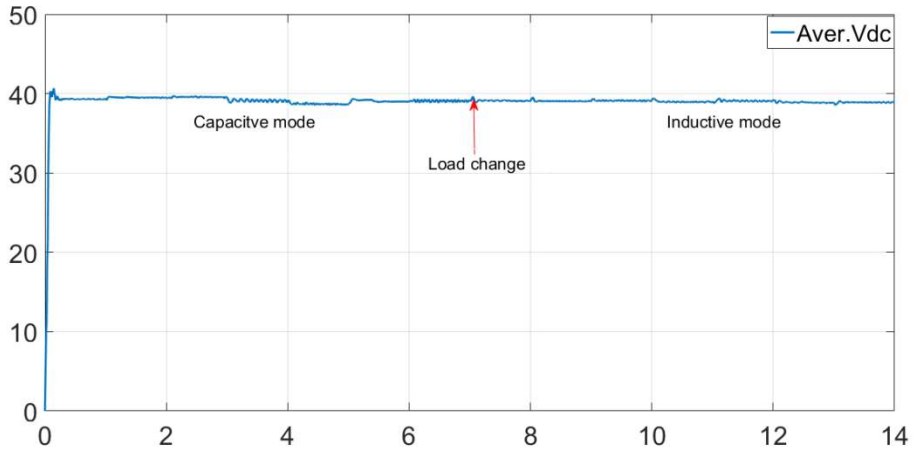

Figure 6.6 The average of DC link capacitor voltages in inductive and capacitive modes under PI control

Figure 6.7 depicts that the STATCOM reactive power is tracking the reference signal properly. It can be concluded that the PI reactive controller for STATCOM is working well. Moreover, Figure 6.8 shows the grid side reactive power, for the time from zero to 7 seconds and with an inductive load, the STATCOM injects reactive power to load and the reactive power which is supplied from the grid side is reduced, for the time from 7 to14 seconds and with a capacitive load, the STATCOM absorbs reactive power from the grid side.

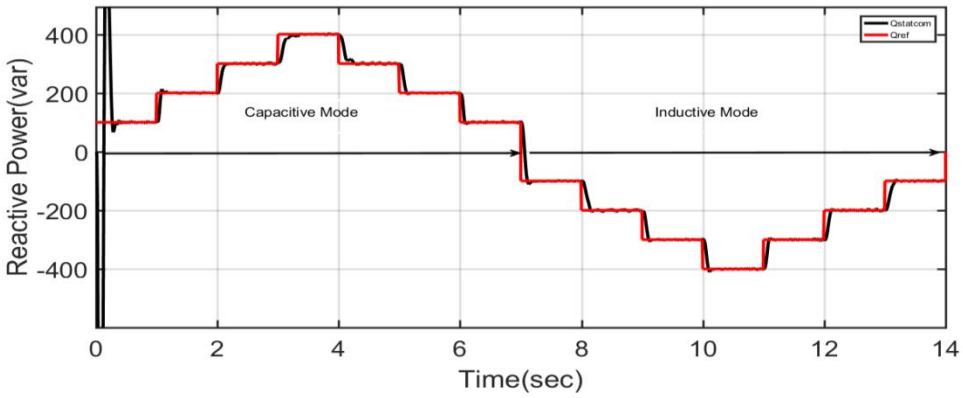

Figure 6.7 STATCOM reactive power with PI control

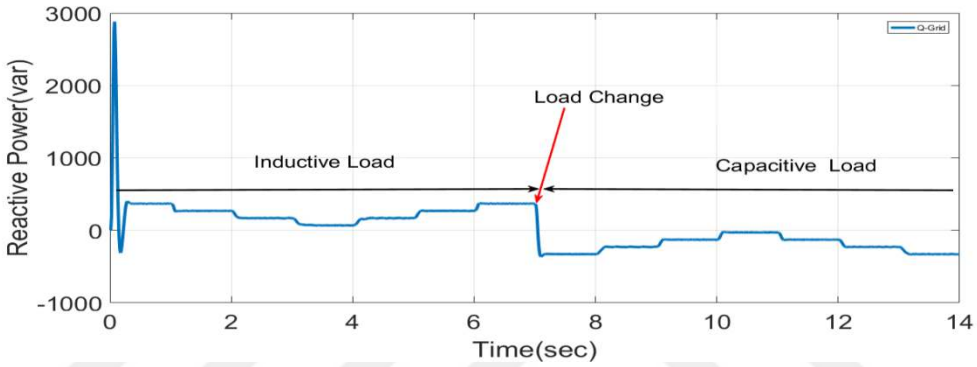

Figure 6.8 Reactive power taken from grid with PI control

6.2.2 Simulation Results of Active and Reactive Power Scheme with FLC

We changed the PI controller discussed in previous section with FLC. There are two FLC controllers implemented in STATCOM, one controller is for reactive power regulation, and second one is for DC link capacitors voltage control which is associated with the phase shift angle. In practical, a small amount of internal power loss is associated with the VSC, making a small phase angle between the AC power system and STATCOM voltage. This small phase shift causes a small amount of active power flow from the power system to the STATCOM. The system model and its parameters are same as in case of using PI controller. Figure 6.9 depicts the nine level of the output voltage for the STATCOM with FLC, while the average DC link capacitor voltage is shown in Figure 6.10.

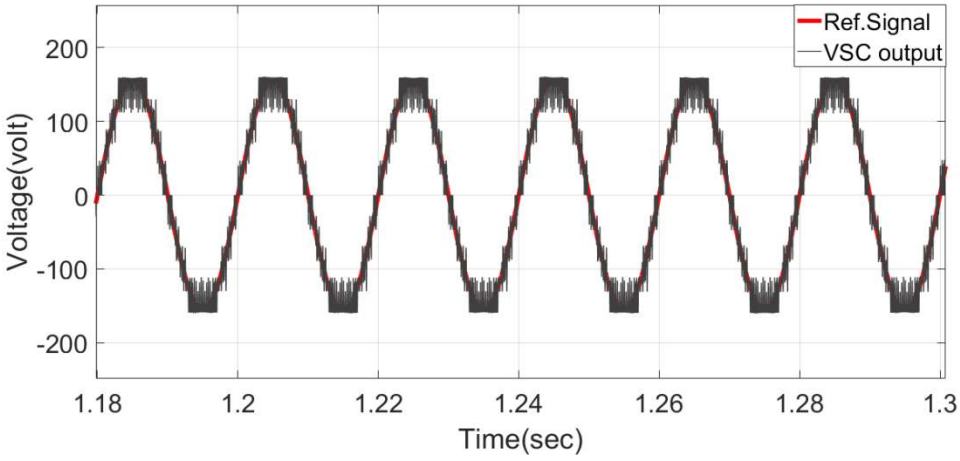

Figure 6.9 Nine-level STATCOM output voltage waveform and reference signal under FLC

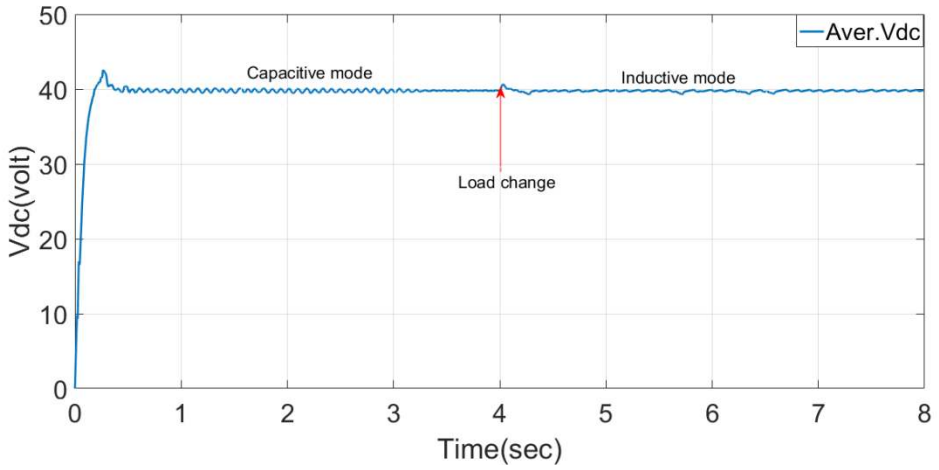

Figure 6.10 The average of DC link capacitor voltages with FLC

Figure 6.11 shows the reactive power when FLC is used and Figure 6.12 shows the grid side reactive power for the capacitive mode. STATCOM injects reactive power to load and the reactive power which is supplied from the grid side is reduced. For the inductive mode, the STATCOM absorbs reactive power from the grid side.

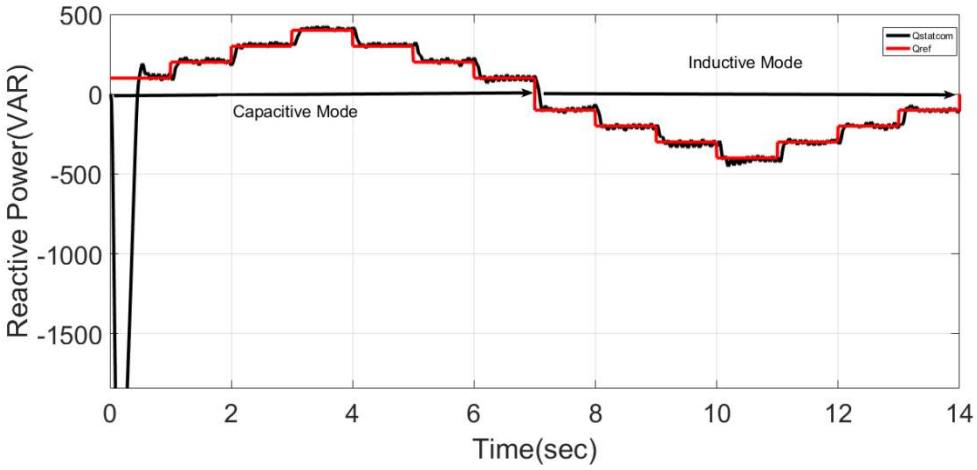

Figure 6.11 STATCOM reactive power with FLC

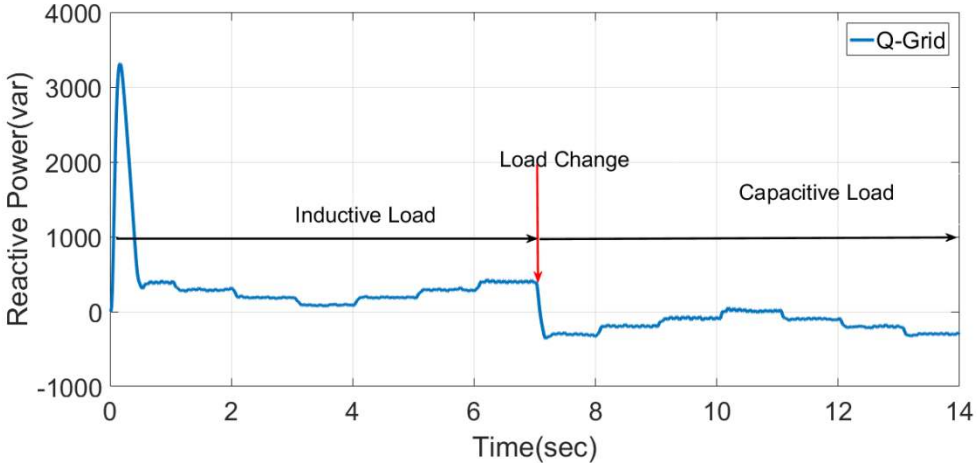

Figure 6.12 Reactive power taken from grid with FLC

The power factor of the load without using STATCOM is 0.7, as shown in Figure 6.2. After the STATCOM is activated, the power factor of the PCC is improved with STATCOM, as shown in Figure 6.13.

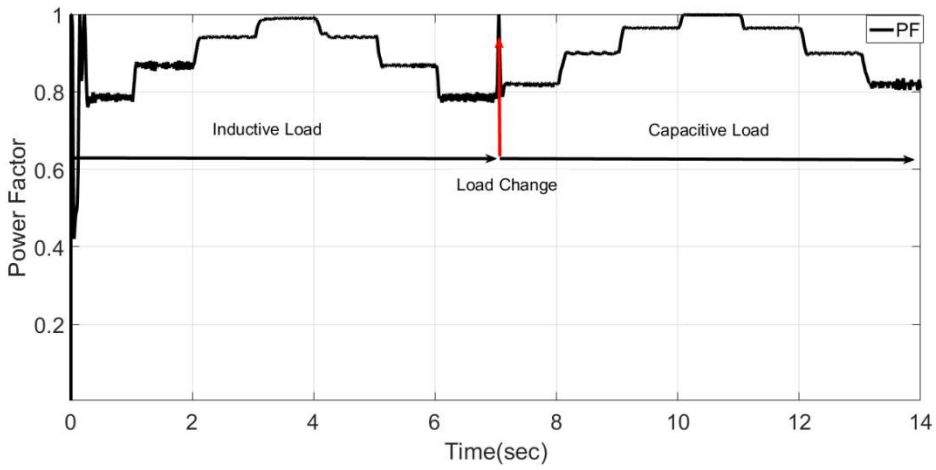

Figure 6.13 Power factor of the PCC with STATCOM

6.2.3 Result Comparison of PI Controller and FLC

In the case of PI controller, the undershoots are present in the waveform of reactive power which is supplied by STATCOM. This situation can be observed clearly by comparing Figure 6.7 and Figure 6.11. These undershoots are removed by FLC as shown in Figure 6.11. In case of reactive power taken from grid side, and with using PI control, the undershoots are observed as shown in Figure 6.8. While this undershoots are removed by using FLC, as shown in Figure 6.12. The FLC is more robust and flexible control technique than PI control, as FLC have more parameters (types membership functions and parameters in the fuzzification and defazzifcation modules).

6.2.4 Conclusion

In this section, two efficient control techniques for the compensation of reactive power using single-phase nine-level STATCOM have been presented. The STATCOM provides reactive power to the system when it is operating in capacitive mode and absorbs reactive power when it is operating in inductive mode. The power factor of the PCC without STATCOM is 0.7 lagging for inductive load and 0.7 leading for capacitive load. Nevertheless, after the addition of STATCOM, the power factor of the PCC is improved and the power factor follows the reference signal with the values of 0.78, 0.87, 0.94 and 0.99 lagging for capacitive mode with inductive load. While in inductive mode with capacitive load, the values followed are 0.8, 0.89, 0.96, and 0.99 leading. At first, we simulated the system using two PI controllers and then a FLC is

used for the second case. The simulations results suggest that FLC is better as compared to the PI control because in PI controller there are undershoots while in case of FLC these undershoots are removed.

6.3 Simulation Model of dq-Control Scheme

A single-phase, 220V, 50 Hz AC source is used. A non-linear load is connected on AC voltage terminals, and an inductive load is implemented for first half period of simulation and later capacitive load is connected instead. However, load draws 450 W and 450 VAR that must be delivered by AC voltage source. The reactive power is consumed by the load, generator is deemed to produce the required current to the load all the times. In such circumstances, transmission line is subjected of power losses with more demand of reactive power in case of inductive load expansion, this in turn degrades the performance of power system. ±400 VAR single-phase CHB-STATCOM model is shown in Figure 6.14. The STATCOM consists of six ($n = 6$) identical CHBs connected in series from their AC sides with thirteen level ($2n + 1$). Single-phase STATCOM is proposed in this thesis to compensate the reactive power and enhance the system performance.

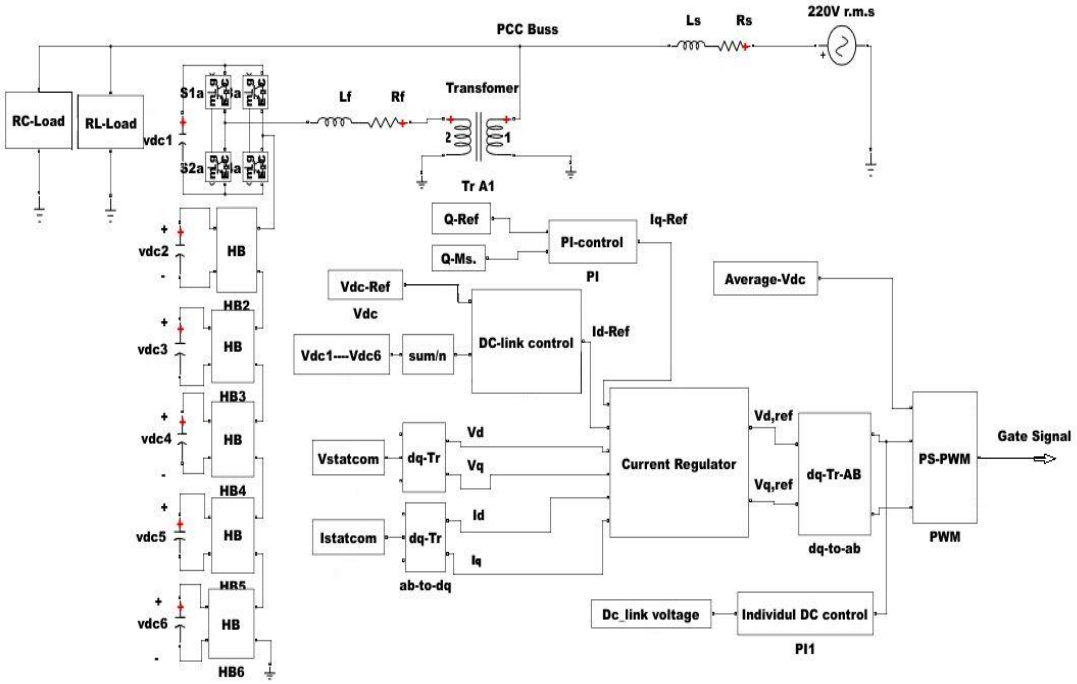

Figure 6.14 Overall simulation model of STATCOM

Table 6.2 is summarizes the model parameters of single-phase 13-level STATCOM system. A 220/110 V coupling transformer is used to provide the connection between power grid and the STATCOM. This means that 110 V rms or equal to 155V max is required to be generated by STATCOM. Each DC capacitor is in turn deemed to produce 25.9 V. This value is the reference of the DC link voltage.

Table 6.2 The model parameters of single-phase 13-level STATCOM system

Type	Parameters	Values
Source	Peak Amplitude	311.12 V
	Frequency	50 Hz
Load	Nominal Voltage	220 V
	Nominal Frequency	50 Hz
	Active Power	450 W
	Reactive Power Inductive	450 VAR
	Reactive Power Capacitive	450 VAR
DC Link	Reference DC Link Voltage	25.9 V
Coupling Transformer	Nominal Power	1000 VA
	Nominal Frequency	50 Hz
Winding-1 Parameters	Voltage	220 V
	Resistance	0.0005 pu
	Inductance	0.0005 pu
Winding-2 Parameters	Voltage	110 V
	Resistance	0.0005 pu
	Inductance	0.0005 pu

6.3.1 Simulation Results of dq-Control

The reactive power reference signal for 13-level STATCOM model is a group of step functions, as shown in Figure 6.15. In order to verify the efficacy of the designed controller, decoupled control strategy is used as shown in Figure 5.16. Detailed simulation is carried out while the total time of simulation is set to 14 seconds. During 0-7 seconds of simulation, the STATCOM works in the capacitive mode and therefore injects about 100-400VAR of reactive power into the system. On the second half of simulation duration 7-14 seconds, the STATCOM works in the inductive mode and therefore absorbs about 100-400VAR of reactive power from the system.

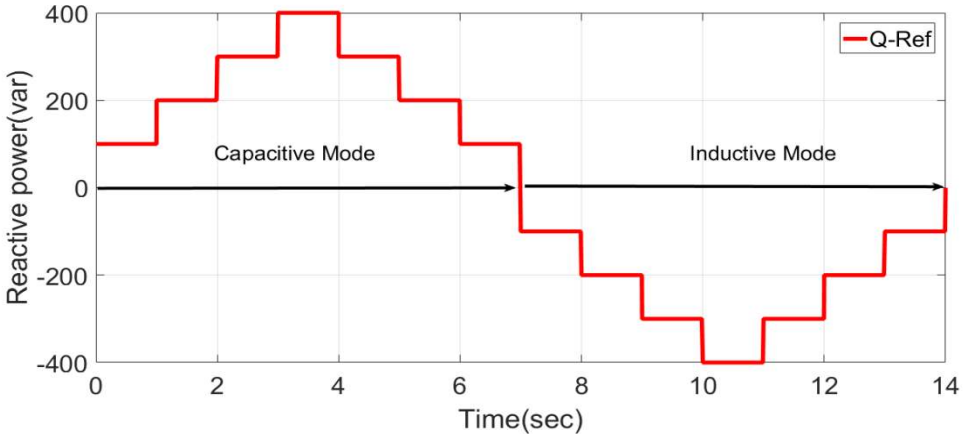

Figure 6.15 Reactive power reference signal for 13-level STATCOM

By using the single-phase dq-transformation, the STATCOM voltage is transformed into dq-frame, as shown in Figure 6.16.

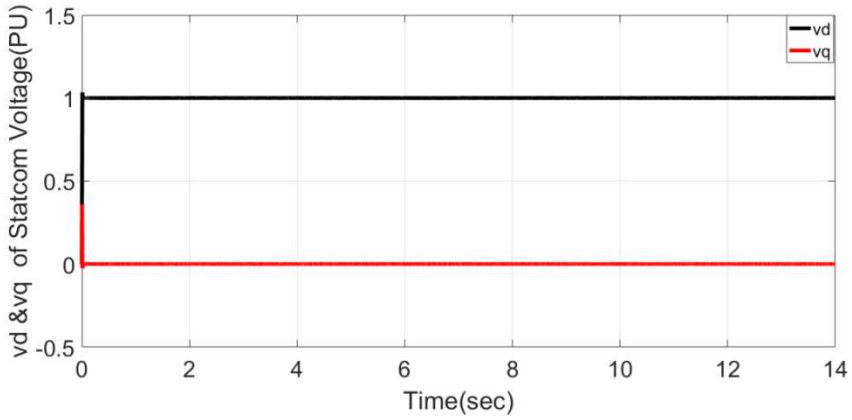

Figure 6.16 STATCOM output voltage in dq- reference component

Figure 6.17 and Figure 6.18 respectively depicts, the d-component (i_d) and q-component (i_q) of STATCOM AC current following towards the reference current signal i_{dref} and i_{qref}. It is understood that is STATCOM well working as per our requirement. For i_q, the negative sign indicates that the STATCOM injects reactive power into the system, while for positive sign, the STATCOM absorbs the reactive power.

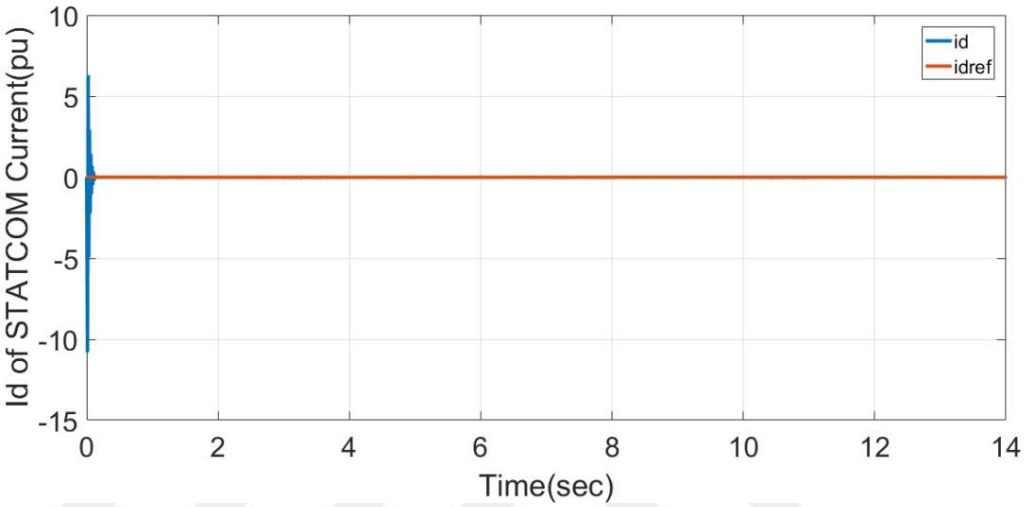

Figure 6.17 D- Component of STATCOM current

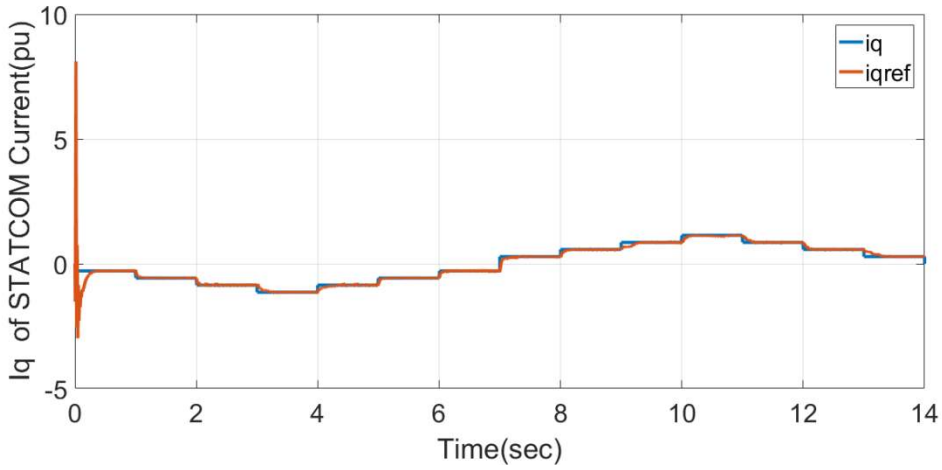

Figure 6.18 Q- Component of STATCOM current

Figure 6.19 depicts that reactive power is tracking the reference signal, which shows that our proposed controller is working well.

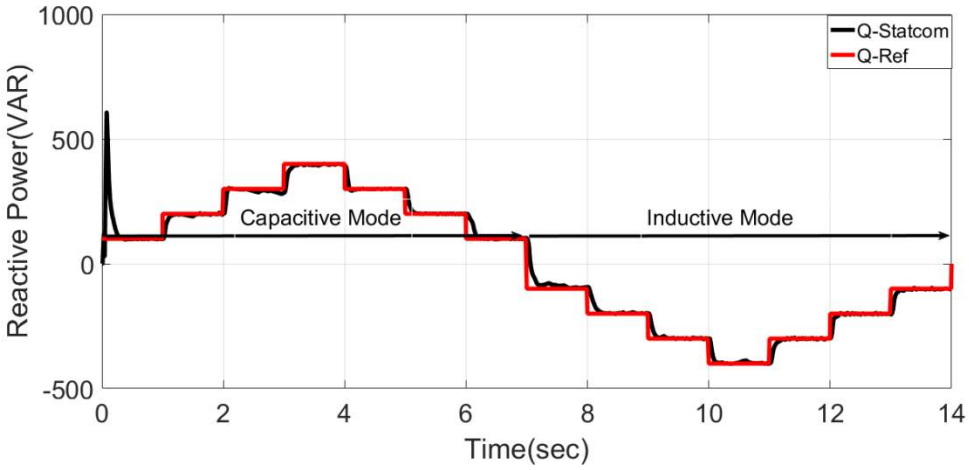

Figure 6.19 Reactive power of STATCOM

Depending on the magnitude of STATCOM voltage ($V_{STATCOM}$) and the magnitude of the voltage at PCC (V_{PCC}), If $V_{STATCOM} > V_{PCC}$, STATCOM generates reactive power, while when, $V_{STATCOM} < V_{PCC}$ reactive power will be absorbed by STATCOM as shown in Figure 6.20.

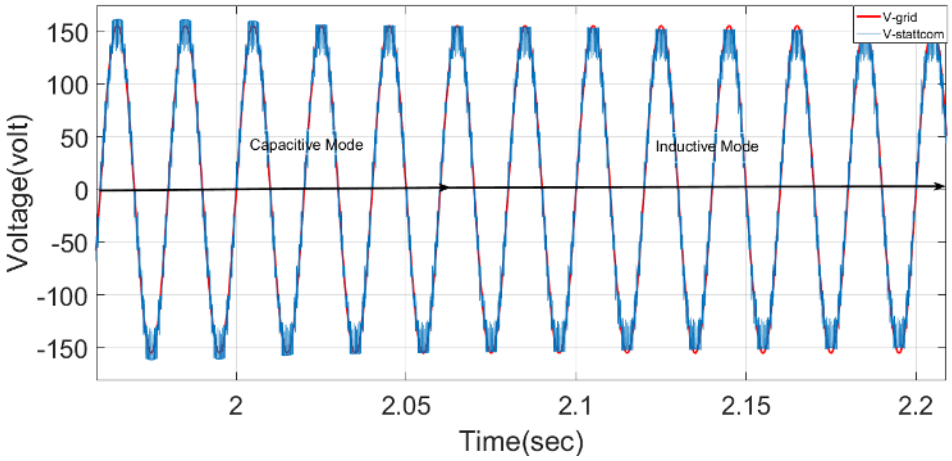

Figure 6.20 STATCOM output voltage with 13-level

Figure 6.21 shows the STATCOM line currents and voltages. At first STATCOM is operated in capacitive mode up to 3 seconds, in inductive mode for the next 3 seconds duration and $I_{STATCOM}$ leads/lags 90° $V_{STATCOM}$ in capacitive/inductive mode. The DC link voltage of each capacitor for 13-level STATCOM is shown in Figure 6.22.

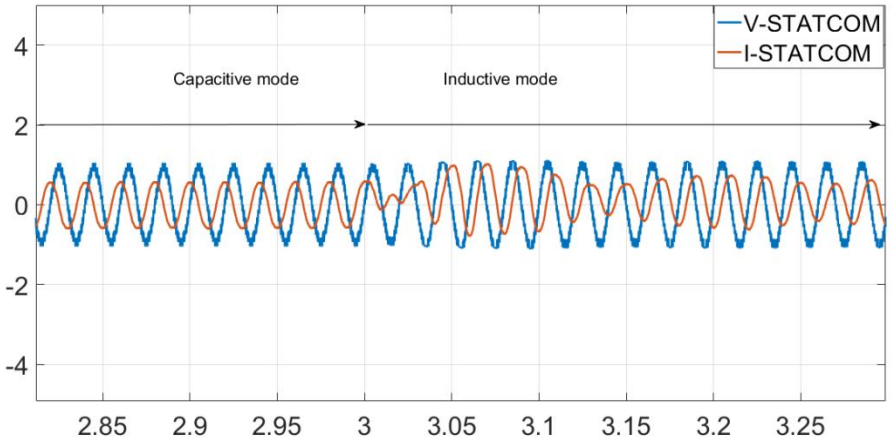

Figure 6.21 13-level STATCOM voltage and current

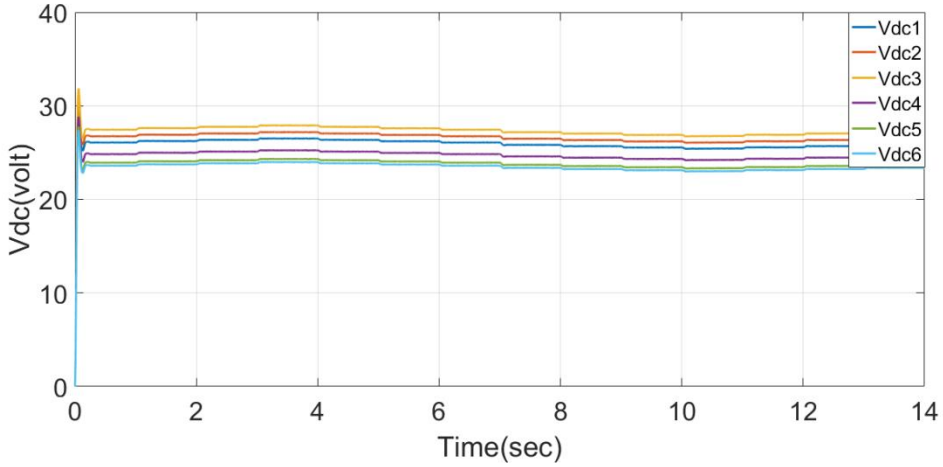

Figure 6.22 Capacitor voltages for each H-bridge

Figure 6.23 depicts that the STATCOM injects about 0.6 pu of reactive power into the AC network at PCC and draws about 0.01pu of real power to compensate the added losses. The active and reactive powers supplied or absorbed by STATCOM to/from system are proportional to d and q-axis currents, respectively.

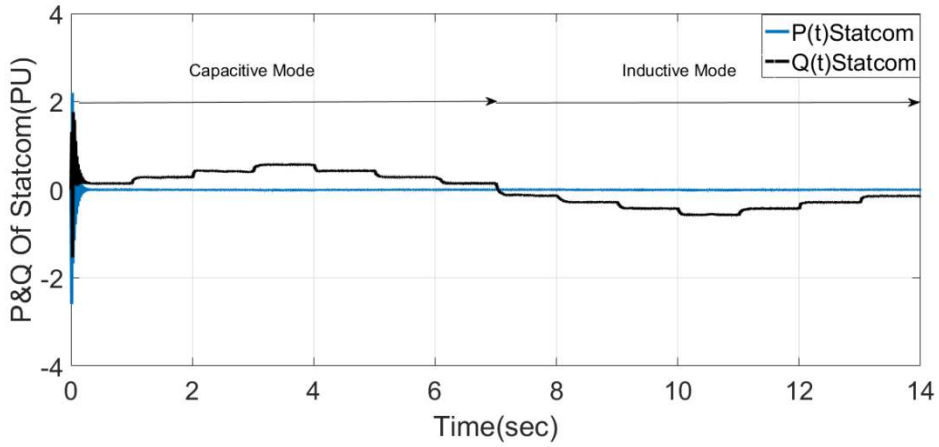

Figure 6.23 Active and reactive powers of STATCOM

6.3.2 Conclusion

In this section, STATCOM is proposed to handle the reactive power demanded by the reactive load. It is compensating reactive power by injecting the same value into power grid. The system is implemented as three separate entities; the power grid, STATCOM and overall controller scheme. The procedure above is clarified that the required arrangements are done on a PI controller so that STATCOM can work in both reactive mode and capacitive mode. The previous detailed structure was implemented by Simulation program and the virtual model of the same has made to run over 14 seconds where inductive load is inserted during the first half of this period and rest of the time is hold for capacitive load. Performance of this model is examined by monitoring the system response of reactive power exchanging between the compensator and power grid. However, reactive power (Q) is injected during the first period of simulation and absorbed in the second half period of simulation. The portion of Q exchanged between system terminals is relative to reactive power amount that supplied or absorbs according to the reference signal.

6.4 Simulation and Results of Dq-Control with Optimization Algorithms

The wye-connected three-phase designed $\pm 25KVAR$ CHB-STATCOM model is shown in Figure 6.24. The STATCOM consists of six ($n = 6$) identical CHBs connected in series from their AC sides. AC side of STATCOM has 13-Levels ($2n + 1$) CHB topology. Each HB has an individual DC link made by a DC capacitor. The proposed DC link voltage control method is applied for reactive power control in the STATCOM, in which it can inject/draw reactive power to/from the system, depending on the magnitude of $V_{STATCOM}$. The phase differences between $V_{STATCOM}$ and V_{PCC} voltages result in active power exchange between STATCOM and the system.

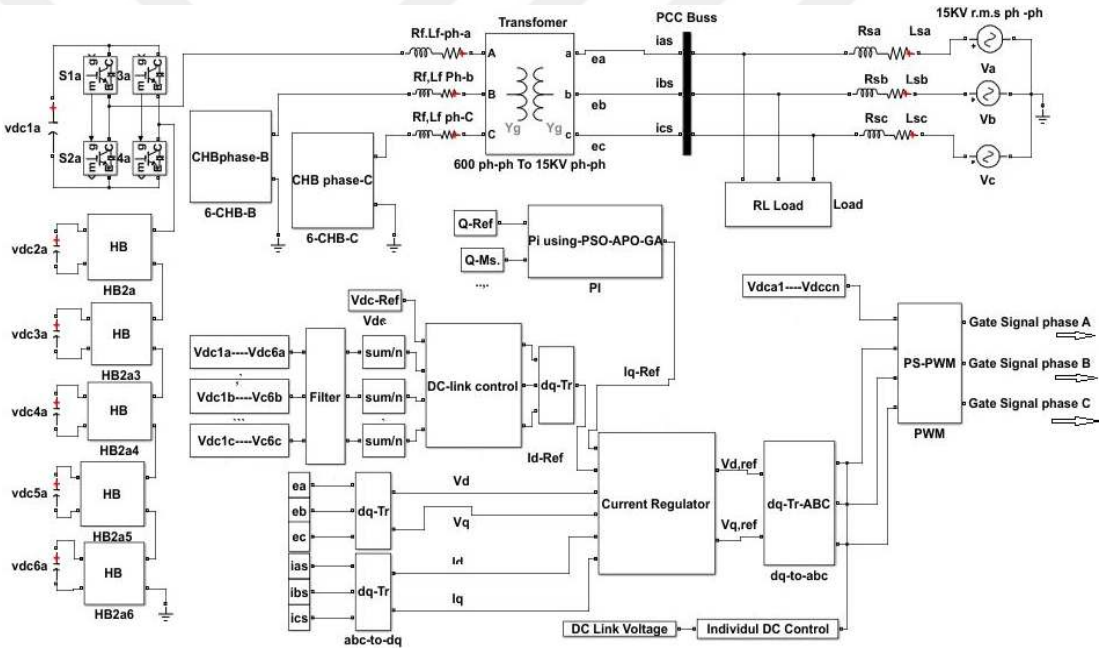

Figure 6.24 Overall simulation model of STATCOM

The reference signal for reactive power is a step function, as shown in Figure 6.25. To verify the efficiency of the designed controller and establish the effectiveness of the optimization techniques, detailed simulations were carried out. An overview of the system parameters is tabulated in Table 6.3.

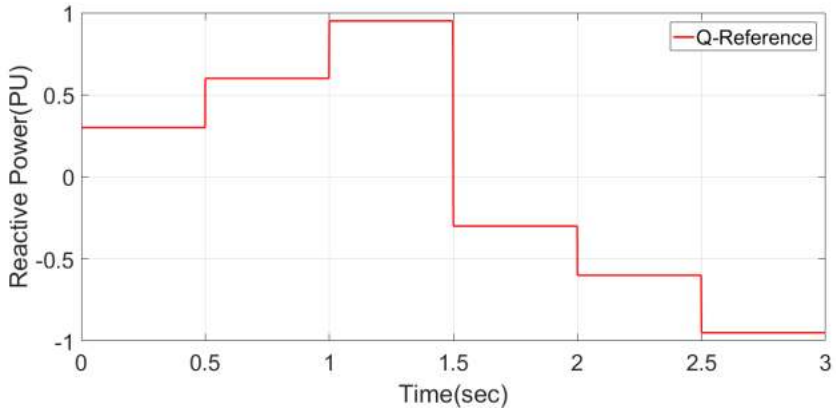

Figure 6.25 Reactive power reference signal

Table 6.3 Parameters of the system model

Parameter	**Value**
PCC Voltage (L-L)	1.5 kV
System frequency	50 Hz
Carrier frequency for PWM	1800 Hz
DC Capacitor value	3500 μF
Filter inductance	10 mH
Filter resistor	0.25 Ω
DC link voltage of each cell	80 V
Number of cells per phase	6
Load Active power Inductive reactive power	 1 MW 100 KVAR

The resulting capacitor voltages in phase (A) are shown in Figure 6.26. The total time of simulation is set to 3 seconds. During 0-1.5 seconds of simulation, STATCOM works in the capacitive mode and therefore injects about 0.3-0.9 pu of reactive power

into the system. This trend gives bulge to the DC capacitor voltage and the q-axis current becomes negative. However, to mitigate IGBT switching loss and core loss in transformer, the STATCOM draws 0.02 pu of reactive power from the system. During the time interval 1.5-3 seconds, the STATCOM undergoes inductive operation and draws about 0.3-0.9 pu of reactive power from the system, thus dropping the DC capacitive voltage and making the q-axis current positive. The voltage ripples are 5V. It can be seen from Figure 6.26 that all the DC capacitor voltages are regulated to 80V reference signal.

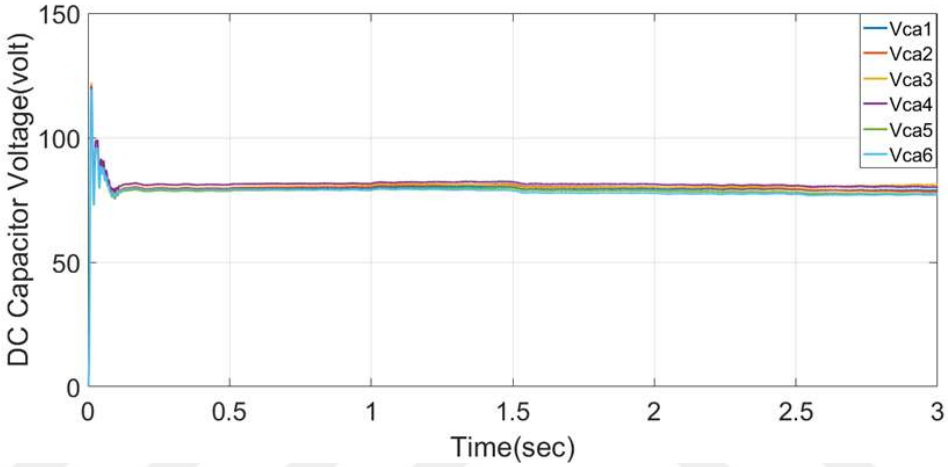

Figure 6.26 Capacitive voltages in phase-a

Figure 6.27 shows the STATCOM line currents and voltages in phase-a. At first STATCOM is operated in capacitive mode up to 1.5 seconds, in inductive mode for the next 1.5 seconds duration and leads/lags 90° in capacitive/inductive mode.

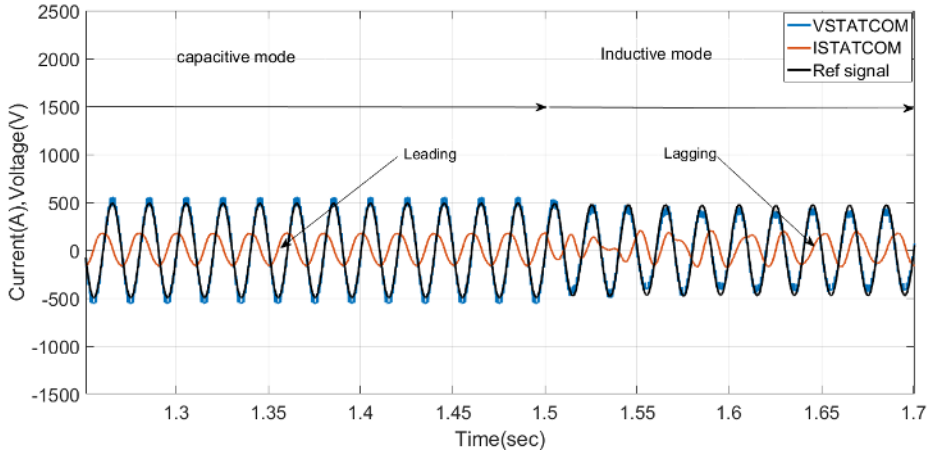

Figure 6.27 STATCOM output voltage and current in phase-a

Figure 6.28 and 6.29 reveal that 13-Levels (0Vdc, ∓1Vdc, ∓2Vdc, ∓3Vdc, ∓4Vd, ∓5Vdc, ∓6Vdc) STATCOM phase-a voltage is synchronized to PCC bus in two capacitive/inductive modes.

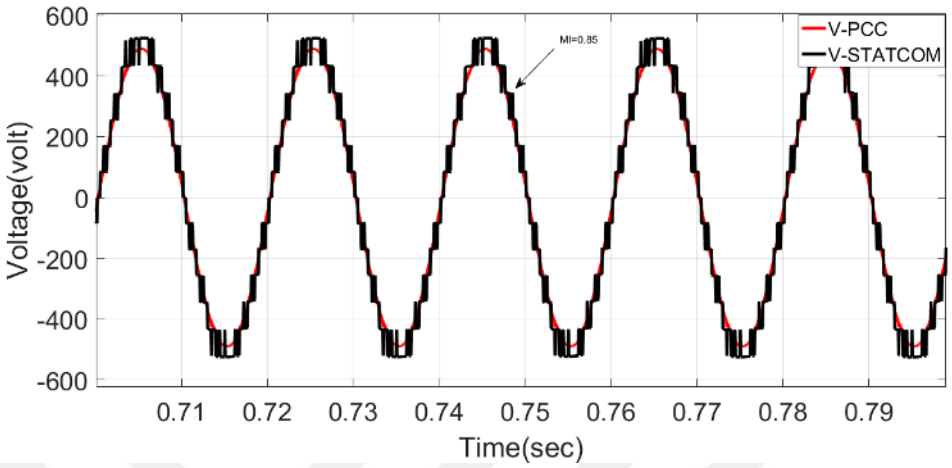

Figure 6.28 STATCOM phase-a voltage: STATCOM line-to-neutral voltage in capacitive mode

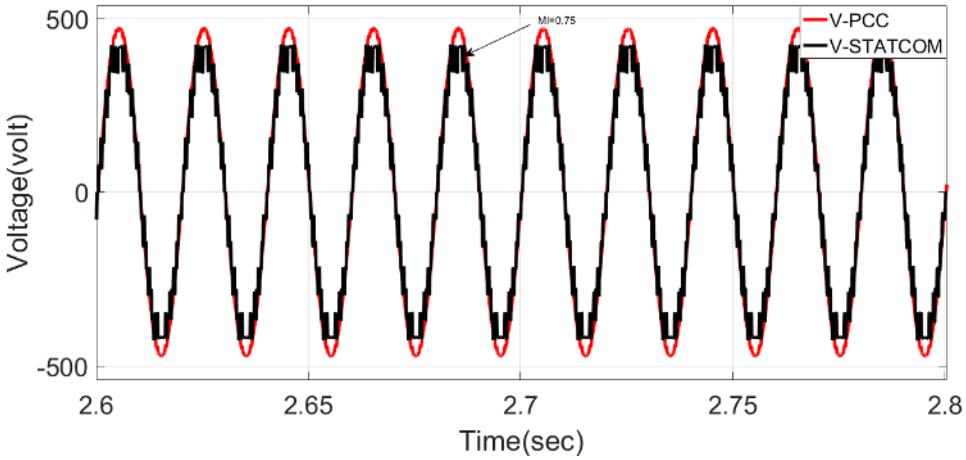

Figure 6.29 STATCOM phase-a voltage: STATCOM line-to-neutral voltage in inductive mode

Another important factor to consider in STATCOM based applications is the Total Harmonic Distortion (THD) introduced in the system. This is tabulated in Table 6.4 for both capacitive and inductive modes together with three different voltage levels.

Table 6.4 Total harmonic distortion

Voltage Level	$V_{STATCOM}$ (Capacitive mode)	VS_{TATCOM} (Inductive mode)	$I_{STATCOM}$ (Capacitive mode)	$I_{STATCOM}$ (Inductive mode)
9	13.1 %	13.7 %	3.98 %	4.71 %
11	11.3 %	12.2 %	3.51 %	4.3 %
13	9.2 %	9.3 %	3.3 %	4.1 %

Next, we present the results of applying PSO, APSO and GSA for the tuning of PI parameters of reactive power control, which are discussed before. The role of optimization techniques is to tune the parameters (K_p and K_i) of the PI controller, such that STATCOM tracks the change in reference reactive power and the resulting reference reactive current, accordingly. To measure the difference between the expected and original signals, Integral of Absolute Error (IAE) is assumed as the metric, based on which the optimization algorithms converge to the optimal solution. For PSO and APSO, 30 initial solutions have been used after some trials. In case of GSA, the initial objects are taken as 30, while the initial value of gravitational constant is taken as 100. The total iterations for PSO, APSO, and GSA are fixed at 50.

6.4.1 PSO

In this section, we present the results of applying PSO for the tuning of PI parameters of reactive power control. The trajectory of performance index and the corresponding shift in the PI parameters are shown in Figure 6.30. IAE in this case, is shown in Figure 6.31 for the PSO over the course of 50 iterations.

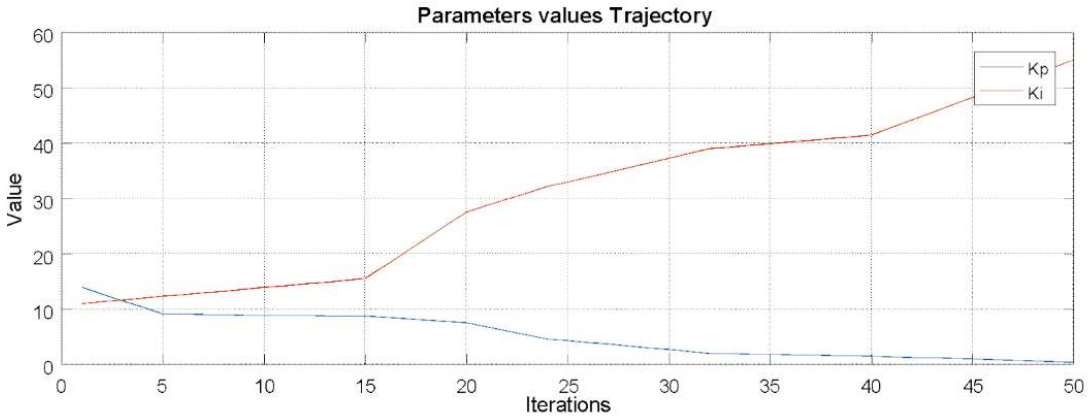

Figure 6.30 Trajectory of PI parameters with iterations in PSO

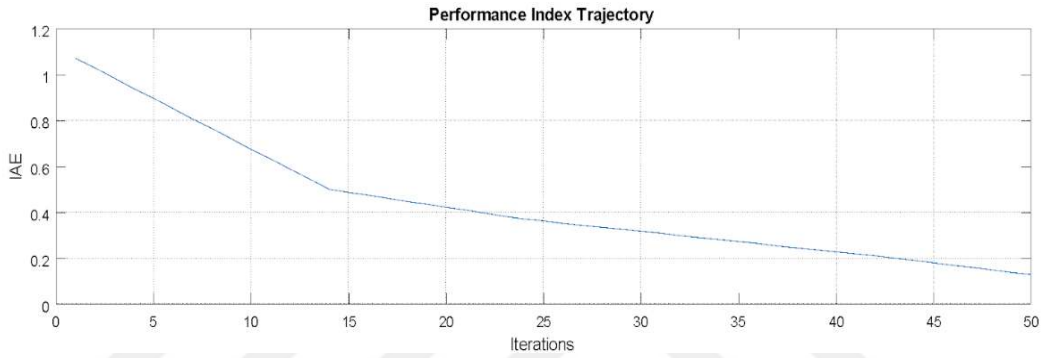

Figure 6.31 Trajectory of IAE with iterations in PSO

As evident from the Figure 6.32, the tracking of the reactive power and reactive current is efficient and STATCOM can track the reference reactive power signals. However, the transients of the tracking are huge in the start. The overshoot can be approximated as 6% in the first stage of the reactive power tracking, while the settling time is around 0.27 seconds. For the tracking of current, all the minor changes are tracked immediately by the STATCOM.

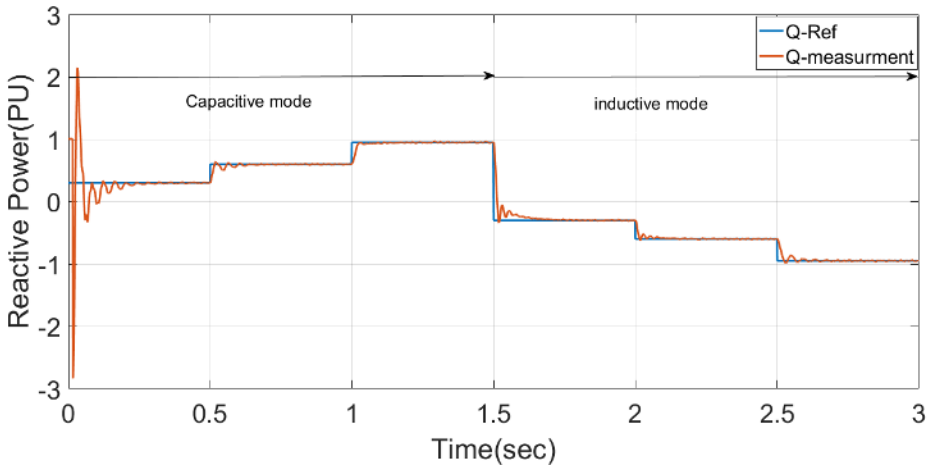

(a) Reference (blue) and measured (red)

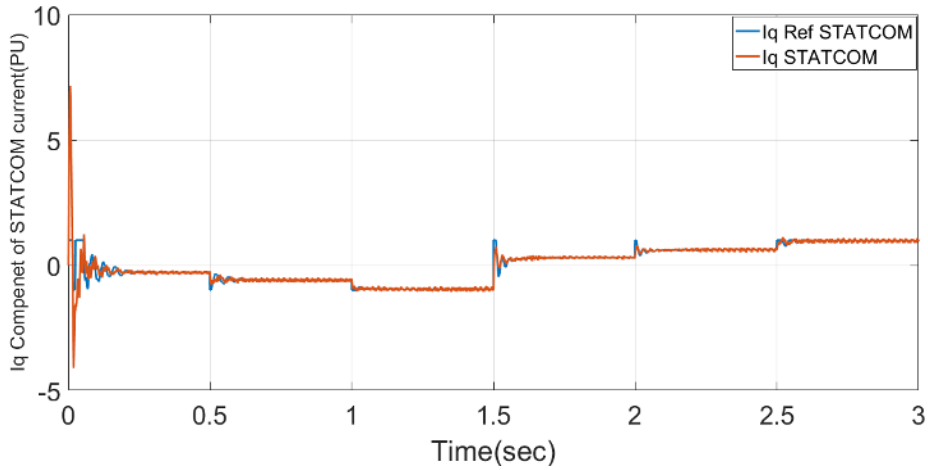

(b) Reference(blue) and measured (red)

Figure 6.32 (a) STATCOM tracking of reactive power Q (b) I_q current through PSO tuning of PI controller

6.4.2 APSO

Similarly, for APSO, the corresponding parameters of reactive power control for each iteration are shown in Figure 6.33. The related stays within 10% of its initial value, but undergoes drastic change in each iteration. The improvement in the cost function for different iterations is shown in Figure 6.34. This can be observed that fall in the IAE over the course of iterations is almost smooth from the beginning, except in the later part, where the slope gets gentler.

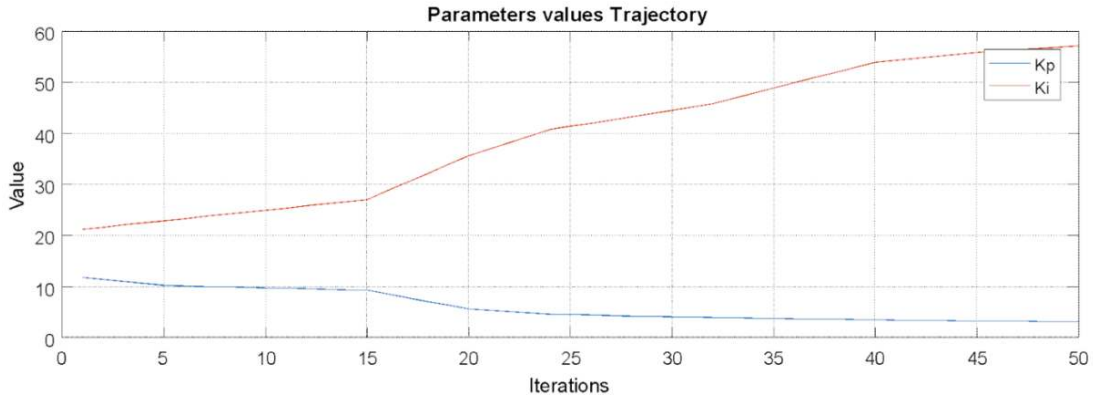

Figure 6.33 Trajectory of PI parameters with iterations in APSO

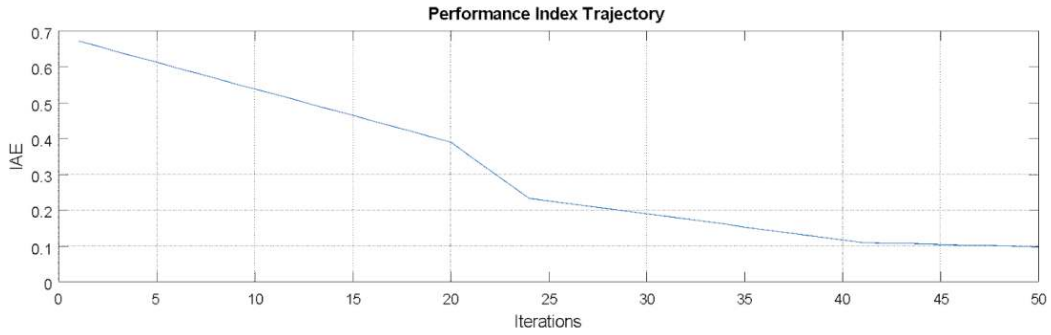

Figure 6.34 Trajectory of IAE with iterations in APSO

The tracking in both cases is efficient with slight perturbation in the start. This is shown in Figure 6.35. The overshoot is slightly less than that of PSO, while the cost (IAE) is less than that of PSO. This can be attributed to the more random approach taken by the APSO which overlooks the local best solution of each particle. However, the tracking of reactive current shows slightly higher overshoot than in the case of PSO.

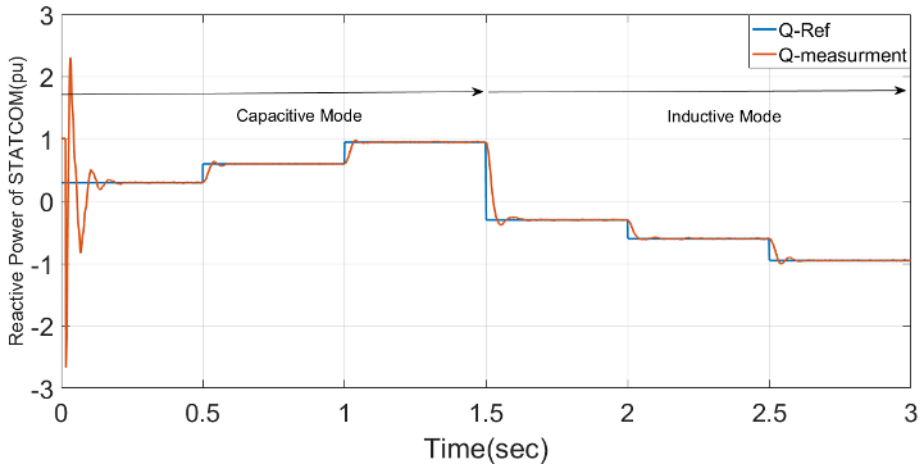

(a) Reference (blue) and measured (red)

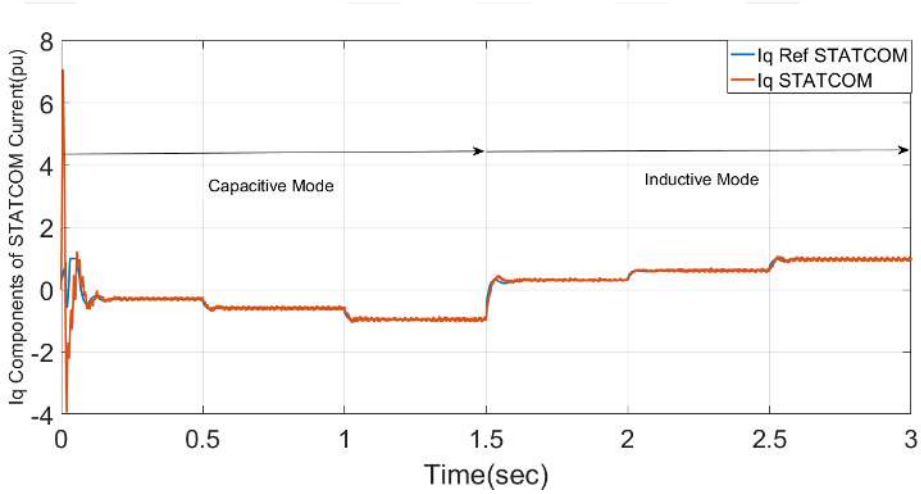

(b) Reference(red) and measured (blue)

Figure 6.35 (a) STATCOM tracking of reactive power Q (b) I_q current through APSO tuning of PI controller

6.4.3 GSA

Similarly, the algorithm runs with continuous improvement in the initial stage, starting from 0.68 seconds. After iteration 23, the cost begins to roll down radically and finally culminates at around 0.1023. On the other hand, the trajectory of PI parameters for reactive power control is shown in Figure 6.36. The parameter undergoes slight change in total 50 iterations, while goes through major shift, the performance index trajectory for GSA is shown in Figure 6.37.

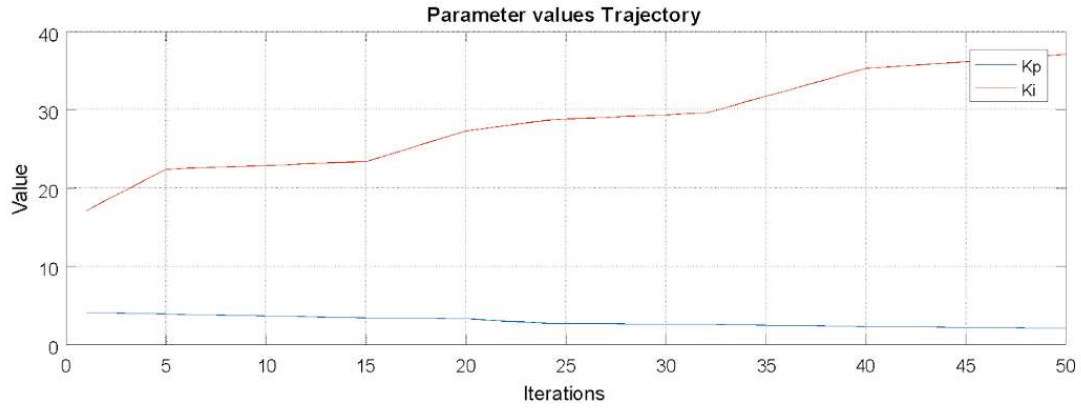

Figure 6.36 Trajectory of PI parameters with iterations in GSA

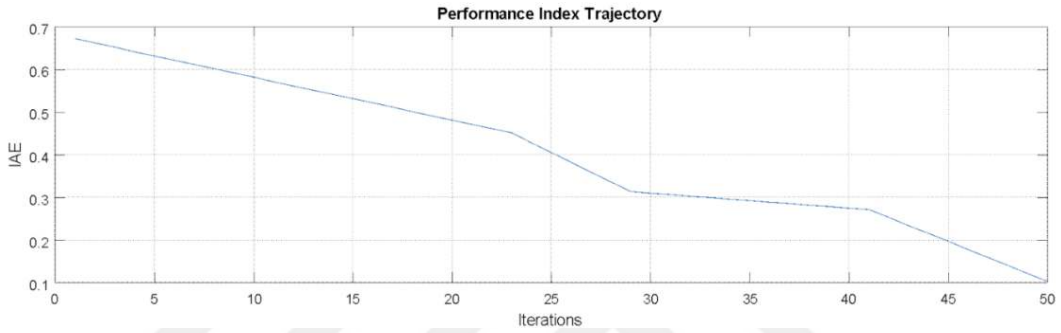

Figure 6.37 Trajectory of IAE with iterations in GSA

In GSA, the tracking of reactive power almost follows the same pattern, as shown in Figure 6.38. The overshoot in the system is observed in the start, for both the reactive power and current tracking, followed by smooth waveforms with slight perturbations. One thing of interest in all three optimization results is that the STATCOM follows positive reactive reference power with higher fidelity, while in case of negative power, more fluctuations around the reference are observed.

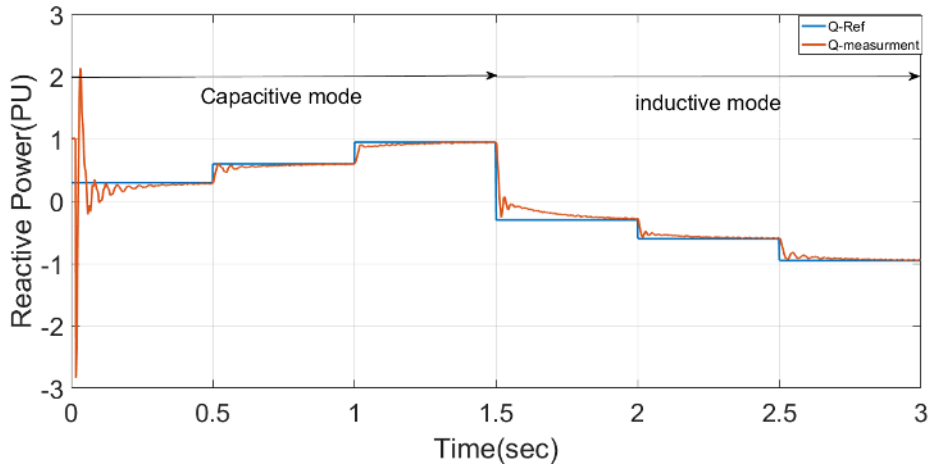

(a) Reference(blue) and measured (red)

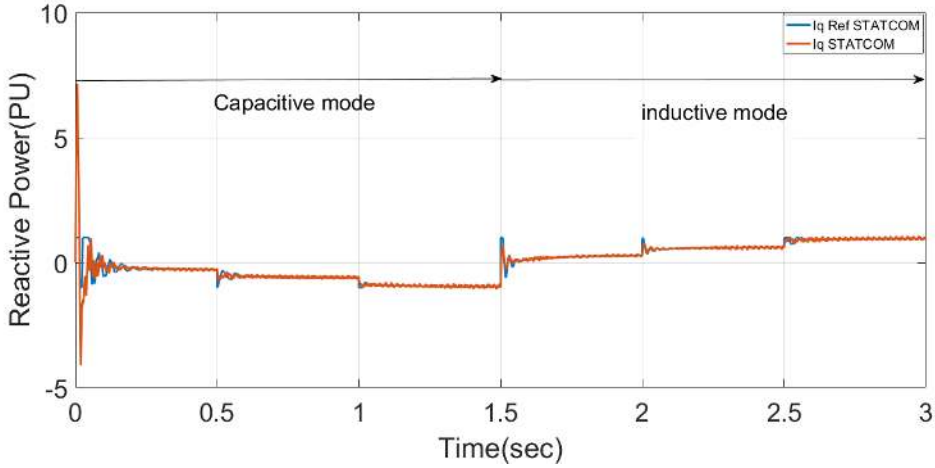

(b) Reference (blue) and measured (red)

Figure 6.38 (a) STATCOM tracking of reactive power Q (b) I_q current through GSA tuning of PI controller

The values of reactive power controller parameter and IAE for each optimization technique are tabulated in Table 6.5, which shows that APSO has the lowest error in estimation, followed by GSA, while the PSO secures third position in the estimation problem.

Table 6.5 Parameters and IAE for each algorithm

Algorithm	**K_P**	**K_I**	**IAE**
PSO	0.35	55.1	0.1274
APSO	3.1	57.1	0.0976
GSA	2.1	37.1	0.1033

6.4.4 Conclusion

In this section, we designed a PI controller for the STATCOM to regulate reactive power at the PCC. The controller is based on individual balance control loop which helps in avoiding capacitor voltage drifting and increases the stability of the system. We have derived system and controller model based on mathematical equations. The PI controller contains adaptive gains for the VAR regulator, which are optimized using three optimization techniques including PSO, APSO and GSA. The results show that APSO outperforms the remaining optimization techniques in optimizing the parameters of PI controller, namely K_P and K_I and produces better tracking of the VAR power. Resulting PI controller can be used efficiently to manipulate the reactive power in the system.

6.5 Simulation Model of CSAPF

The designed CSAPF model was implemented in simulation program environment as in shown in Figure 6.39. The CSAPF consists of four identical CHBs connected in series from their AC sides. The performance of the aimed p-q theory method was tested inside the simulations. The CSAPF was made to make up harmonics current. The model parameters are tabulated in Table 6.6.

Table 6.6 Detail of system parameters

Type	**Parameters**
Supply phase voltage	220 V
Supply frequency	50 Hz
Filter inductor	7.5 mH
DC link capacitor	250 µF
Load	R-Load (R= 30 Ω) RL-Load (R= 60 Ω and the L= 20 mH) RC-Load (R= 60 Ω and the C= 25 µF) Electrical motor (DC motor 5 HP 240V field 300V)

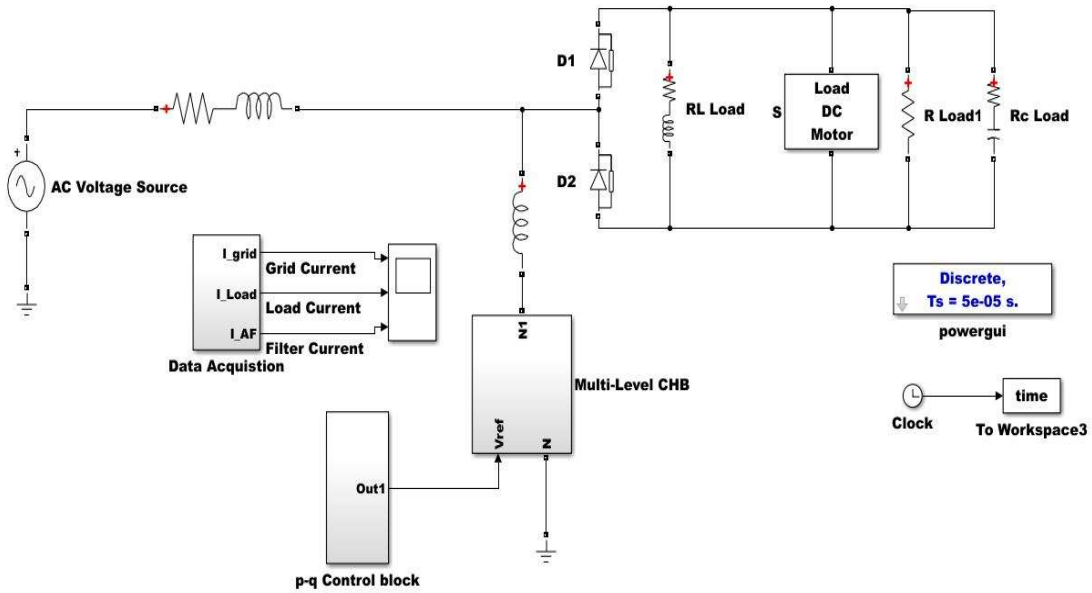

Figure 6.39 CSAPF topology

6.5.1 Simulation Model of CSAPF

The supply current can be seen in Figure 6.40, while the load current waveform can be seen in Figure 6.41 and the filter current is shown in Figure 6.42. The DC capacitor voltage is depicted in Figure 6.43.

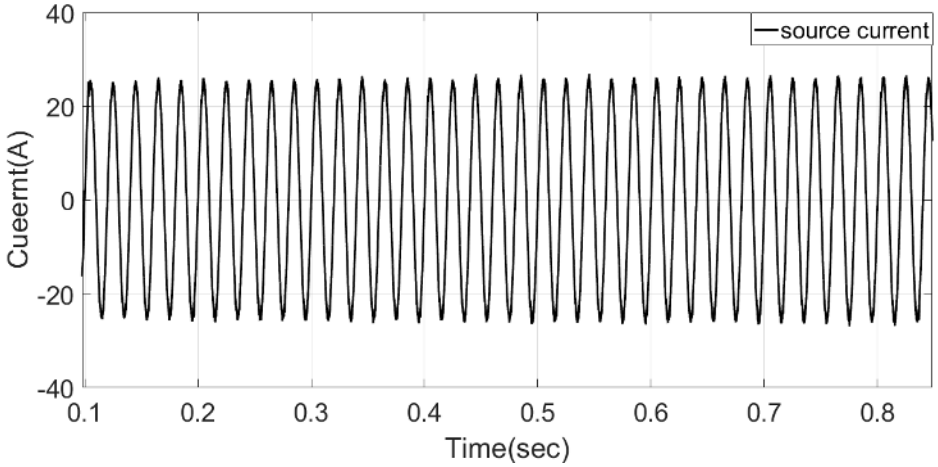

Figure 6.40 Supply current waveforms

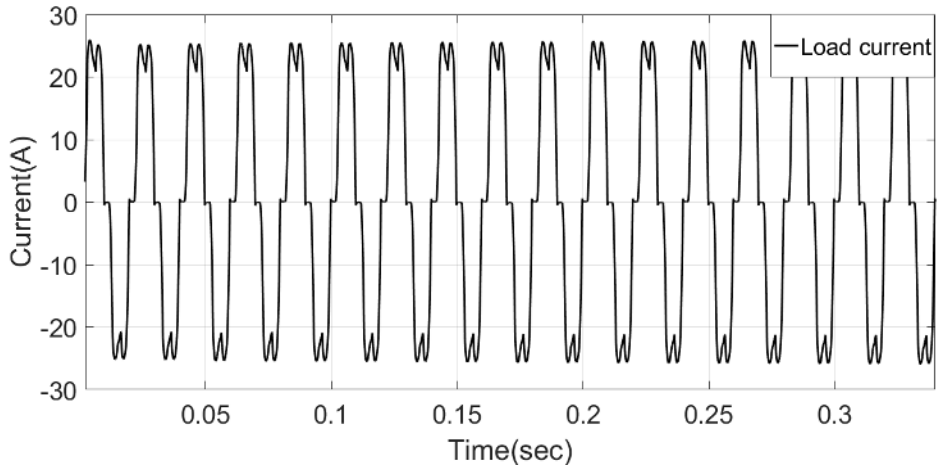

Figure 6.41 load current waveforms

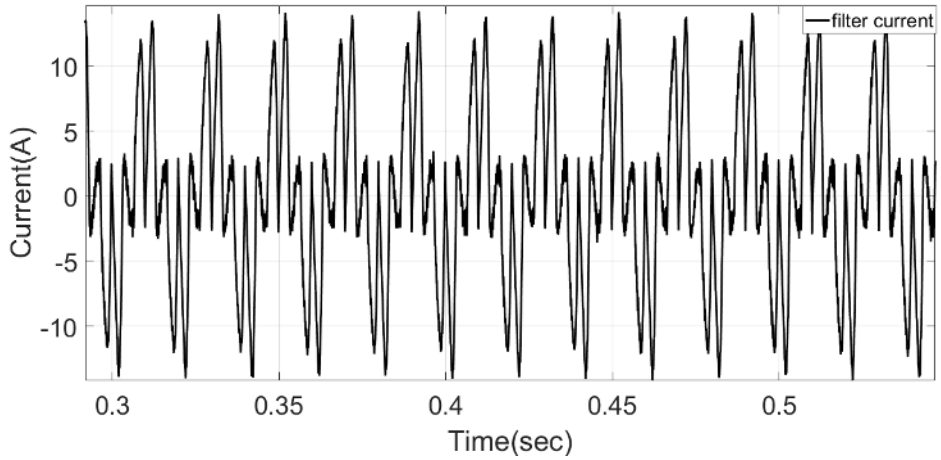

Figure 6.42 Filter current waveforms

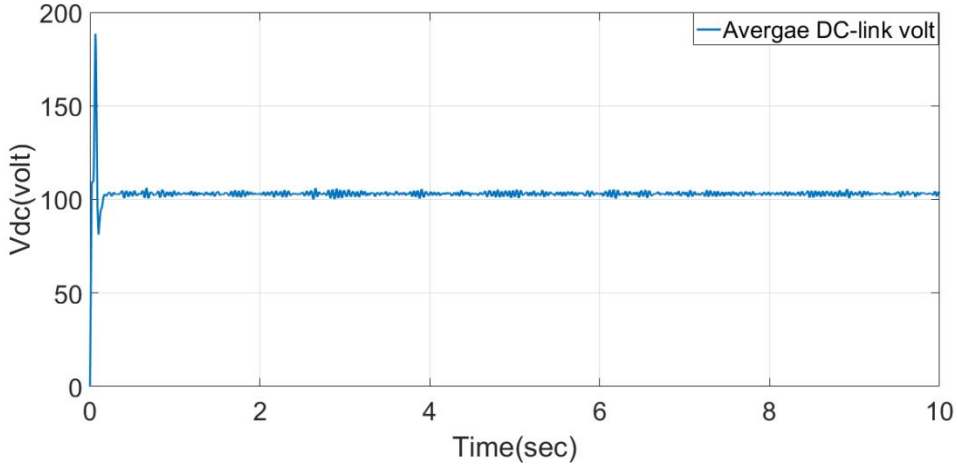

Figure 6.43 Average DC link voltage

Without using SAPF, the THD is equal to 22.8%, which has now dropped to about 2.5%. CHB converter-based APF is examined with different levels and resulted a THD in range of (7.2%-2.5%). This can be seen in Table 6.7, Figure 6.44, Figure 6.45, Figure 6.46 and Figure 6.47, respectively.

Table 6.7 Results of each simulation

No of H-bridge	Number of Level	THD Current Value
1	3	7.2%
2	5	4.88%
3	7	2.9%
4	9	2.5%

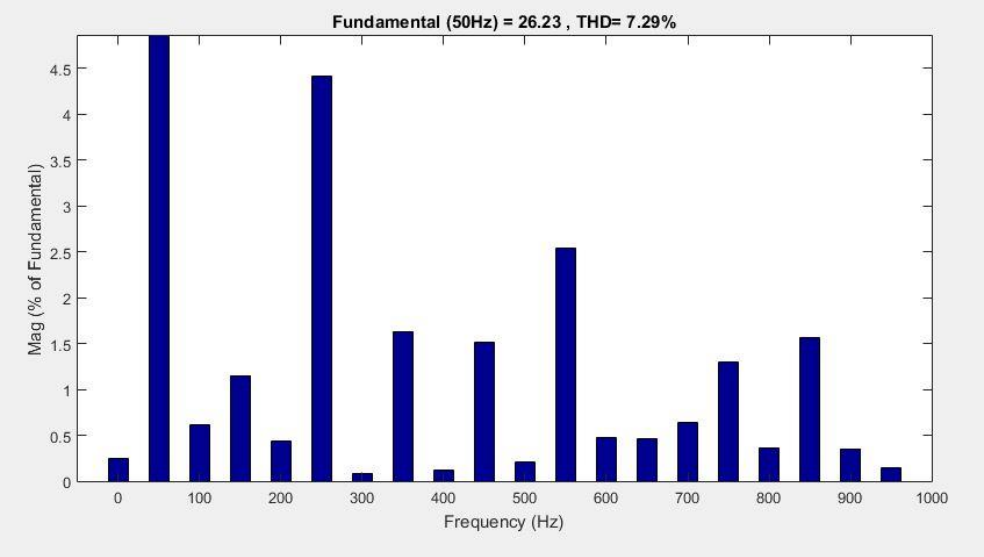

Figure 6.44 Source current THD spectrum with 3-Level STATCOM

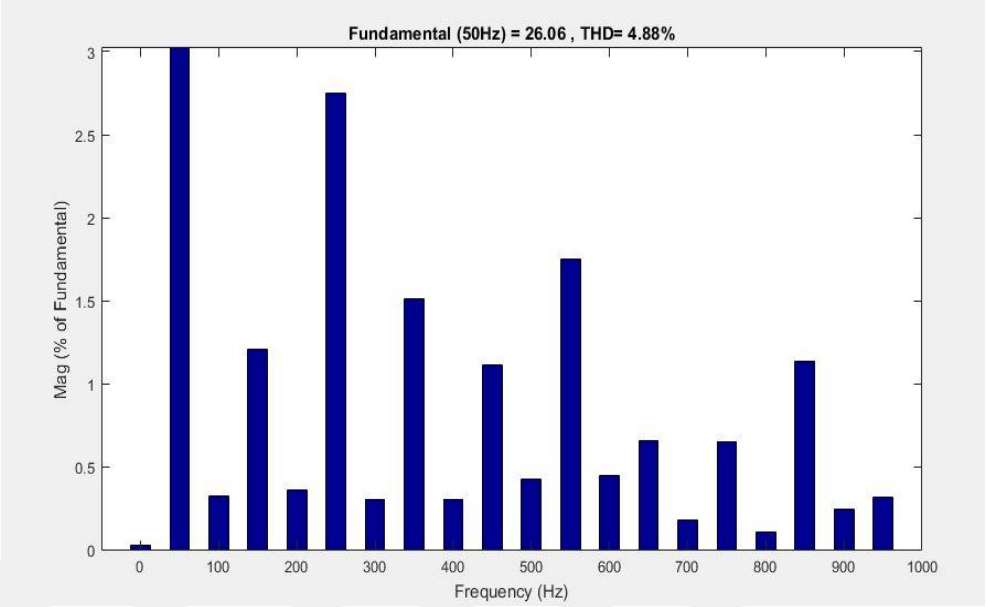

Figure 6.45 Source current THD spectrum with 5-Level STATCOM

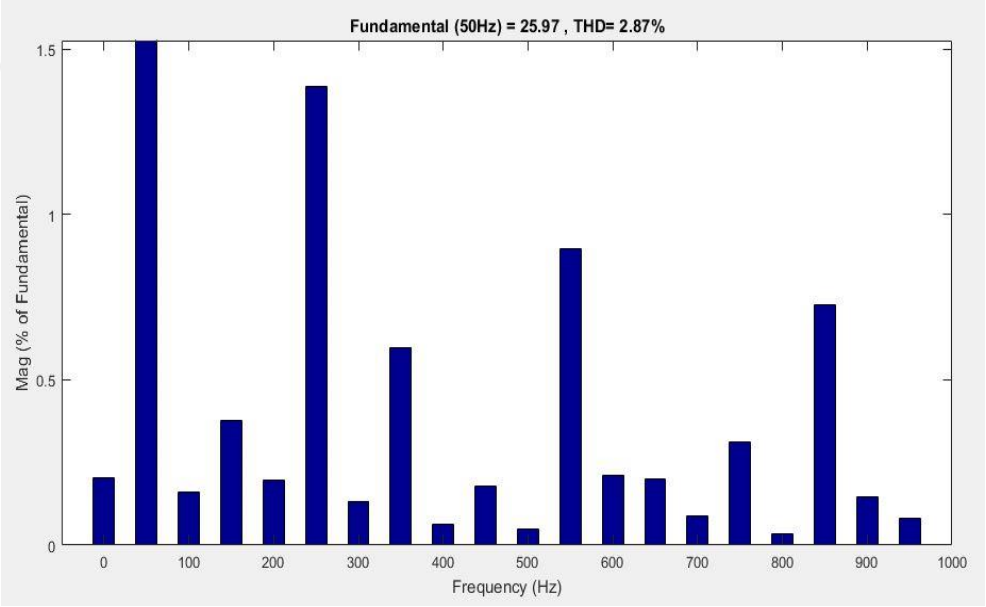

Figure 6.46 Source current THD spectrum with 7-Level STATCOM

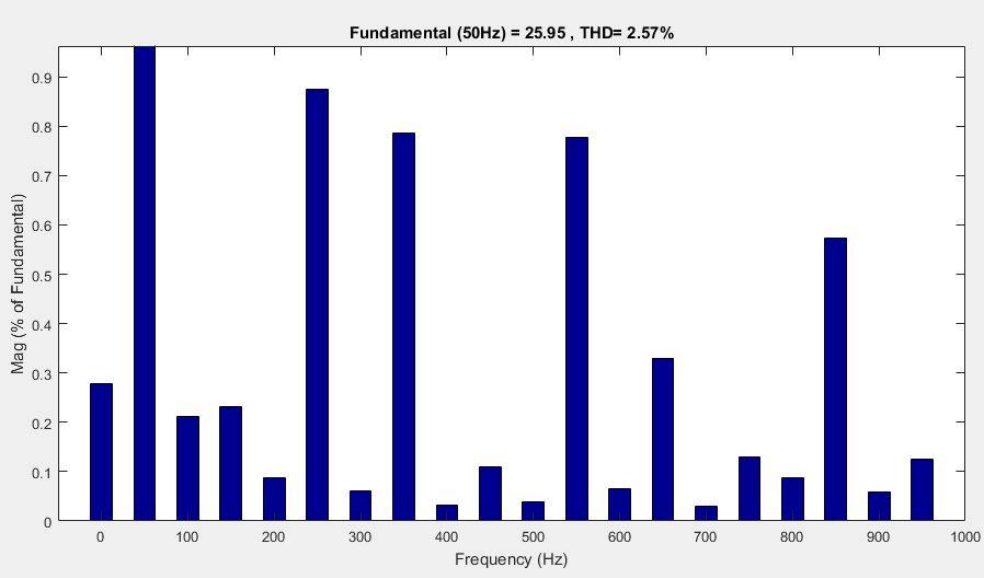

Figure 6.47 Source current THD spectrum with 9-Level STATCOM

6.5.2 Conclusions

This section examines the performance of proposed CSAPF under different controllers. The (p-q theory) is verified through simulation studies. The (p-q theory) contains integrated (PI) controller, added to regulate the capacitor DC voltage of the CSAPF. The complete CSAPF structure has been implanted to compensate harmonics caused by nonlinear loads. The results show that, we can apply it to lower THD of any system. GSAPF is proposed to reduce the THD from 22.8% to around 2.5% under given loading conditions.

6.6 Results and Discussion of STATCOM Control Based on ANN

To study the efficiency of the designed STATCOM and the ANN based estimation techniques, we tested the system on IEEE-30 bus system. The duty of STATCOM is to regulate bus voltage around 1pu. While the estimation schemes have been used to estimate the STATCOM voltage, phase angle, and the reactive power at STATCOM. STATCOM has been connected at the load bus 12. ANN has been trained by a variety of different optimization techniques such as Back-Propagation, PSO, SFLA and GA. As mentioned earlier, the real and reactive powers of the IEEE-30 bus systems were perturbed by increasing the powers at the load buses by introducing a 5% change in each iteration. The corresponding voltages, phase angles, and reactive powers of the STATCOM are estimated using the Newton-Raphson method. This combination of

real and reactive powers and corresponding voltages, phase angles, and reactive powers becomes the dataset for the three cases of ANN. Out of the total dataset, a random 70% of the data is used for training and the remaining is used for the testing purposes. For the purpose of summarizing the results, only 21 samples of input and output results are generated for each of the three cases of ANNs. In all cases, the ANNs have been designed with one input, one hidden layer containing 10 neurons and one output layer containing one output neuron. The neural network configuration is 'feed forward network' with no back links. In the case of back-propagation training, Levenberg-Marquardt back-propagation algorithm is used which is the most widely used back-propagation method. The input contains real and reactive powers of all the buses, hence the size of input is 60. The weights to be trained include hidden layer weights and biases plus the output layer weights and biases. In the cases of PSO, 10 initial solutions were assumed. Similarly, in the case of SFLA, a total of 24 initial solutions (frogs) have been assumed, with 4 memeplexes and 3 shuffles. In case of GA, 30 initial solutions were produced in the population.

The performance of the first case of ANN is tabulated in Table 6.8. This Table compares the original STATCOM voltage calculated at the bus 12 with the help of Newton-Raphson with the four ANNs which have been trained using back-propagation, PSO, SFLA and GA. In Figure 6.48, this performance comparison of different optimization techniques is illustrated for the 9 test cases. This is obvious from the Table 6.8 and Figure 6.48 that SFLA based ANN performs the best in this category and estimates the STATCOM voltage with minimum error. While, GA and Back-propagation algorithms perform quite alike and produce better results after SFLA. The worst performance in this scenario is shown by PSO. The SFLA's performance can be attributed to the concept of memeplexes which help the individual particles escape the local minima. The mean squared errors (MSE) are shown in Table 6.9.

Table 6.8 STATCOM voltage estimation

Actual Voltage (pu)	**ANN_BP**	**ANN_PSO**	**ANN_SFLA**	**ANN_GA**
0.969135	0.95716	0.96854	0.978241	0.962651
0.976864	0.97241	0.97772	0.982655	0.973999
1.000053	1.0057	1.0067	0.998007	1.003856
1.002879	1.0111	1.0143	1.001886	1.009219
1.013198	1.0209	1.0296	1.010445	1.018492
1.016203	1.0254	1.0309	1.015159	1.022415
1.052532	1.049	1.0341	1.046581	1.044392
1.061034	1.0616	1.0543	1.064762	1.059902
1.095348	1.0975	1.1055	1.107148	1.102465

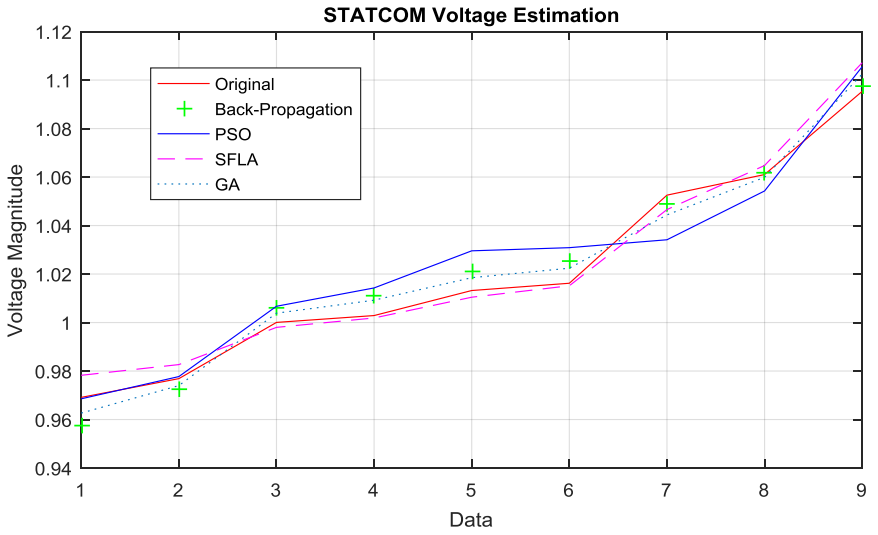

Figure 6.48 Comparison of STATCOM voltage estimation with different optimization techniques

Table 6.9 MSE for voltage estimation

Algorithm	MSE
Back-Propagation	5.2361e-06
PSO	1.416e-05
SFLA	**3.5771e-06**
GA	3.9367e-06

In Table 6.10, the ANNs performance is shown, which have been developed for the estimation of STATCOM bus phase angles. These values are also plotted and shown in Figure 6.49, while Table 6.11 shows the MSE for each case. It is evident that back-propagation method outperforms other algorithms in phase estimation. This difference in result from the previous case shows that ANN also depends on the nature of the dataset and sometimes hidden features in the dataset lead to change in the performance of the ANN. PSO and SFLA have similar results.

Table 6.10 STATCOM phase estimation

Actual Phase (degrees)	ANN_BP	ANN_PSO	ANN_SFLA	ANN_GA
-15.4719	-15.779	-15.9132	-14.3293	-18.4958
-16.8681	-16.89	-17.2127	-15.6629	-19.8726
-20.4668	-20.145	-19.3617	-19.6911	-20.2012
-21.1561	-20.884	-19.9518	-20.6146	-20.2087
-22.683	-22.456	-22.4967	-22.5677	-20.2343
-23.3962	-23.291	-24.1178	-23.5912	-20.2806
-28.0485	-27.973	-27.6542	-28.9894	-29.3734
-29.7182	-30.09	-28.9323	-31.1672	-32.1666
-34.3413	-34.747	-34.5266	-35.2818	-26.6616

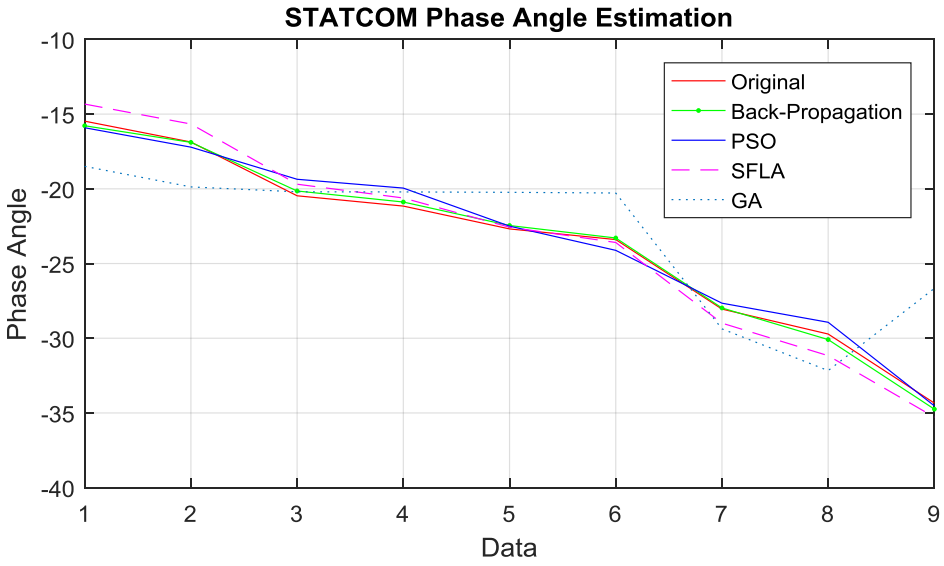

Figure 6.49 Comparison of STATCOM phase angle estimation with different optimization techniques

Table 6.11 MSE for phase angle estimation

Algorithm	**MSE**
Back-Propagation	0.0079424
PSO	0.053676
SFLA	0.093501
GA	1.2539

Table 6.12 contains the data obtained from the third case: the estimation of STATCOM reactive powers. In this case, the performance of SFLA closely resembles that of Back propagation, with SFLA performing slightly better than ANN. The strength of SFLA is obvious due to its memeplex structure. The results are plotted in Figure 6.50 and the MSE is shown in Table 6.13.

Table 6.12 STATCOM reactive power estimation

Actual Reactive Power-Q (VAR)	**ANN_BP**	**ANN_PSO**	**ANN_SFLA**	**ANN_GA**
0.308599	0.26023	0.344767	0.34151	0.33022
0.231335	0.21638	0.238442	0.25949	0.33022
-0.00053	0.045224	-0.03443	-0.02285	0.00514
-0.02879	-0.0022	-0.08225	-0.07813	-0.16844
-0.13198	-0.11168	-0.14738	-0.16161	-0.14128
-0.16205	-0.17333	-0.16897	-0.20128	-0.17115
-0.52545	-0.50661	-0.35157	-0.55022	-0.55583
-0.61051	-0.61863	-0.77518	-0.63837	-0.6059
-0.95389	-0.87355	-0.88589	-1.0182	-0.60589

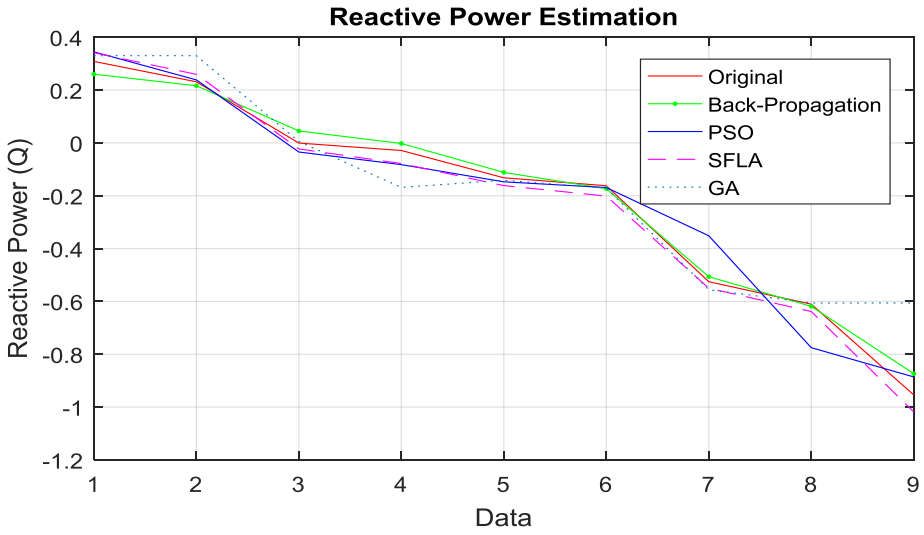

Figure 6.50 Comparison of STATCOM reactive power estimation with different optimization techniques

Table 6.13 MSE for reactive power estimation

Algorithm	**MSE**
Back-Propagation	0.00015776
PSO	0.00083491
SFLA	**0.00015735**
GA	0.0018765

6.6.1 Conclusion

This section is focused on fine-tuning the weights of ANN using different optimization techniques. Then, the developed ANN is used to estimate voltages and reactive powers of STATCOM. We have discussed the role of STATCOM in power buses for the voltage regulation of the buses. We have presented an efficient iterative method to solve the power systems which involve STATCOM. The STATCOM introduces some new variables in the system which must be accounted for. In the next stage, we have provided an alternative method to calculate the unknown variables in STATCOM using ANN curve fitting, which is faster and requires less memory and processing power. We have trained ANN with different optimization techniques such as Back-Propagation, PSO, SFLA and GA. The results show that SFLA can perform better than the back-propagation and other methods when the parameters are fine-tuned according to the given dataset.

CHAPTER 7

EXPERMENTAL STUDIES

7.1 Circuit & Block Diagram of STATCOM

To validate simulation results, the single-phase five-level converter based STATCOM was built and tested in the laboratory. The rating of the prototype STATCOM was around ±40 VAR reactive power to/from single-phase 220V power socket. The proposed STATCOM consists of two identical CHBs, coupling reactance, and stepdown transformer. The reduced scale STATCOM was used specifically to show the proof of concept, and the rating was limited only by voltage and current ratings of the utilized components, such as power semiconductor switches and capacitors. In this work, single-phase prototype is aimed only to decrease the overall costs. Table 7.1 shows the ratings of the MOSFETs used in the STATCOM prototype.

Table 7.1 Product summary of IRF 260N MOSFET

Parameter Name	**Parameter Value**
Drain-to-Source Breakdown Voltage (VDS)	200 V
Drain-to-Source Leakage Current (Id)	Gate Threshold Voltage (VGS)=10 V: 35 A
Static Drain-to-Source On-Resistance RDS (on)	VGS=10 V: 0.04 Ohm
Total Gate Charge Q_g	234 nC
Gate-to-Source Charge Q_{gs}	38 nC
Gate-to-Drain Charge Q_{gd}	110 nC

As shown, voltage and current ratings of these semiconductor devices are low which consequently limits the converter ratings. In fact, the ratings of prototype converter models can be expanded easily only by replacing the components with larger rated elements such as higher rated MOSFETs or IGBTs. The controller system can be expanded to higher ratings with minor modifications such as voltage and current sensor, isolation, converters, microcontroller, and the stepdown transformer, and etc. Figure 7.1 shows the schematic of the single-phase CHB multi-level converter based STATCOM comprised of the control board, converter board, single-phase transformer, current (ACS712) and voltage (ASL160212) sensors, LCD and etc. Figure 7.2 shows the details of experimental setup used for testing the proposed multilevel converter based STATCOM.

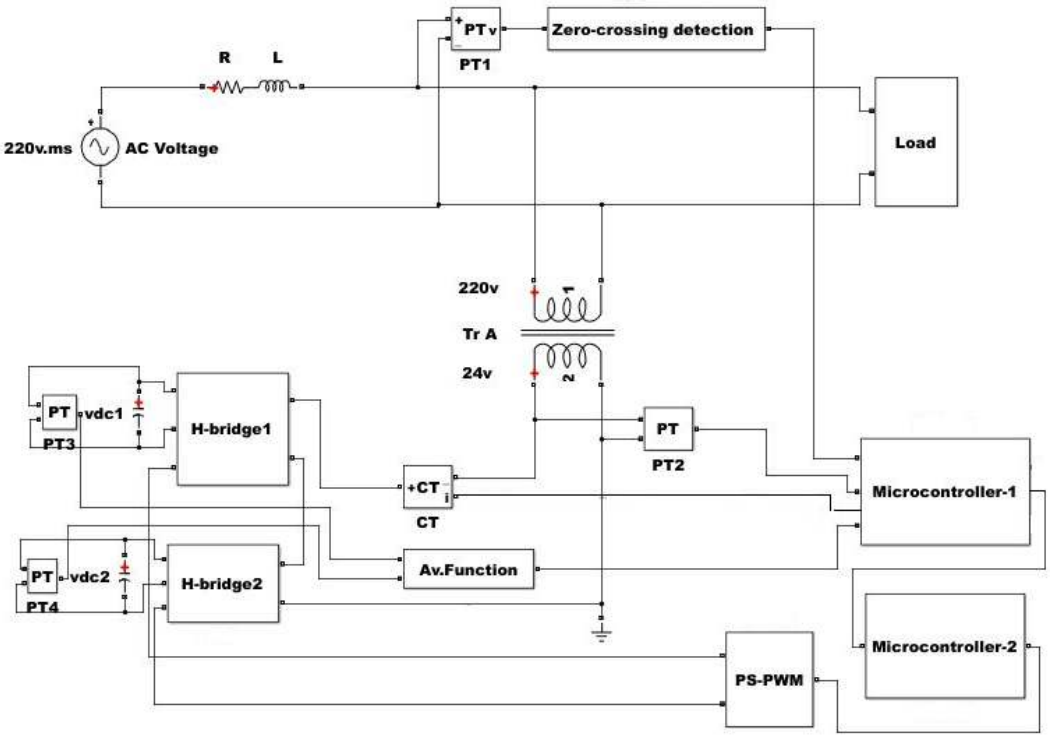

Figure 7.1 Schematic of the experimental setup

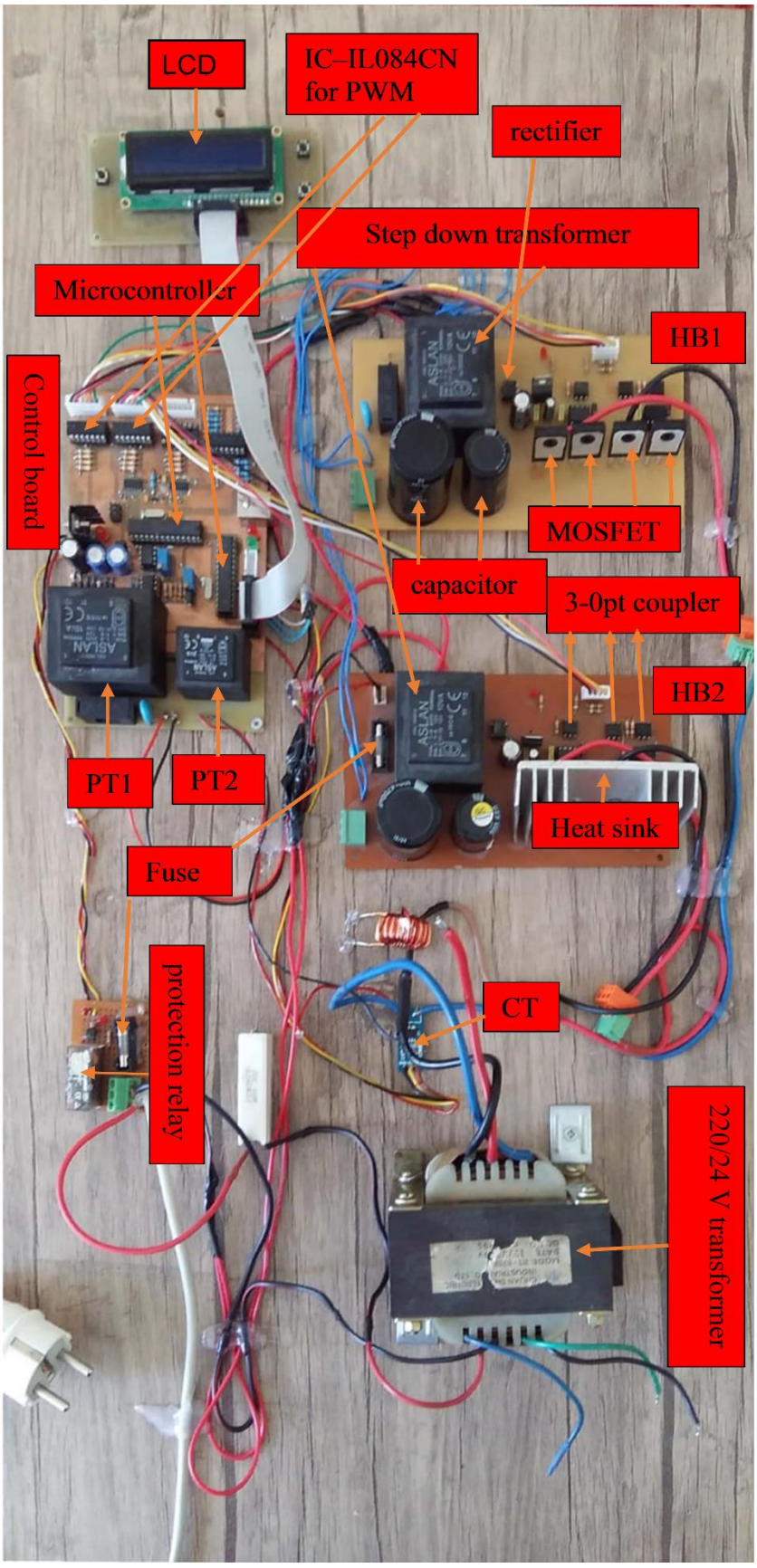

Figure 7.2 The details of experimental setup

In the experimental setup, potential transformer (PT1) is used to sense the voltage at PCC of the power system and STATCOM. The sensed voltage is passed through the zero cross detector (ZCD) circuit to sense the zero cross of the voltage at PCC. Potential transformer (PT2) is used to sense the STATCOM output voltage. Current transformer (CT) is used to sense the STATCOM current. At the same time, these inputs (the STATCOM current and the STATCOM voltage) are utilized to calculate the reactive power of STATCOM using Microcontroller-1. The differential amplifier (7812) is used to sense the two capacitor voltages. Four inputs are provided to the Microcontroller-1. These are STATCOM voltage, STATCOM current, average of two capacitor voltage, and zero cross of the supply source voltage. These inputs are utilized to calculate the phase angle (ϕ) difference between converter AC output voltage (STATCOM voltage) and source voltage. The difference between reference and measured reactive power is used to calculate the modulation index. The Microcontroller-1 calculates these values and sends these reference values of phase angle and modulation index information to the Microcontroller-2 using universal asynchronous receiver transmitter (UART) module for asynchronous communication between Microcontroller-1 and Microcontroller-2. The Microcontroller-2 generates the reference voltage (sinusoidal) using the data obtained from the Microcontroller-1 and an 8-bit digital-to-analogue converter (DAC). The generated reference voltage is compare with carrier signal using PS-SPWM technique. The controller (IC–IL084CN) compares the reference sinusoidal signal with four triangular carrier signal to generate the eight switching gate signals for the converter, four gate signals for each H-bridge. Figure 7.3 depicts the flowchart of the experimental setup of STATCOM.

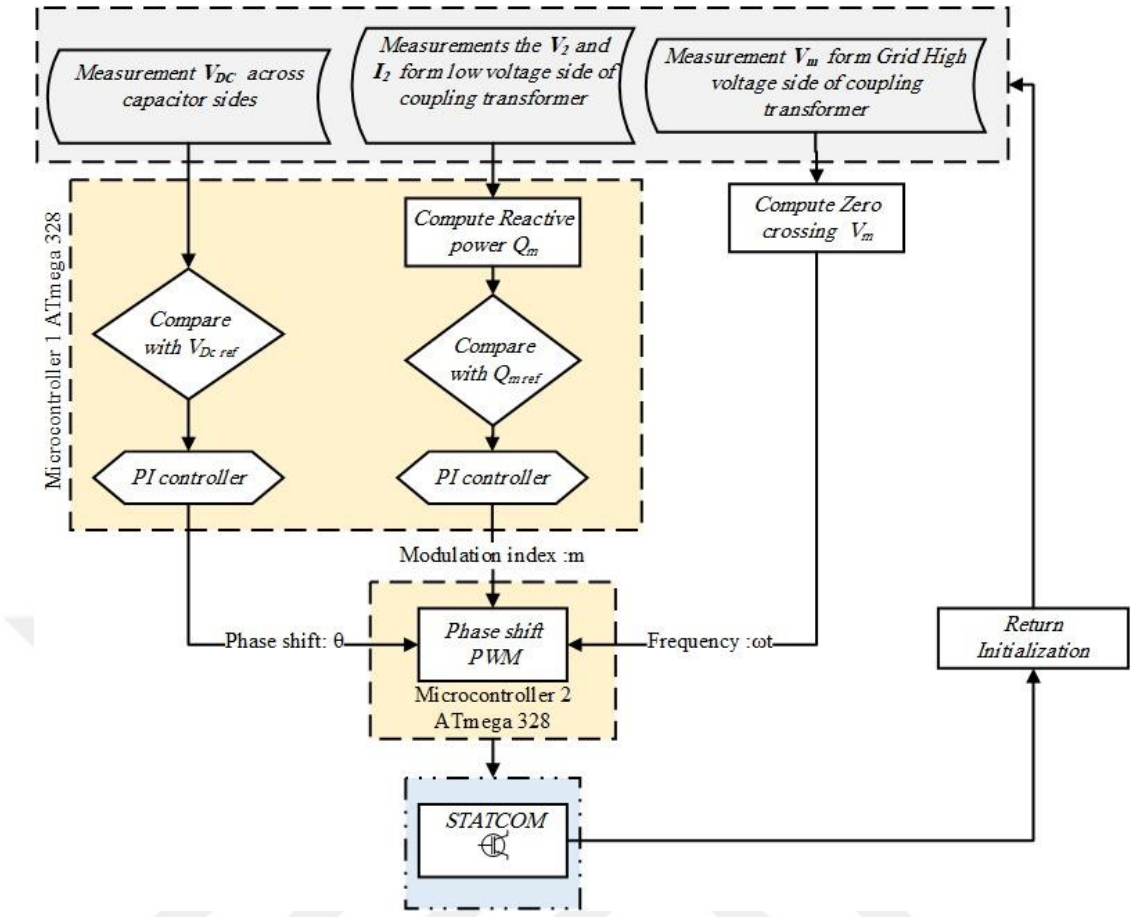

Figure 7.3 Operation logic of STATCOM

7.2 H-Bridge Module

To validate simulation results, a 5-level STATCOM model of the system was built by two cascaded connected H-bridges. The H-bridge module consists of four power MOSFETs (IRFP260N), DC link capacitors (820µF), three-opt couplers (HCPL3120), step down transformer (220/12 Volt), rectifier 12VAC to 12VDC, linear voltage regulation, and power terminals. Table 7.2 shows the number of major components used in H-bridge. The H-bridge module uses four MOSFETs as switches in this circuit. MOSFETs are switched using a MOSFET driver (IC IR2104). The driver converts the digital gate signal into required gate voltages of the MOSFETs. If the MOSFETs on the same leg of the H-bridge are turned ON at the same instant, it creates a short circuit. Thus, in order to prevent this condition, the signal to the lower MOSFET is inverted to the higher MOSFET using the (IR2104) MOSFET drivers. Figure 7.4 shows the implemented hardware module by using two H-bridges as the cascaded multilevel

converter using one capacitor as DC input source for each H-bridge, eight power MOSFETs, and six-optocoupler.

Table 7.2 Major components used to implement one H-bridge

Component Name	Specification	Number of Component
IRF260 (power MOSFET)	Continuous Drain Current $ID \approx 35A$	4
DC link capacitor	820 μF	1
Gate drive optcoupler (HCPL 3120)	2.5 A output current	3
IR2104 MOSFET drivers	Package power dissipation P_D (8 lead)	2

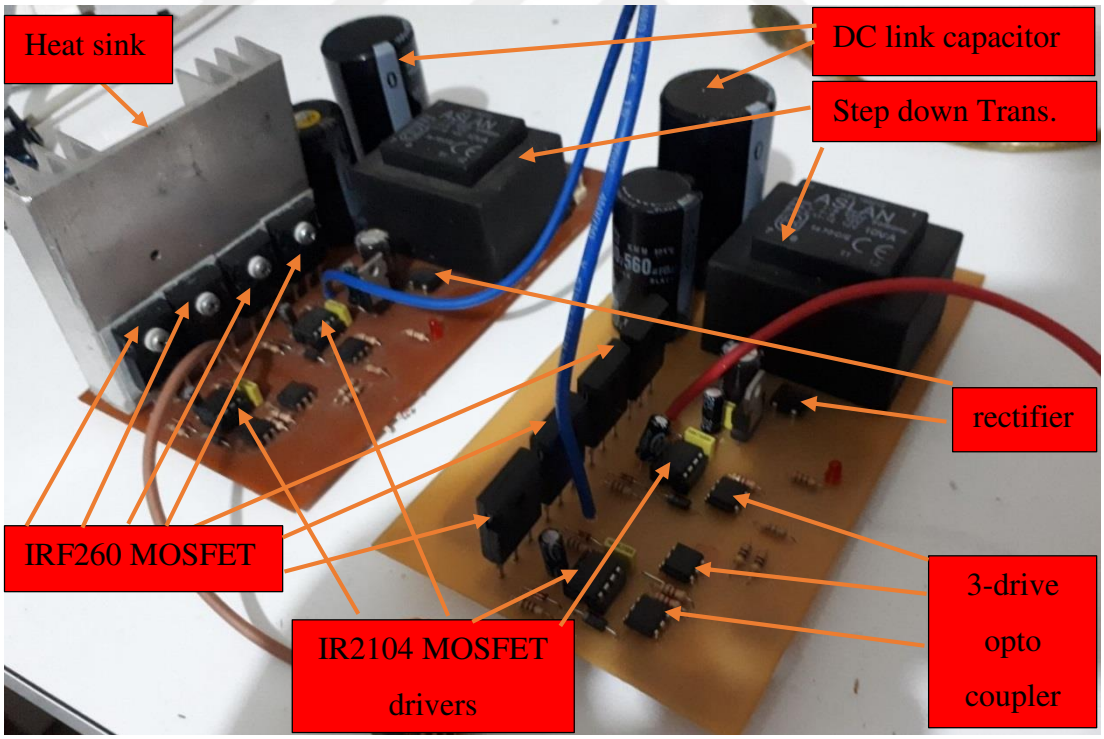

Figure 7.4 5-Level CHB prototype model

7.3 Controller Board

For the development of STATCOM, two ATMEGA328P microcontrollers have been used. Controller board operating in normal mode runs the code. This controller manages all outputs which are PWM gate signals to turn on and off MOSFET switches as well as all the inputs' feedback signals originating from various parts of the circuit. Input feedback signals include: 1) capacitor voltages, 2) output voltage and current of the 5-Level CHB STATCOM, and 3) reactive power measurements. The output PWM signals are a combination of logic 0 and logic 1, thus determining the status of the switches to be ON or OFF. These logic values are converted to actual voltage values (15 V) through gate drive circuits. The other task of gate drive circuit is to electrically isolate the power stage from the control board. In order to protect the control board, all system I/O signals are connected to the controller board through the IDC connector, as shown in Figure 7.5.

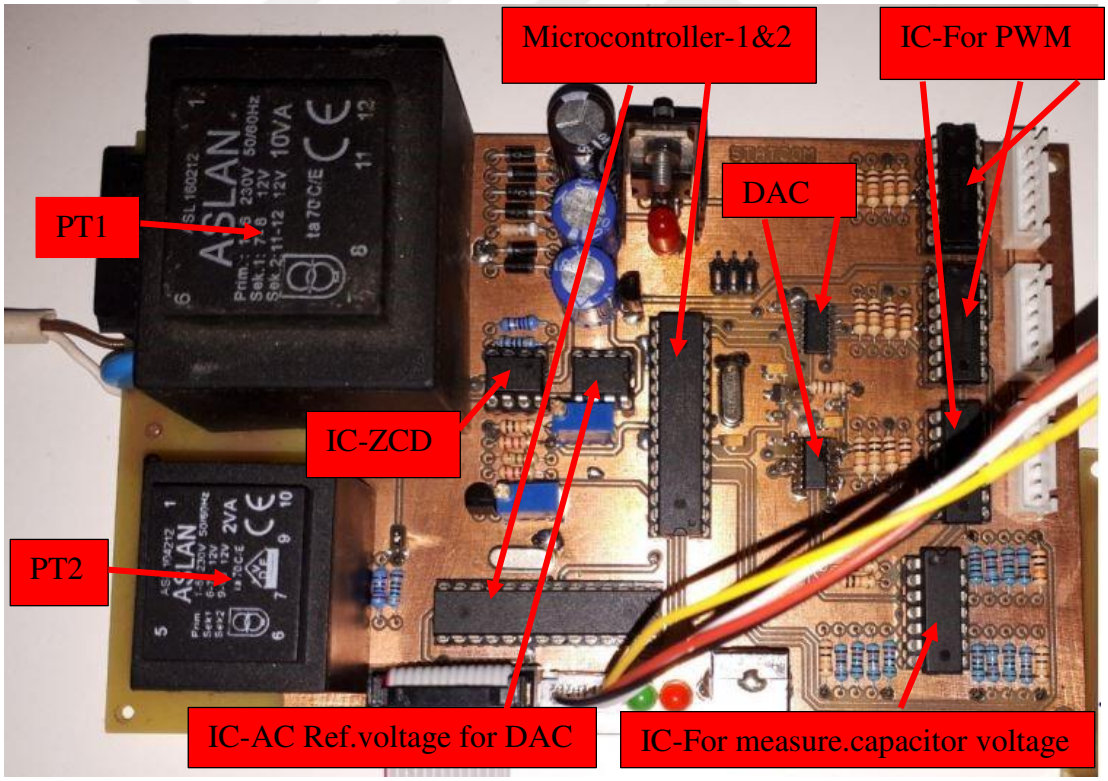

Figure 7.5 Controller board

Microcontrollers are the brain of the system. A microcontroller is defined in simple word as "a computer in a chip". The microcontroller brand used in this thesis is Microchip. The project needs to perform two operations simultaneously, one is the

sensing of STATCOM voltage and current and calculates the reference reactive power and the other one is to generate continuously the sinusoidal reference voltage. Thus, for this purpose, two ATMEGA328P microcontrollers are needed. The first ATMEGA328P microcontroller is used for the former task (to sense STATCOM current, voltage and their phase angle and to determine the phase angle and magnitude of the reference voltage) and the second one is used for the later task (to generate continuously the PWM signals). The first AT-MEGA328P microcontroller has a clock input of 16 MHz while the second ATMEGA328P microcontroller has a clock speed of 20 MHz. Hence, first one is faster than the second one. The first one continuously generates the digital value of the real-time magnitude of the sinusoidal reference voltage.

7.4 ZCD Circuit

A ZCD circuit is one type of voltage comparator. A ZCD circuit can be used to measure the phase angle difference between two voltage values. Figure 7.6 shows the operational amplifier (LM311), which is used in this project as ZCD.

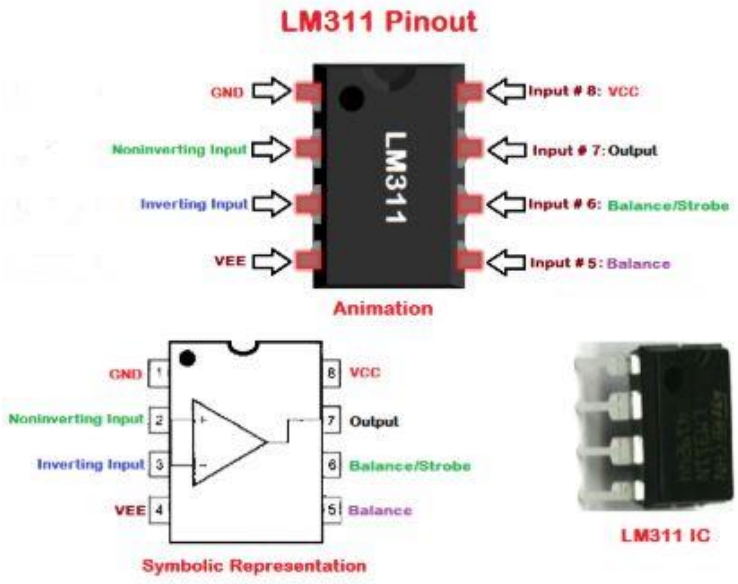

Figure 7.6 Operational amplifier (LM311) used as ZCD

A sequence of pulses in the +ve and -ve cycles are acquired to measure the voltage between the time interval of the pulse of sine wave voltage and second sine wave. This interval of time is related to the phase difference between the two input sine wave voltages. The use of phase meter ranges from 0° to 360°. The Figure 7.7 shows the sinusoidal input voltage and the output of the ZCD circuit.

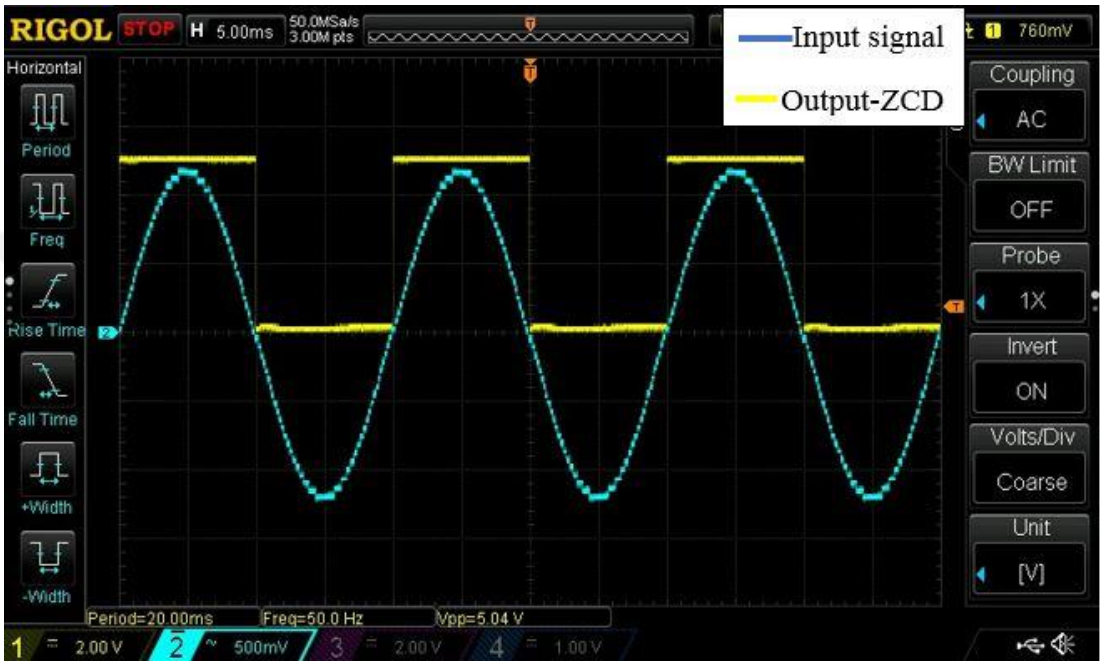

Figure 7.7 Input and output signal of ZCD

7.5 LCD

LCD stands for Liquid Crystal Display [107]. It is a device that can be used with microcontrollers to display different messages. Here, this display (LCD 1602) has 5V an operating voltage with power supply for logic (Vdd=3.0V±10%), is used to display the value of measured rms voltage and current as well as the magnitude and phase angle of the generated reference signal. LCD has a controller chip that controls the action of LCD. To control the LCD, different command word must be sent to this controller using the pins of LCD. In this way, any messages on the LCD can be displayed by using any microcontroller. Figure 7.8 shows the LCD 1602 which is used in this work.

Figure 7.8 LCD 1602 used in this work

7.6 Other Hardware Components

For easiness, the whole hardware system is divided into mainly two sections. Section 1 refers to the block of hardware that senses the STATCOM reactive power, modulation index and phase angle, and finally generates the reference voltage waveform signal for the next block. Section 2 refers to the block of hardware consisting of 5-Level CHB STATCOM. Each hardware component used in these parts are discussed briefly in the following sub titles.

7.6.1 Voltage Transformer

As shown in Figure 7.9, a step-down transformer of 230-12VAC was used to rectify to a pure 12V DC and then adjusted to voltage within 5V DC using the linear voltage regulator (LM7805) to be fed the DC voltage signal into the electronic device for H-bridge circuit.

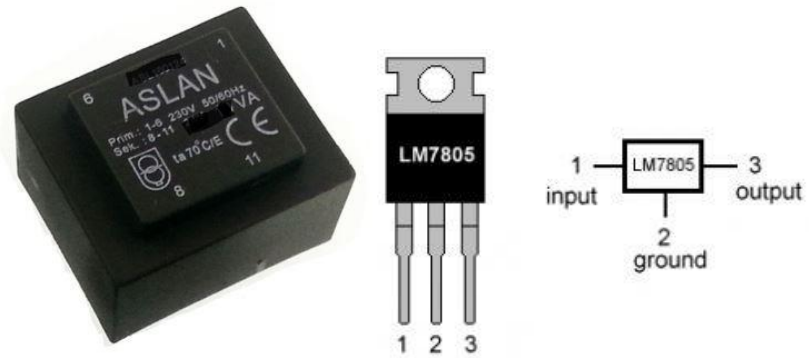

(a) (b)

Figure 7.9 (a) Step down transformer, (b) Voltage regulator (LM780)

7.6.2 PT and CT

Potential transformer (PT) and current transformer (CT) are used to sense the voltage and current of the STATCOM.

In PT sensors, a step down transformer of 230-12VAC (ASL160212) was used and rectified to a pure DC and then adjusted to voltage within 5V AC using the potentiometer in order to fed the analogue signal into the ADC without burning the ADC converter, and based on the Microcontroller-1, the input voltage can be monitored [108].

A CT sensor is used to sense the current value. ACS712 current sensor is used in this project, and it operates from 5V and outputs an analog voltage, which is proportional to the measured current. Figure 7.10 shows the PT and CT which is used in this work.

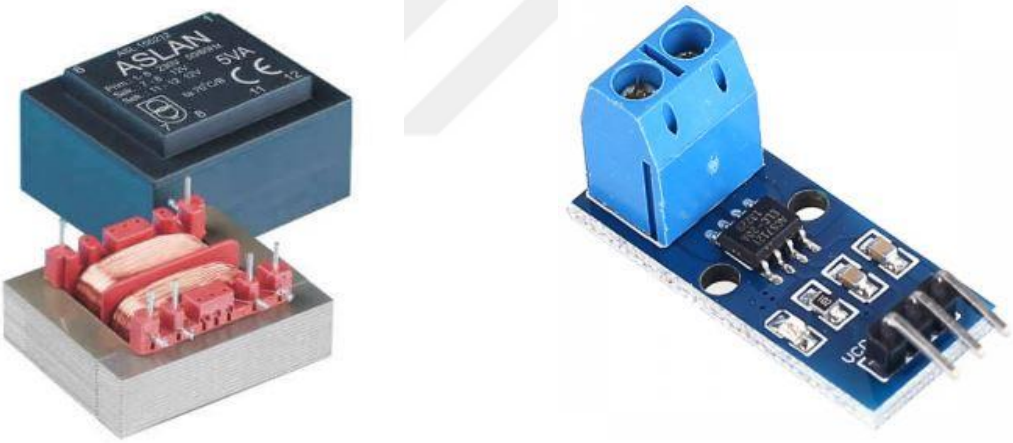

(a) (b)

Figure 7.10 (a) PT (ASL160212), (b) CT (ACS712)

7.7 Simulation Results

The proposed system is designed and simulated using simulation software with libraries for electrical components and systems. The complete simulation model of STATCOM is shown in Figure 7.11.

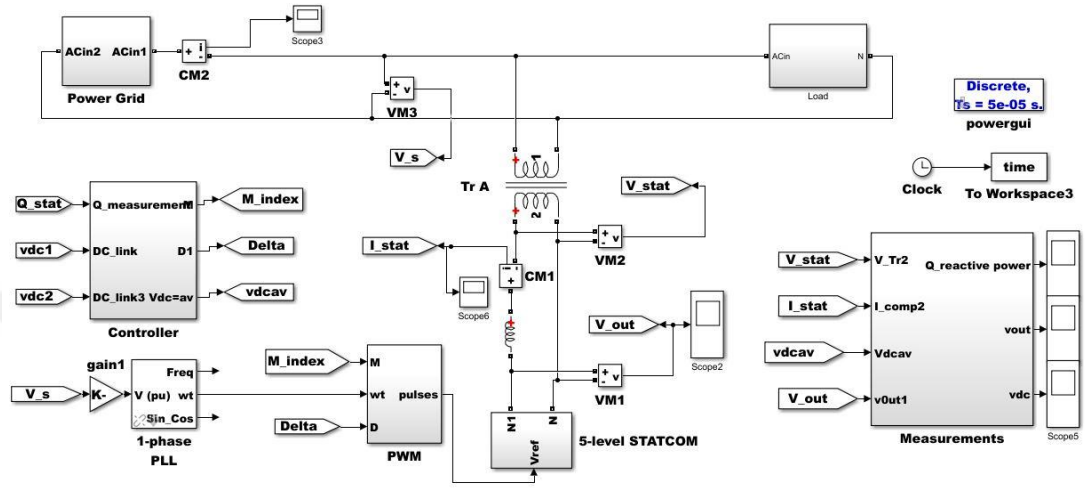

Figure 7.11 Complete simulation model of STATCOM

The model parameters are tabulated in Table 7.3. In this case, for the testing of system, a step reactive power signal combination is used. We have considered a purely sinusoidal waveform as source voltage and a non-linear load. The IGBTs are used as switching devices in the H-bridge circuit. The system is simulated for 8 seconds. During the first two seconds, the STATCOM system supplies 10 VAR reactive power and in the next two seconds this value increases until 40 VAR reactive power.

Table 7.3 System parameters

Type	Parameter	Value
Source	Peak Amplitude	311.12 V
	Frequency	50 Hz
Load	Nominal Voltage	220 Vrms
	Active Power	450 W
	Reactive Power Inductive	450 VAR
DC Link	Reference DC Link Voltage	17 V
Coupling Transformer	Nominal Power	5000 VA
Winding-1 Parameters	Voltage	220 Vrms
Winding-2 Parameters	Voltage	24 Vrms

Figure 7.12 depicts 5-Level output voltage of the multilevel converter. The average DC link capacitor voltage is shown in Figure 7.13, while Figure 7.14 shows that the measured reactive power is tracking the reactive power reference signal. Figure 7.15 is demonstrating the resultant voltage of converter, reference voltage, and the STATCOM current leads the STATCOM voltage by 90°.

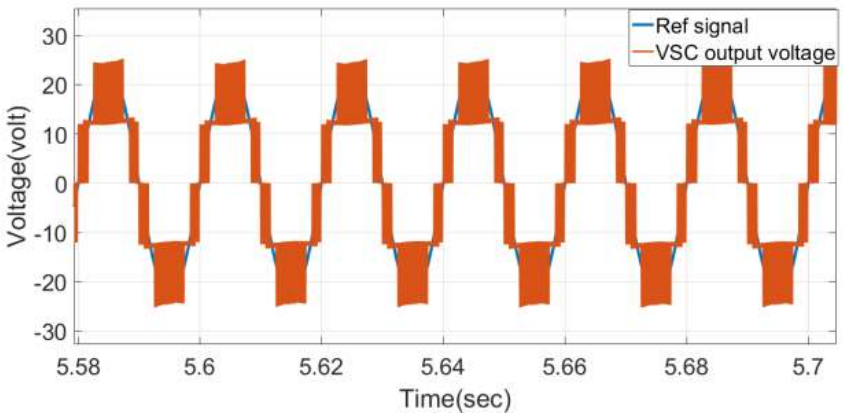

Figure 7.12 5-Level converter output voltage and the reference signal

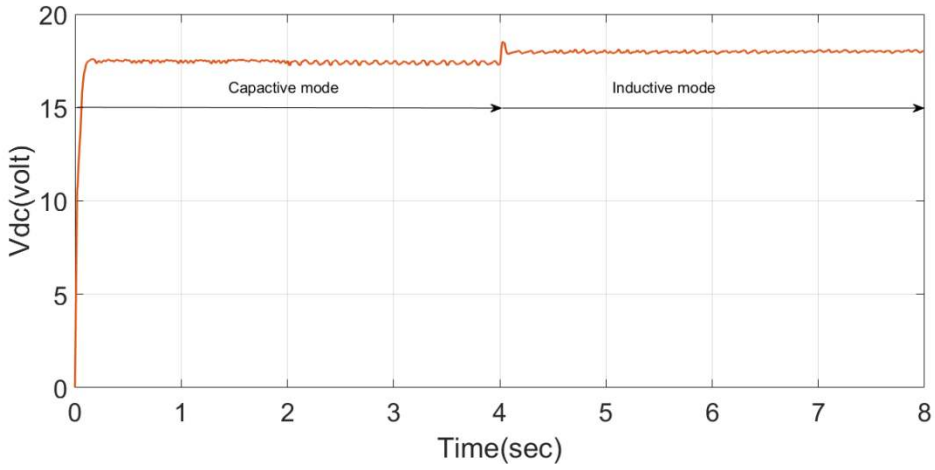

Figure 7.13 Average capacitor voltage

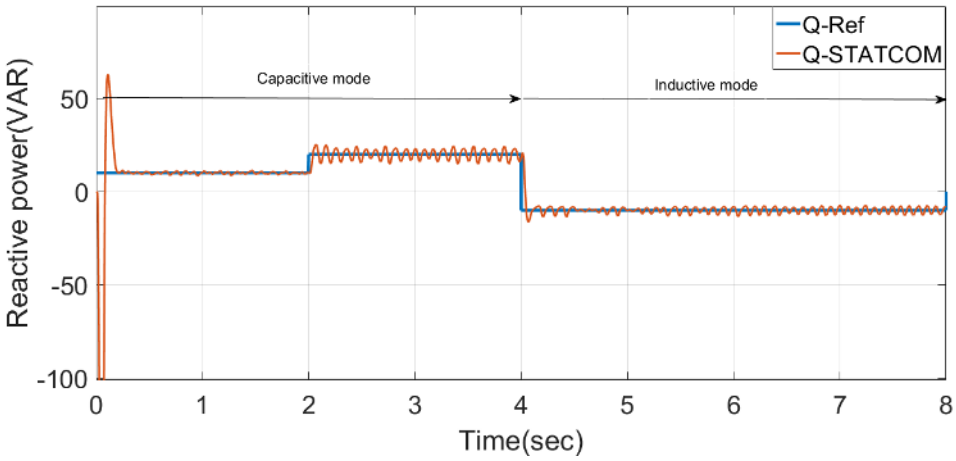

Figure 7.14 STATCOM reactive power

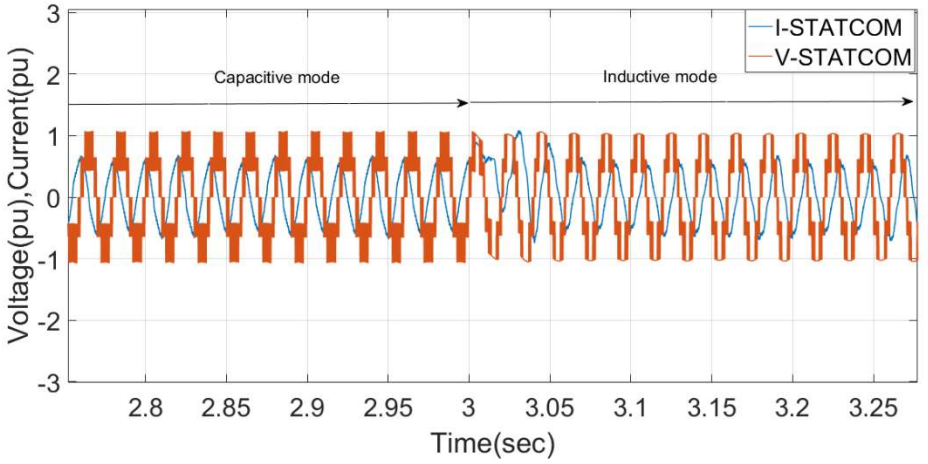

Figure 7.15 STATCOM output voltage and current

7.8 Experiment Results

To validate the simulation results that is presented in Chapter 6, a prototype has been constructed. This prototype consists of a 2 CHB connected to the grid via coupling reactance, which is used for source connection with the grid and filter out the current. A 220/24V step down coupling transformer is used for adjusting voltage levels between the STATCOM converter and PCC. For each H-bridge a 17V-DC voltage is used as reference DC capacitor voltage. For capacitive mode, the test signal value is used to supply the reactive power to grid changed from (10VAR to 40VAR), while for inductive mode, absorbs the reactive power from grid, it is changed from (-2 VAR to -10VAR). The PS-PWM switching strategy has been selected, and the switching frequency that is used in the test bench is 2KHz, which is the same frequency that is used in the simulations. The 5-Level converter output voltage (yellow) with zero cross output (blue) signal is depicted in Figure 7.16. On the other hand, Figure 7.17 depicts the converter output voltage following towards the secondary winding transformer voltage.

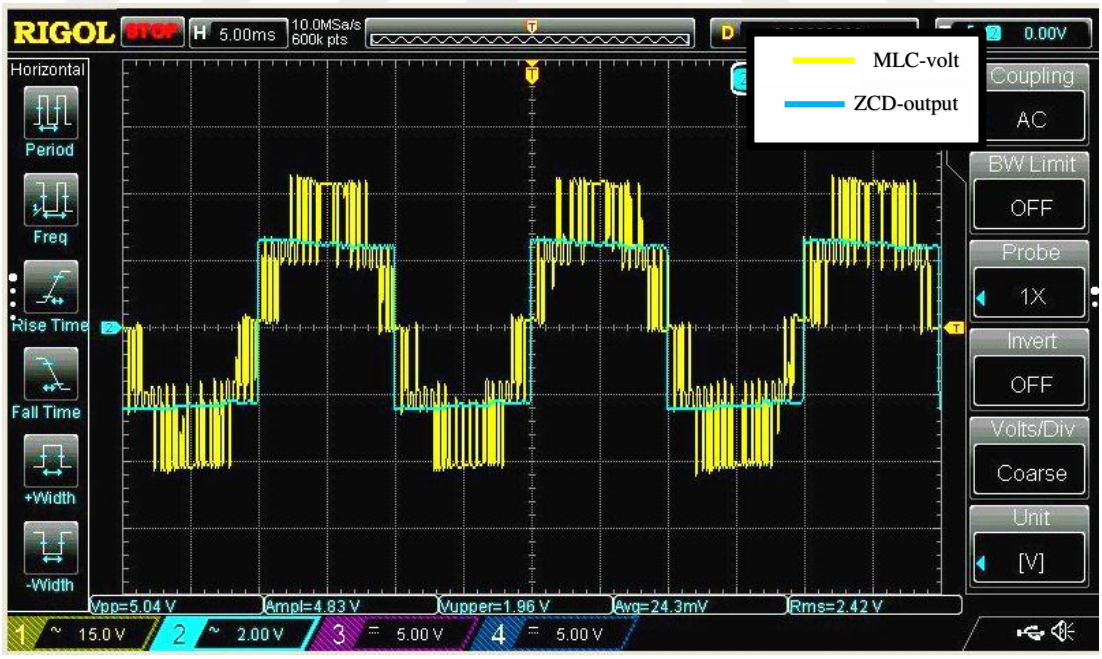

Figure 7.16 Multilevel inverter voltage and zero cross signal

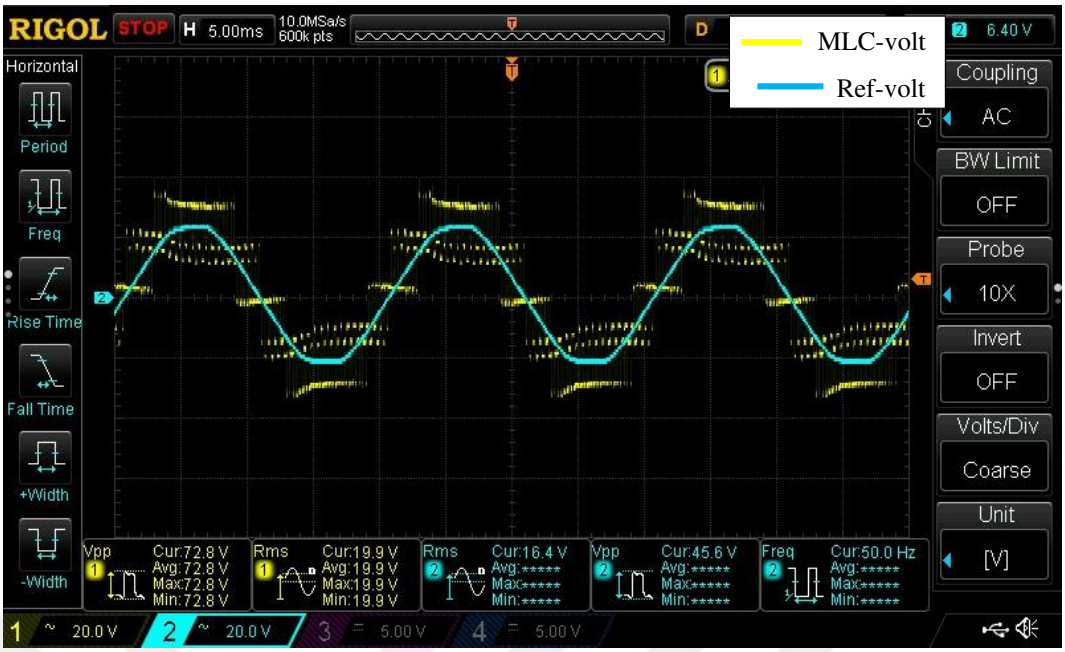

Figure 7.17 Multilevel inverter voltage and reference signal

Figure 7.18 reveals that STATCOM voltage after the primary of the transformer is synchronized to source voltage at the PCC bus.

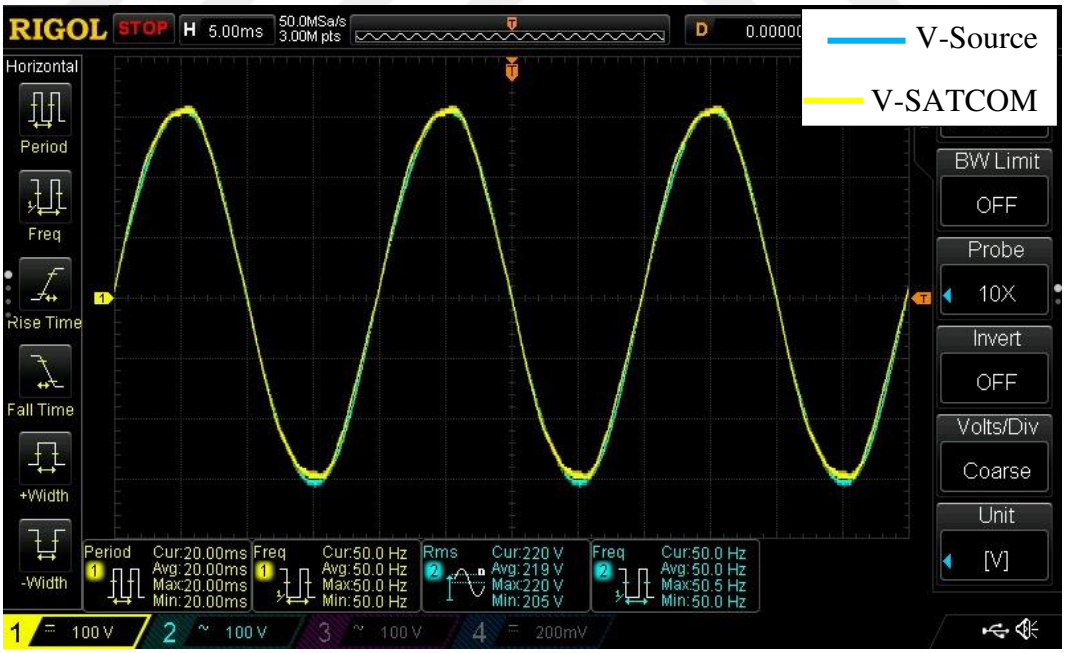

Figure 7.18 STATCOM output voltage with source voltage

7.8.1 STATCOM Operating in Capacitive Mode

In this mode the STATCOM can inject the reactive power to grid, and the STATCOM current leads 90° STATCOM voltage. Figure 7.19 shows the STATCOM current and voltage for reference reactive power equal to 10 VAR with modulation index equal to 0.74. While Figure 7.20 shows the STATCOM current and voltage for reference reactive power equal to 20 VAR with modulation index equal to 0.874.

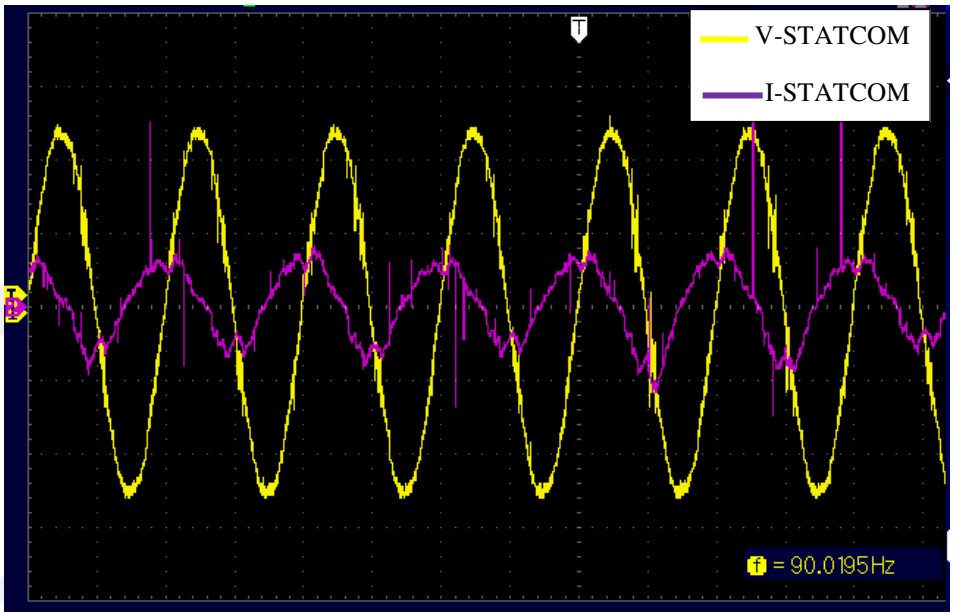

Figure 7.19 Reactive power Q =10 VAR, Modulation index M = 0.74

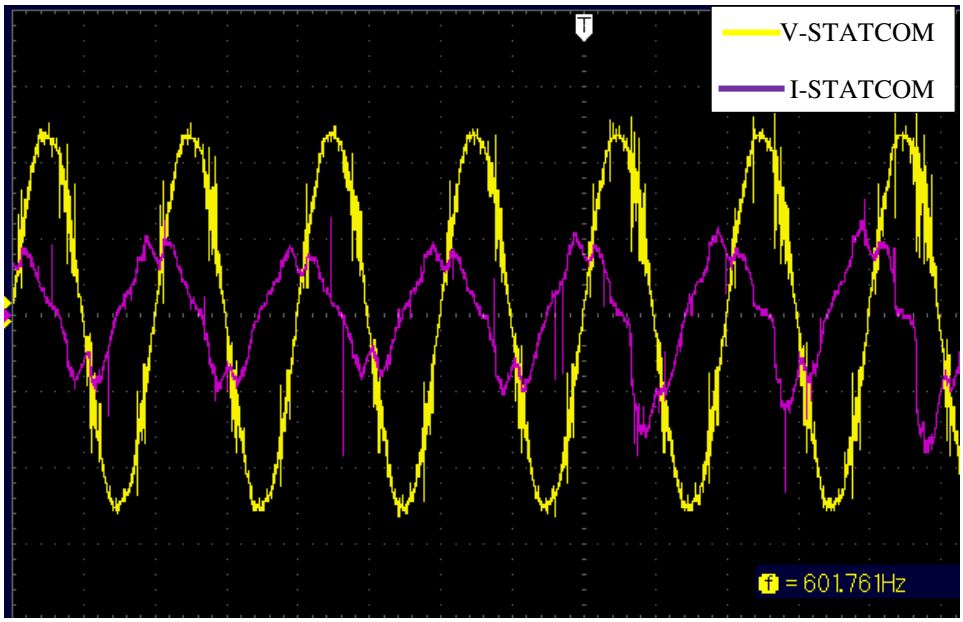

Figure 7.20 Reactive power Q =20 VAR, Modulation index M = 0.87

Figure 7.20 shows the STATCOM current and voltage for reference reactive power equal to 30VAR with modulation index equal to 0.9. In Figure 7.20 shows the STATCOM current and voltage for reference reactive power equal to 40VAR with modulation index equal to 0.94.

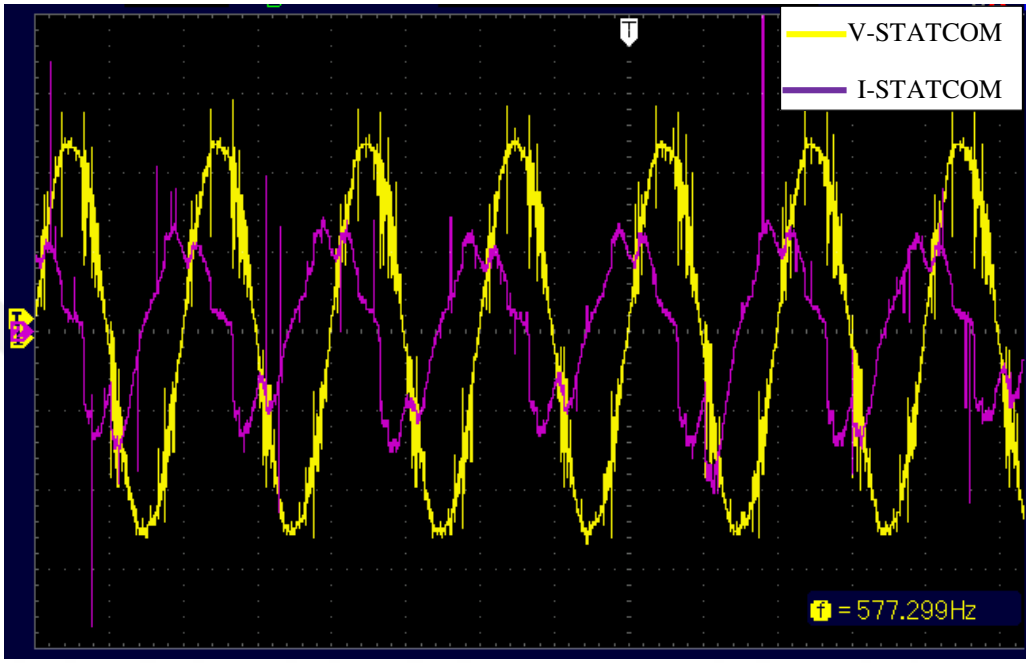

Figure 7.21 Reactive power Q = 30 VAR, Modulation index M = 0.9

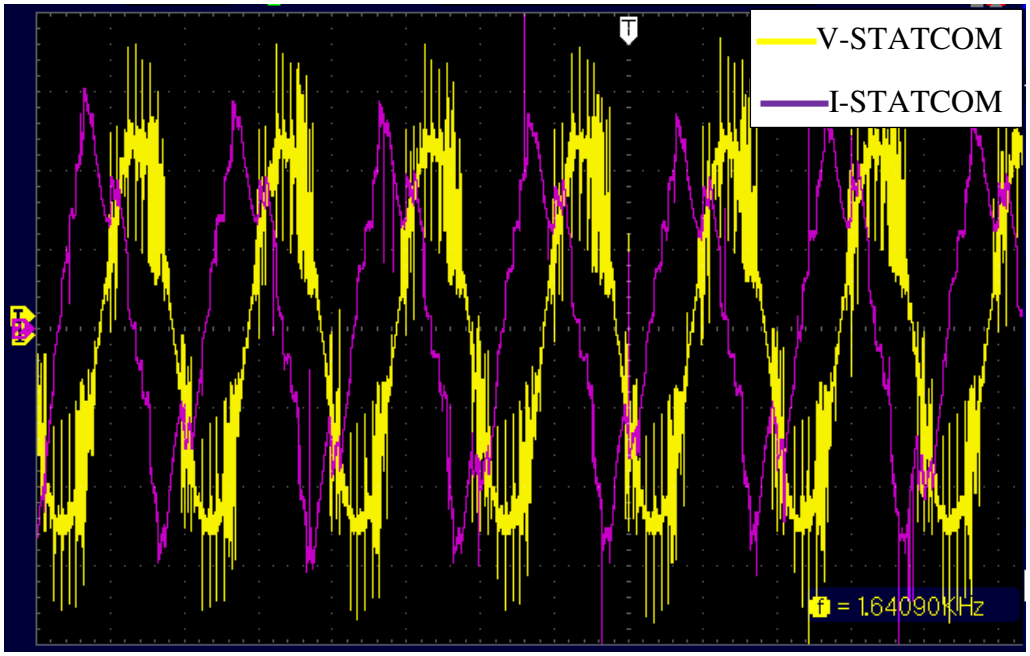

Figure 7.22 Reactive power Q = 40 VAR, Modulation index M = 0.94

Figure 7.23 depicts the reactive power set point (S) and reactive power measurement (Q) of the STATCOM, while Figure 7. 24 depicts that the average DC link V_{dc} voltage for STATCOM operation in capacitive mode.

Figure 7.23 Reference and measured STATCOM reactive power in capacitive mode

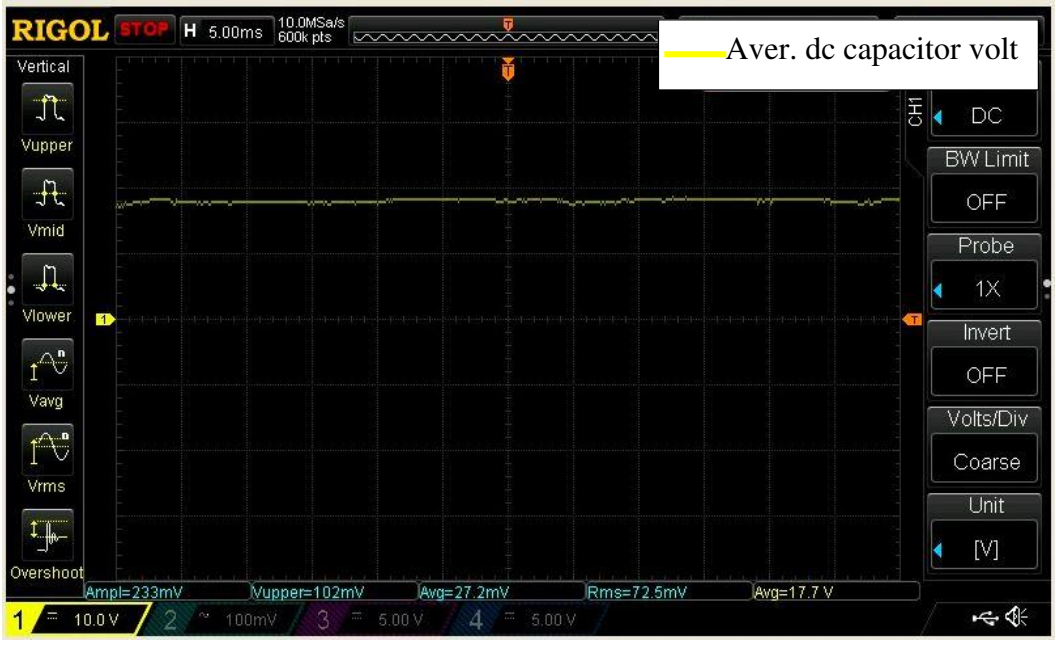

Figure 7.24 Average DC link voltage in capacitive mode

7.8.2 STATCOM Operating in Inductive Mode

In this mode the STATCOM can absorbs the reactive power from the grid, and the STATCOM current lagging 90° STATCOM voltage. Figure 7.25 shows the STATCOM current and voltage for reference reactive power equal to -10 VAR with modulation index equal to 0.9 operation in inductive mode.

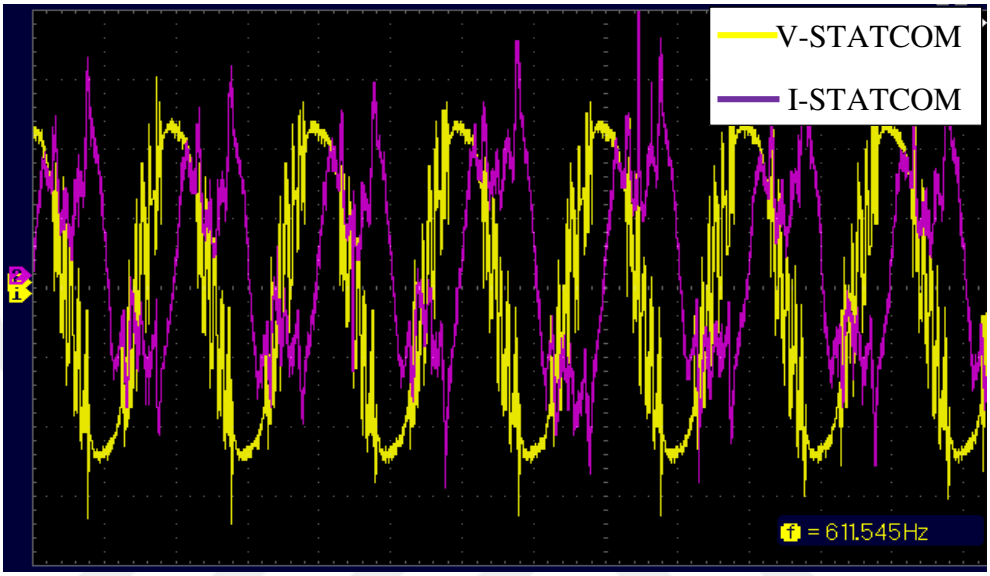

Figure 7.25 Reactive power Q = -10 VAR, Modulation index M = 0.9

For inductive mode, Figure 7.26 depicts the reactive power set point (S = -10 VAR) and reactive power measurement (Q = -10 VAR) of the STATCOM with modulation index (PI = 0.9), while Figure 7.27 depicts the average DC link V_{dc} voltage for STATCOM operation in inductive mode.

Figure 7.26 Reference and measured STATCOM reactive power in inductive mode

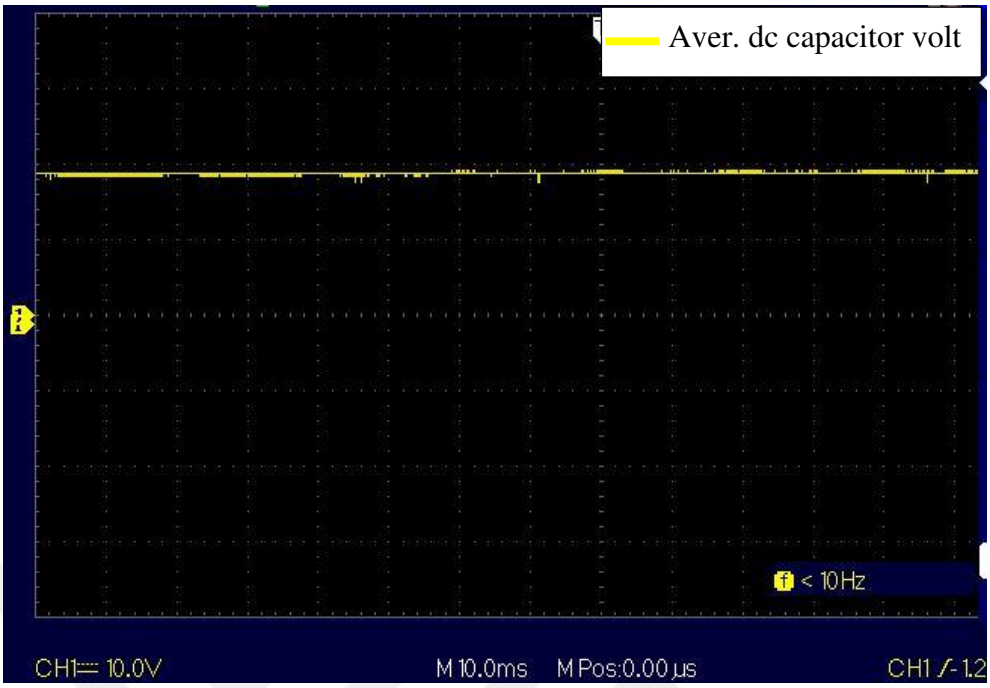

Figure 7.27 Average DC link voltage in inductive mode

7.9 Conclusion

In this chapter, we have presented the single-phase 5-Level STATCOM topology as the appropriate topology for the reactive power compensation applications. Additionally, it can be shown that reactive power as well as DC link voltage control strategy with respect to the single-phase cascaded H-bridge multilevel-converter based STATCOM applications can be enough for PWM techniques. The PI controller contains adaptive gains for DC-Link voltage and reactive power regulator. The hardware experiments as well as simulation propound the proposed control approach and, in all cases, it verifies the accurate performance.

CHAPTER 8

CONCLUSIONS AND FUTURE WORK

8.1 Conclusions

This thesis has dealt with the control and modulation of single-phase cascaded H-bridge (CHB) converters for STATCOM applications. With focus on the reactive power compensation, the STATCOM performance under capacitive mode and inductive mode operation have been investigated, trying to highlight the advantages but also the challenges and possible pitfalls.

After an introductory overview of the main multilevel converter topologies and overview of STATCOM that are available in today's market, the overall control structure for the single-phase CHB-STATCOM has been described in Chapter 5.

This thesis has presented analysis, simulation and experimental results focusing on modeling, control, and analysis of single-phase CHB-STATCOM, according to the following steps:

1. Modeling and analysis of single-phase CHB-STATCOM circuit by using a technique based on the active and reactive power frame.

2. Enhancement of the PI controller performance by controlling the single-phase CHB-STATCOM based on the active and reactive power by using FLC.

3. Modeling and analysis of single-phase CHB-STATCOM circuit by using a technique based on the synchronous rotating reference frame.

4. Modeling and analysis of single-phase CHB-STATCOM for the reduction of THD associated with the nonlinear load.

5. Modeling and analysis of single-phase CHB-STATCOM allowing a reactive power to be imported and exported from the grid and enhancement of the power factor of the grid.

6. The developed ANN is used to estimate voltages, phases, and reactive powers of STATCOM.

7. The effectiveness of the proposed system has been verified by simulation and experimentation.

8.2 Future work

The CHB converter and more in general the modular multilevel concept is still rather new and offers both opportunities and challenges for the researchers to improve its efficiency and performance. One important aspect that still needs research effort is the control and modulation of the converter. Different types of control techniques and other modulation schemes, in both directions are of high interest and need further investigation to preserve (or even increase) the performance of the system and at the same time reduce to the minimum the number of switching events. Also, the operation of the CHB-STATCOM in case of connection to weak grids is a challenge, especially when utilized for balancing purpose. The result obtained from this low power STATCOM project will be used in near future for the design and implementation of larger three-phase STATCOMs and/or active power filters for harmonic reduction. For this reason, it can be of high interest to investigate alternative configurations for modular multilevel STATCOMs, to extend its operational range under unbalanced conditions.

REFERENCES

[1] Kolenc, M., Papič, I., & Blažič, B. (2014). Coordinated reactive power control to achieve minimal operating costs. International Journal of Electrical Power & Energy Systems, 63, 1000-1007.

[2] Chopade, P., Bikdash, M., Kateeb, I., & Kelkar, A. D. (2011, March). Reactive power management and voltage control of large Transmission System using SVC (Static VAR Compensator). In Southeastcon, 2011 Proceedings of IEEE(pp. 85-90). IEEE

[3] Mithulananthan, N., Canizares, C. A., Reeve, J., & Rogers, G. J. (2003). Comparison of PSS, SVC, and STATCOM controllers for damping power system oscillations. IEEE transactions on power systems, 18(2), 786-792.

[4] Gerbex, S., Cherkaoui, R., & Germond, A. J. (2001). Optimal location of multi-type FACTS devices in a power system by means of genetic algorithms. IEEE transactions on power systems, 16(3), 537-544.

[5] Singh, B., Saha, R., Chandra, A., & Al-Haddad, K. (2009). Static synchronous compensators (STATCOM): a review. IET Power Electronics, 2(4), 297-324.

[6] Colak, I., Kabalci, E., & Bayindir, R. (2011). Review of multilevel voltage source inverter topologies and control schemes. Energy conversion and management, 52(2), 1114-1128.

[7] Rodríguez, J., Bernet, S., Wu, B., Pontt, J. O., & Kouro, S. (2007). Multilevel voltage-source-converter topologies for industrial medium-voltage drives. IEEE Transactions on industrial electronics, 54(6), 2930-2945.

[8] Rodriguez, J., Lai, J. S., & Peng, F. Z. (2002). Multilevel inverters: a survey of topologies, controls, and applications. IEEE Transactions on industrial electronics, 49(4), 724-738.

[9] Rao, P., Crow, M. L., & Yang, Z. (2000). STATCOM control for power system voltage control applications. IEEE Transactions on power delivery, 15(4), 1311-1317.

[10] Barrena, J. A., Marroyo, L., Vidal, M. Á. R., & Apraiz, J. R. T. (2008). Individual voltage balancing strategy for PWM cascaded H-bridge converter-based STATCOM. IEEE Transactions on Industrial Electronics, 55(1), 21-29.

[11] Prasad, K. N. V., Kumar, G. R., Kiran, T. V., & Narayana, G. S. (2013, January). Comparison of different topologies of cascaded H-Bridge multilevel inverter. In Computer Communication and Informatics (ICCCI), 2013 International Conference on (pp. 1-6). IEEE.

[12] Atalik, T., Deniz, M., Koc, E., Gercek, C. Ö., Gultekin, B., Ermis, M., & Cadirci, I. (2012). Multi-DSP and-FPGA-based fully digital control system for cascaded multilevel converters used in FACTS applications. IEEE transactions on industrial informatics, 8(3), 511-527.

[13] Gultekin, B., Gercek, C. O., Atalik, T., Deniz, M., Biçer, N., Ermis, M., ... & Açik, A. (2012). Design and Implementation of a 154-kV $\pm $50-Mvar Transmission STATCOM Based on 21-Level Cascaded Multilevel Converter. IEEE Transactions on Industry Applications, 48(3), 1030-1045.

[14] Hingorani, N. G., Gyugyi, L., & El-Hawary, M. (2000). Understanding FACTS: concepts and technology of flexible AC transmission systems (Vol. 1). New York: IEEE press.

[15] Zhang, X. P., Rehtanz, C., & Pal, B. (2012). Flexible AC transmission systems: modelling and control. Springer Science & Business Media.

[16] Reed, G. F., Takeda, M., & Iyoda, I. (1999, January). Improved power quality solutions using advanced solid-state switching and static compensation technologies. In Power Engineering Society 1999 Winter Meeting, IEEE (Vol. 2, pp. 1132-1137). IEEE.

[17] Davidson, C. C., & De Préville, G. (2009, September). The future of high power electronics in transmission and distribution power systems. In Power Electronics and Applications, 2009. EPE'09. 13th European Conference on(pp. 1-14). IEEE.

[18] Sood, V. K. (2006). HVDC and FACTS controllers: applications of static converters in power systems. Springer Science & Business Media.

[19] Akagi, H., Inoue, S., & Yoshii, T. (2007). Control and performance of a transformerless cascade PWM STATCOM with star configuration. IEEE Transactions on Industry Applications, 43(4), 1041-1049.

[20] Lesnicar, A., & Marquardt, R. (2003, June). An innovative modular multilevel converter topology suiTable for a wide power range. In Power Tech Conference Proceedings, 2003 IEEE Bologna (Vol. 3, pp. 6-pp). IEEE.

[21] Townsend, C. D., Cox, S. M., Watson, A. J., Summers, T. J., Betz, R. E., & Clare, J. C. (2012, September). Voltage balancing characteristics for a cascaded H-bridge multi-level StatCom employing space vector modulation. In Power Electronics and Motion Control Conference (EPE/PEMC), 2012 15th International (pp. DS3b-3). IEEE.

[22] Behrouzian, E. (2016). Operation and control of cascaded H-bridge converter for STATCOM application.

[23] Shinde, O. K., BharathPulavarthi, V. R. S. V., & Patil, S. S. (2017, April). Five level inverter based STATCOM with PI control. In Circuit, Power and Computing Technologies (ICCPCT), 2017 International Conference on (pp. 1-5). IEEE.

[25] Zhang, Y., Wu, X., Yuan, X., Wang, Y., & Dai, P. (2016). Fast Model Predictive Control for Multilevel Cascaded H-Bridge STATCOM With

Polynomial Computation Time. IEEE Trans. Industrial Electronics, 63(8), 5231-5243.

[26] Wang, Y., Cong, W., Li, M., Li, N., Cao, M., & Lei, W. (2014, March). Model predictive control of modular multilevel converter with reduced computational load. In Applied Power Electronics Conference and Exposition (APEC), 2014 Twenty-Ninth Annual IEEE (pp. 1776-1779). IEEE.

[27] Xu, R., Yu, Y., Yang, R., Wang, G., Xu, D., Li, B., & Sui, S. (2015). A novel control method for transformerless H-bridge cascaded STATCOM with star configuration. IEEE Transactions on Power Electronics, 30(3), 1189-1202.

[28] Benachaiba, C., Dib, S., & Abdelkhlek, O. (2006). Genetic algorithm-based self-learning fuzzy PI controller for shunt active filter. International Journal of Applied Engineering Research, 1(2), 203-216.

[29] Stott, B. (1974). Review of load-flow calculation methods. Proceedings of the IEEE, 62(7), 916-929.

[30] Zhang, L., & Suganthan, P. N. (2016). A survey of randomized algorithms for training neural networks. Information Sciences, 364, 146-155.

[31] Kamel, S., & Jurado, F. (2015). Modeling of STATCOM in load flow formulation. In Static Compensators (STATCOMs) in Power Systems (pp. 405-435). Springer, Singapore.

[32] Mesic, S. (2015). Investigation of Harmonic Content in Chain-Link Statcom with a Non-Integer Frequency Modulation INdex(Doctoral dissertation, Masters Thesis. Chalmers University of Technology).

[33] Rodriguez, J., Lai, J. S., & Peng, F. Z. (2002). Multilevel inverters: a survey of topologies, controls, and applications. IEEE Transactions on industrial electronics, 49(4), 724-738.

[34] Debnath, S., Qin, J., Bahrani, B., Saeedifard, M., & Barbosa, P. (2015). Operation control and applications of the modular multilevel converter: A review. IEEE Trans. Power Electron, 30(1), 37-53.

[35] Vivas, J. H., Bergna, G., & Boyra, M. (2011, August). Comparison of multilevel converter-based STATCOMs. In Power Electronics and Applications (EPE 2011), Proceedings of the 2011-14th European Conference on (pp. 1-10). IEEE.

[36] Soto, D., & Green, T. C. (2002). A comparison of high-power converter topologies for the implementation of FACTS controllers. IEEE transactions on industrial electronics, 49(5), 1072-1080.

[37] Rodriguez, J., Lai, J. S., & Peng, F. Z. (2002). Multilevel inverters: a survey of topologies, controls, and applications. IEEE Transactions on industrial electronics, 49(4), 724-738.

[38] Tolbert, L. M., & Peng, F. Z. (1998, February). Multilevel converters for large electric drives. In Applied Power Electronics Conference and Exposition,

1998. APEC'98. Conference Proceedings 1998., Thirteenth Annual (Vol. 2, pp. 530-536). IEEE.

[39] Nabae, A., Takahashi, I., & Akagi, H. (1981). A new neutral-point-clamped PWM inverter. IEEE Transactions on industry applications, (5), 518-523.

[40] Rodríguez, J., Bernet, S., Wu, B., Pontt, J. O., & Kouro, S. (2007). Multilevel voltage-source-converter topologies for industrial medium-voltage drives. IEEE Transactions on industrial electronics, 54(6), 2930-2945.

[41] Bruckner, T., Bernet, S., & Guldner, H. (2005). The active NPC converter and its loss-balancing control. IEEE Transactions on Industrial Electronics, 52(3), 855-868.

[42] Grunbaum, R., Sannino, A., & Wahlberg, C. (2010). Use of FACTS for enhanced flexibility and efficiency in power transmission and distribution grids. In World Energy Congress, Montreal.

[43] Meynard, T. A., & Foch, H. (1992, June). Multi-level conversion: high voltage choppers and voltage-source inverters. In Power Electronics Specialists Conference, 1992. PESC'92 Record., 23rd Annual IEEE (pp. 397-403). IEEE.

[44] Fujii, K., Schwarzer, U., & De Doncker, R. W. (2005, June). Comparison of hard-switched multi-level inverter topologies for STATCOM by loss-implemented simulation and cost estimation. In Power Electronics Specialists Conference, 2005. PESC'05. IEEE 36th (pp. 340-346). IEEE.

[45] Agarwal, S., & Deore, S. R. (2015, January). Level shifted SPWM of a seven level cascaded multilevel inverter for STATCOM applications. In Nascent Technologies in the Engineering Field (ICNTE), 2015 International Conference on(pp. 1-7). IEEE.

[46] Tolbert, L. M., Peng, F. Z., Cunnyngham, T., & Chiasson, J. N. (2002). Charge balance control schemes for cascade multilevel converter in hybrid electric vehicles. IEEE Transactions on Industrial Electronics, 49(5), 1058-1064.

[47] Mariethoz, S., & Rufer, A. (2002, November). Design and control of asymmetrical multi-level inverters. In IECON 02 [Industrial Electronics Society, IEEE 2002 28th Annual Conference of the] (Vol. 1, pp. 840-845). IEEE.

[48] Manohar, P., & Dutta, K. K. (2011, January). Effect of SCFCL on the performance of BTB-HVDC system. In Electrical Energy Systems (ICEES), 2011 1st International Conference on (pp. 288-293). IEEE.

[49] Du, Z., Tolbert, L. M., Ozpineci, B., & Chiasson, J. N. (2009). Fundamental frequency switching strategies of a seven-level hybrid cascaded H-bridge multilevel inverter. IEEE Transactions on Power Electronics, 24(1), 25-33.

[50] Khoucha, F., Ales, A., Khoudiri, A., Marouani, K., Benbouzid, M. E. H., & Kheloui, A. (2010, September). A 7-level single DC source cascaded H-bridge multilevel inverters control using hybrid modulation. In Electrical Machines (ICEM), 2010 XIX International Conference on (pp. 1-5). IEEE.

[51] Lu, S., & Corzine, K. A. (2007). Advanced control and analysis of cascaded multilevel converters based on PQ compensation. IEEE transactions on power electronics, 22(4), 1242-1252.

[52] Barrena, J. A., Aurtenechea, S., Canales, J. M., Rodriguez, M. A., & Marroyo, L. (2005, September). Design, analysis and comparison of multilevel topologies for DSTATCOM applications. In Power Electronics and Applications, 2005 European Conference on (pp. 10-pp). IEEE.

[53] Kouro, S., Malinowski, M., Gopakumar, K., Pou, J., Franquelo, L. G., Wu, B., ... & Leon, J. I. (2010). Recent advances and industrial applications of multilevel converters. IEEE Transactions on industrial electronics, 57(8), 2553-2580.

[54] Rodriguez, J., Franquelo, L. G., Kouro, S., Leon, J. I., Portillo, R. C., Prats, M. A. M., & Perez, M. A. (2009). Multilevel converters: An enabling technology for high-power applications. Proceedings of the IEEE, 97(11), 1786-1817.

[55] Agarwal, S., & Deore, S. R. (2015, January). Level shifted SPWM of a seven level cascaded multilevel inverter for STATCOM applications. In Nascent Technologies in the Engineering Field (ICNTE), 2015 International Conference on(pp. 1-7). IEEE.

[56] Hassanpoor, A., Norrga, S., Nee, H. P., & Ängquist, L. (2012, October). Evaluation of different carrier-based PWM methods for modular multilevel converters for HVDC application. In IECON 2012-38th Annual Conference on IEEE Industrial Electronics Society (pp. 388-393). IEEE.

[57] Du, Z., Tolbert, L. M., Ozpineci, B., & Chiasson, J. N. (2009). Fundamental frequency switching strategies of a seven-level hybrid cascaded H-bridge multilevel inverter. IEEE Transactions on Power Electronics, 24(1), 25-33.

[58] Vural, Ahmet Mete.(2016). Self-capacitor voltage balancing method for optimally hybrid modulated cascaded H-bridge D-STATCOM.IET Power Electronics 9.14 . 2731-2740.

[59] Ribeiro, P. F., Johnson, B. K., Crow, M. L., Arsoy, A., & Liu, Y. (2001). Energy storage systems for advanced power applications. Proceedings of the IEEE, 89(12), 1744-1756.

[60] Styvaktakis, E., Bollen, M. H., & Gu, I. Y. (2000). Classification of power system events: Voltage dips. In Harmonics and Quality of Power, 2000. Proceedings. Ninth International Conference on (Vol. 2, pp. 745-750). IEEE.

[61] http://www.learnemc.com/tutorials/Transient_Protection/t-protect.html.

[62] Deshmukh, S. M., Dewani, B., & Gawande, S. P. (2013). A review of power quality problems-voltage sags for different faults. International Journal of Scientific Engineering and Technology, 2(5), 392-397.

[63] Rojin, R. K. (2013). A review of power quality problems and solutions in electrical power system. International Journal of Advanced Research in Electrical, Electronics and Instrumentation Engineering, 2(11), 5605-5614.

[64] Agarwal, A., Kumar, S., & Ali, S. (2012). A research review of Power Quality problems in Electrical Power System. MIT International Journal of Electrical and Instrumentation Engineering, 2(2), 88-93.

[65] VURAL, A. M. (2012). Modelling of Multi-Converter FACTs (Flexible Alternating Current Transmission Sytstems) (Doctoral dissertation, PhD Dissertation, Cukurova University).

[66] Murali, D., & Rajaram, M. (2013). Use of ANFIS control approach for SSSC based damping controllers applied in a two-area power system. Journal of applied research and technology, 11(6), 895-902.

[67] VURAL, A. M., & BAYINDIR, K. C. (2012). Understanding the steady-state modeling and analysis of power systems embedded with VSC-based FACTS devices. IEEE EnergyTech2012.

[68] Padiyar, K. R. (2007). FACTS controllers in power transmission and distribution.

[69] Gyugyi, L., Schauder, C. D., & Sen, K. K. (1997). Static synchronous series compensator: a solid-state approach to the series compensation of transmission lines. IEEE Transactions on power delivery, 12(1), 406-417.

[70] GYUGYI L., 1992. Unified power-flow control concept for flexible AC transmission systems, IEE Proceedings C, Generation, Transmission and Distribution, vol.139, no. 4, pp. 323-331.

[71] Vural, A. M., & Hamad, M. S. (2018, May). Comparison of dynamic performances of IPFC, UPFC and back to back HVDC transmission on local and inter-area oscillation damping in power systems. In 2018 5th International Conference on Electrical and Electronic Engineering (ICEEE)(pp. 31-35). IEEE.

[72] Yu, Qingguang, et al.(2004). Overview of STATCOM technologies. Electric Utility Deregulation, Restructuring and Power Technologies, 2004.(DRPT 2004). Proceedings of the 2004 IEEE International Conference on. Vol. 2. IEEE.

[73] Wang, H. F. (2000). Applications of damping torque analysis to STATCOM control. International Journal of Electrical Power & Energy Systems, 22(3), 197-204.

[74] Çetin, Alper, and Muammer Ermis.(2009). VSC-based D-STATCOM with selective harmonic elimination. IEEE Transactions on Industry Applications 45.3 . 1000-1015.

[75] Cetin, A. (2007). Design and implementation of a voltage source converter based STATCOM for reactive power compensation and harmonic filtering. METU Electrical and Electronic Engineering Department Phd Thesis, Pages, 222.

[76] Patel, S. N., Patel, C. R., & Mehta, A. J. (2011, May). Modeling and control of current source converter (CSC) based STATCOM. In National Conference on Recent Trends in Engineering & Technology (pp. 1-5).

[77] Muñoz, J., Rohten, J., Espinoza, J., Melín, P., Baier, C., & Rivera, M. (2015, March). Review of current control techniques for a cascaded H-Bridge STATCOM. In Industrial Technology (ICIT), 2015 IEEE International Conference on(pp. 3085-3090). IEEE.

[78] Akagi, H., Inoue, S., & Yoshii, T. (2007). Control and performance of a transformerless cascade PWM STATCOM with star configuration. IEEE Transactions on Industry Applications, 43(4), 1041-1049.

[79] Neyshabouri, Y., Iman-Eini, H., & Miranbeigi, M. (2015). State feedback control strategy and voltage balancing scheme for a transformer-less STATic synchronous COMpensator based on cascaded H-bridge converter. IET Power Electronics, 8(6), 906-917.

[80] Vural, A. M. (2016). Self-capacitor voltage balancing method for optimally hybrid modulated cascaded H-bridge D-STATCOM. IET Power Electronics, 9(14), 2731-2740.

[81] Wallmark, O., & Harnefors, L. (2006). Sensorless control of salient PMSM drives in the transition region. IEEE transactions on industrial electronics, 53(4), 1179-1187.

[82] Sotoodeh, P. (2014). A single-phase multi-level D-STATCOM inverter using modular multi-level converter (MMC) topology for renewble energy sources (Doctoral dissertation, Kansas State University).

[83] Mak, L. O., Ni, Y. X., & Shen, C. M. (2000). STATCOM with fuzzy controllers for interconnected power systems. Electric Power Systems Research, 55(2), 87-95.

[84] Barua, A., La, S. M., & Olga K.(2014) .Why trapezoidal and triangular membership functions work so well. Towards a theoretical explanation." *Journal of Uncertain Systems*.

[85] Li, S., Fu, X., Ramezani, M., Sun, Y., & Won, H. (2015). A novel direct-current vector control technique for single-phase inverter with L, LC and LCL filters. Electric Power Systems Research, 125, 235-244.

[86] Behrouzian, E., Bongiorno, M., & Teodorescu, R. (2014, September). Impact of frequency modulation ratio on capacitor cells balancing in phase-shifted PWM based chain-link STATCOM. In Energy Conversion Congress and Exposition (ECCE), 2014 IEEE (pp. 1931-1938). IEEE.

[87] Eberhart, R., & Kennedy, J. (1995, October). A new optimizer using particle swarm theory. In Micro Machine and Human Science, 1995. MHS'95., Proceedings of the Sixth International Symposium on (pp. 39-43). IEEE.

[88] Clerc, M. (2010). Particle swarm optimization (Vol. 93). John Wiley & Sons.

[89] Shinde, S. U., Sharmila, M., Patil, R. S., & Malkhede, D. V. (2016, March). Performance comparison of PI & ANN based STATCOM for 132 KV transmission line. In Electrical, Electronics, and Optimization Techniques (ICEEOT), International Conference on (pp. 2730-2734). IEEE.

[90] Chen, H., Li, J., & Zhou, X. (2012, June). PSO-based self-tuning PI control for STATCOM. In Power Electronics and Motion Control Conference (IPEMC), 2012 7th International(Vol. 4, pp. 2710-2715). IEEE.

[91] Yang, X. S. (2010). Nature-inspired metaheuristic algorithms. Luniver press.

[92] Yang, X. S., Deb, S., & Fong, S. (2011, July). Accelerated particle swarm optimization and support vector machine for business optimization and applications. In International Conference on Networked Digital Technologies (pp. 53-66). Springer, Berlin, Heidelberg.

[93] Rashedi, E., Nezamabadi-Pour, H., & Saryazdi, S. (2009). GSA: a gravitational search algorithm. Information sciences, 179(13), 2232-2248.

[94] Rafiei, M. (2006, July). Verification of global optimality of the OFC active power filters by means of genetic algorithms. In Proc. WSEAS Int. Conf. on Systems, Vouliagmeni, Athens, Greece (pp. 559-564).

[95] Rahmani, S., Al-Haddad, K., & Fnaiech, F. (2006, July). A three-phase shunt active power filter for damping of harmonic propagation in power distribution systems. In Industrial Electronics, 2006 IEEE International Symposium on (Vol. 3, pp. 1760-1764). IEEE.

[96] Ortúzar, M. E., Carmi, R. E., Dixon, J. W., & Morán, L. (2006). Voltage-source active power filter based on multilevel converter and ultracapacitor DC link. IEEE Transactions on Industrial Electronics, 53(2), 477-485.

[97] Komurcugil, H., & Kukrer, O. (2006). A new control strategy for single-phase shunt active power filters using a Lyapunov function. IEEE Transactions on Industrial Electronics, 53(1), 305-312.

[98] Shyu, K. K., Yang, M. J., Chen, Y. M., & Lin, Y. F. (2008). Model reference adaptive control design for a shunt active-power-filter system. IEEE Transactions on Industrial Electronics, 55(1), 97-106.

[99] Liu, C. C., McArthur, S., & Lee, S. J. (Eds.). (2016). Smart grid handbook, 3 volume set (Vol. 1). John Wiley & Sons.

[100] Zhu, J. (2015). Optimization of power system operation (Vol. 47). John Wiley & Sons.

[101] Padilla, E. (2015). Substation Automation Systems: Design and Implementation. John Wiley & Sons.

[102] Cajori, F. (1911). Historical note on the Newton-Raphson method of approximation. The American Mathematical Monthly, 18(2), 29-32.

[103] Hu, X., Shi, Y., & Eberhart, R. (2004, June). Recent advances in particle swarm. In Evolutionary Computation, 2004. CEC2004. Congress on (Vol. 1, pp. 90-97). IEEE.

[104] Radman, G., & Raje, R. S. (2007). Power flow model/calculation for power systems with multiple FACTS controllers. Electric power systems research, 77(12), 1521-1531.

[105] Vui, C. S., Soon, G. K., On, C. K., Alfred, R., & Anthony, P. (2013, November). A review of stock market prediction with Artificial neural network (ANN). In Control System, Computing and Engineering (ICCSCE), 2013 IEEE International Conference on (pp. 477-482). IEEE.

[106] Ahmad, A. S., Hassan, M. Y., Abdullah, M. P., Rahman, H. A., Hussin, F., Abdullah, H., & Saidur, R. (2014). A review on applications of ANN and SVM for building electrical energy consumption forecasting. Renewable and Sustainable Energy Reviews, 33, 102-109.

[107] Eusuff, M., Lansey, K., & Pasha, F. (2006). Shuffled frog-leaping algorithm: a memetic meta-heuristic for discrete optimization. Engineering optimization, 38(2), 129-154.

[108] Panda, S., Sarangi, A., & Panigrahi, S. P. (2014). A new training strategy for neural network using shuffled frog-leaping algorithm and application to channel equalization. AEU-International Journal of Electronics and Communications, 68(11), 1031-1036.

[109] Goldberg, D. E., & John, H. (1988). Holland. Genetic algorithms and machine learning. Machine learning, 3(2-3), 95-99.

[110] Ezoji, H., Sheikholeslami, A., Tabasi, M., & Saeednia, M. M. (2009). Simulation of dynamic voltage restorer using hysteresis voltage control. European journal of scientific research, 27(1), 152-166.

[111] Wu, W. C., & Lin, H. P. (2005). U.S. Patent No. 6,837,469. Washington, DC: U.S. Patent and Trademark Office.

[112] Ekdahl, C. A. (1980). Voltage and current sensors for a high-density z-pinch experiment. Review of scientific Instruments, 51(12), 1645-1648.

[113] Microchip. discussion forum. 7 September 2010. Document. 23 July 2013. <http://www.microchip.com/forum>.

[114] Edaboard. Microcontroller Hardware and programming forum. 25 March 2013. Web. 29 March 2013. <http://www.edaboard.com/forum31.html>.

APPENDIX A

A.1 Transistors

Transistors are the semiconductor devices which can be controlled electrically. It has three terminals as collector, base and emitter. The current value through the base controls the flow of current from collector to emitter. This control helps to use this electronic component to preform different actions. The transistor is solely used in this section to convert the +15 Volt and -15 Volt signal in to +5 Volt and 0 Volt signal, such that, they can be used by microcontroller.

Figure A.1 Transistor

A.2 Microcontrollers

Microcontrollers are the brain of the system. A microcontroller is defined in simple word as “a computer in a chip”. The microcontroller used in this section is of micro-chip [109]. The project needs to perform two operations simultaneously, one is the sensing STATCOM voltage and current and calculates the reference reactive component and the other is to generate continuously the sinusoidal reference voltage. Thus, for this purpose two ATMEGA328P microcontrollers are needed. The first ATMEGA328P is used for the former task (to sense STATCOM current, voltage and their phase and determine the phase and magnitude of the reference voltage) and is

used for the later task (to generate continuously the reference voltage digital value). The first AT-MEGA328P has the clock input of 16 MHz while the second ATMEGA328P has clock speed 20 MHz Hence, first one is faster than the second one. The first one continuously generates the digital value of the real-time magnitude of the sinusoidal reference voltage. Table A.1 shows describe the configuration about the ATMEGA328P.

Table A.1 Major microcontroller parameters

Features	**ATmega328P**
Pin Count	28/32
Flash (Bytes)	32K
SRAM (Bytes)	2K
EEPROM (Bytes)	1K
General Purpose I/O Lines	23
SPI	2
TWI (I2C)	1
USART	1
ADC	10-bit 15k SPS
ADC Channels	8
8-bit Timer/Counters	2
16-bit Timer/Counters	1

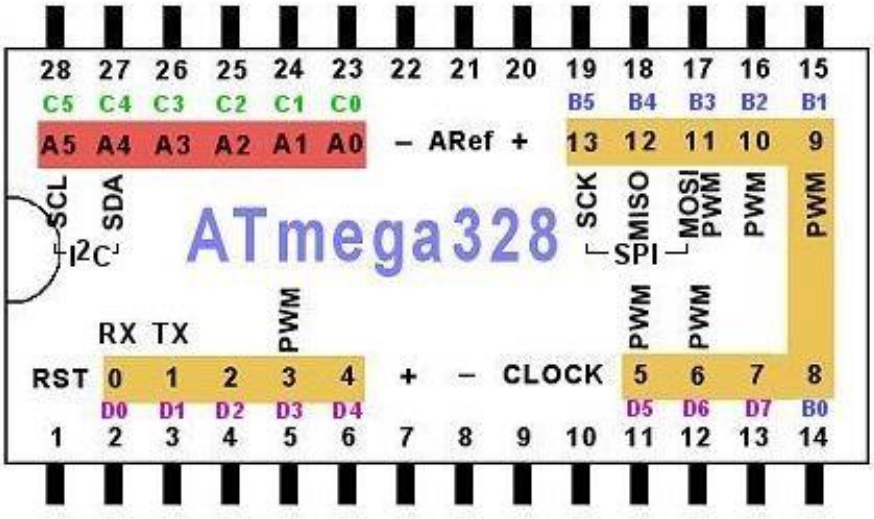

Figure A.2 Microcontroller (AT Mega 328)

A.3 Operational Amplifier

It is one of the versatile electronic devices in various applications. Op-amp in short, it refers to a class of high-gain DC coupled amplifiers with two inputs and a single output [110]. The modern integrated circuit version is typified by the famous 741 op-amp. Some of the general characteristics of the IC version are:

- High gain, on the order of a million,
- High input impedance, low output impedance,
- Used with split supply usually +/- 15V or with single supply mode as + and ground
- Used with feedback, with gain determined by the feedback network
- The main principle of op-amp is that its terminal is virtually short. It means that the op-amp tries to maintain same potential in its both input terminal in anyway it can.

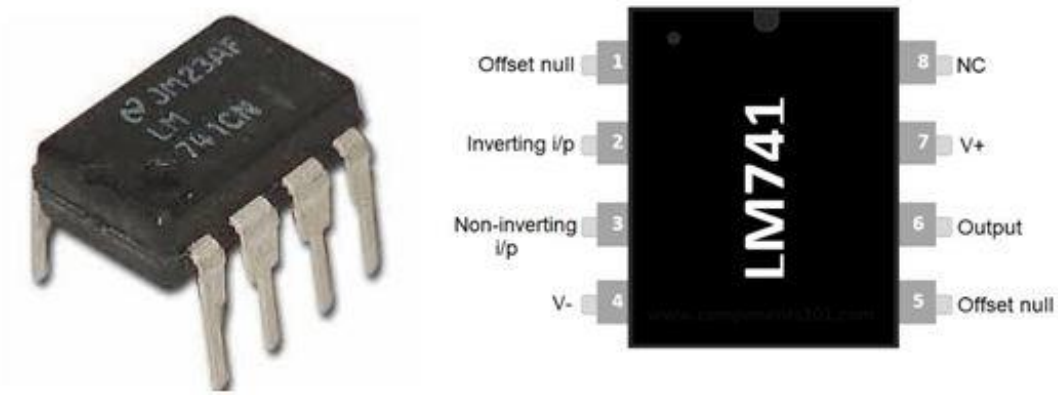

Figure A.4 Operational amplifier

LM741 is one of the famous op-amp with +/- 15 V split supply and LM348 is simply a quad version of 741 op-amp. Op-amp is used in this thesis as zero crossing detector, peak detector and to convert the current output of DAC into voltage.

A.4 DAC

DAC stands for digital to analog converter. It is used to convert the digital 1 (+5 Volt) and 0 (0 Volt) data into analog values. The reference wave is generated in the digital circuit using the inputs and mathematics, which is then communicated with the DAC chip which converts the digital data into corresponding analog values. In this way, the reference signal is generated [111].

Here, the DAC chip used is DAC 4922, which is a 12-bit DAC i.e. It takes 12-bit digital data as input with represents 2^{12} different analog values. It is a parallel DAC; thus, it requires 12 data lines from the microcontroller to its input. The output of DAC 4922 is in voltage form, The DAC 4922 devices are dual 12-bit buffered voltage output Digital-to-Analog Converters (DACs), respectively, the devices provide high accuracy and low noise performance for consumer and industrial applications where calibration or compensation of signals (such as temperature, pressure and humidity) are required.

Figure A.5 DAC

A primary design objective of this CHB-SATCOM is minimal total cost. The total cost increases with increasing the number of levels of the model because the number of components increases at higher voltage levels. Prices of these components for 5-Level single-phase CHB-STATCOM are tabulated in Table A.2.

Table A.2 Cost of each component

Component	Item /required	Price/item
Transformer 12V / 8VA	1	$ 7.00
Transformer 12V*2 / 2VA	1	$ 3.50
ZMPT107Voltage Sensor	2	$ 5.00 Each: $ 2.5
ZMCT103C Current Sensor	2	$ 4.00 Each: $2
MCP6002Rail-to-Rail OP-AMP	3	$ 3.00 Each: $ 1
TL072 OP-AMP	1	$ 0.50
LM339 Differential Comparators	1	$ 0.50
ICL7660 Capacitor Inverter	1	$ 0.50
RT9193-3.3 300mA, Ultra-Low Noise, LDO	1	$ 1.50
LM7805 VOLTAGE REGULATOR	1	$ 0.20
ULN2003 7- Darlington arrays	1	$ 0.25
LCD 1602	1	$ 5.00
F232RL USB TO UART	1	$ 1.50
ATMEGA328P Microcontroller	2	$ 3.00
TERMINAL CONNECTORS	6	$ 10.00 Each:$ 1.6

IDC Connector	4	$ 4.50 Each: $ 1.125
PCB	3	$ 45.00 Each: $ 15
IRFP260N N-Channel Mosfet Transistor	8	$ 14.70 Each: $1.8
IR2104 high speed power MOSFET drivers	4	$ 6.64 Each: $ 1.6
1000uF/100V DC link capacitor	8	$ 8.00 Each: $ 1
Heatsink	2	$ 6.00 Each: $ 3
TLP281-4 Photo coupler	2	$ 3.00 Each: $ 1.5
TVS 1,5KE82A	2	$ 0.66 Each: $ 0.33
BUZZER	1	$ 0.80
PUSH BUTTON	5	$ 2.00 Each: $ 0.4
RELAY 12V 10A	1	$ 1.00
1.5mH / 15A Inductor	1	$ 35.00
USB Connector	1	$ 1.50
Total amount	*$ 170.15*	